Geometrically Open Inverted Granular Filters

R.A. Lengkeek

TU Delft

Geometrically Open Inverted Granular Filters

by

R.A. Lengkeek

in partial fulfilment of the Master of Science
at the Delft University of Technology,
to be defended publicly on Tuesday January 11, 2022 at 15:30.

This thesis is confidential and cannot be made public until January 11, 2023.

Student number:	4531752	
Project duration:	February 8, 2021 – January 11 2022	
Thesis committee:	Dr. ir. B. Hofland,	TU Delft, Chair
	Dr. ir. A. Antonini,	TU Delft
	Ir. D.C.P. van Kester,	TU Delft & Van Oord, Daily Supervisor

An electronic version of this thesis is available at `http://repository.tudelft.nl/`.

Preface

Dear Reader,

This thesis is written to complete the MSc program Hydraulic Engineering at the Delft University of Technology (TU Delft). This project was an experimental study into the stability of an open inverted filter. The TU Delft, and Van Oord Dredging and Marine Contractors (Van Oord) provided supervision.

I would like to thank Van Oord for allowing me to do my graduation project within their company. This gave me context to learn about many interesting projects where an open filter could be of benefit. In particular I appreciate the support from Dennis van Kester who guided me well during our weekly meetings.

I really value my time and experiences in the TU Delft Hydraulic Engineering laboratory. Holding the gravel and sand used for the filters in my own hands made me appreciate the The process of doing an experimental study presented many interesting practical challenges alongside the intellectual challenges. I appreciate the assistance I had for these challenges from Pieter, Kevin, Arno, Arie and Chantal.

I value the support I received from people at the TU Delft. I would like to thank my Bas Hofland and Alessandro Antonini for being in my graduation committee and for the theoretical discussions of the processes in my experimental setup.

And lastly, I would like to thank my friends and family who kept me motivated throughout the project and helped with proofreading of my report.

R.A. Lengkeek
Delft, January 2022

Abstract

The ability to stabilise the core-backfill interface with an open filter has been investigated. This will allow for easier construction of a land reclamation and therefore is a potential cost saving. This study is the continuation of a research line into the interface stability at the rear of a breakwater in a land reclamation structure. A diagram of the situation studied is shown in Figure 1.

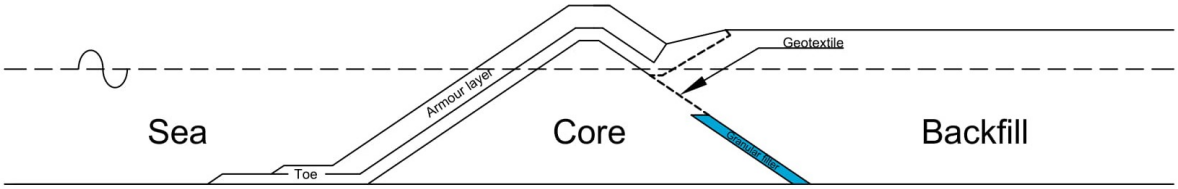

Figure 1: A schematic of the type of land reclamation structures were the filter studied (shown in blue) is used to stabilise the core-backfill interface.

Sea waves breaking on the armour layer cause a cyclic porous flow, that extends into the core and backfill material. This flow transports unsecured backfill material into the core and then into the sea so it is unable to return to the land reclamation. This can lead to unwanted settlements of the surface of the reclamation area. This thesis focuses on stabilising the backfill with a geometrically open, but hydraulically closed granular filter. Geometrically open entails that the base material (Backfill) can physically fit through the pores within the filter material. Hydraulically closed implies that the flow forces are not sufficient to transport the base material. Currently there is little knowledge about the stability of such a filter, especially for an inverted situation where the base material is on top of the filter material.

Multiple base particles can interlock to close pores larger than the base particles themselves are. This mechanism is referred to as arching and provides the strength for an open filter. Factors identified which affect arching are: the effective stress at the base-filter interface, the angularity of the base material and the stability ratio (SR). SR is ratio between the size exceeded by 15% (by mass) of the filter particles and the size exceeded 85% (by mass) of the base particles ($\frac{d_{15,f}}{d_{85,b}}$). The forces due to porous flow are the loading on the base particles, which is quantified by the hydraulic gradient (i). Two principal directions of the hydraulic gradient are defined, parallel ($i_{\parallel}$) and perpendicular ($i_{\perp}$) to this interface.

This study investigates the way the above described factors influence the interface stability of a geometrically open inverted filter. An experimental investigation was conducted using a modification of the set-up designed by Boersma (2020), shown in Figure 2. The current study focuses on the possible stabilising influence of a surcharge on the stability at the filter backfill interface.

This model has three compartments. Hydraulic gradients were generated in the filter structure in compartment B, by changing the water level in compartment A using a plunger. The speed of the plunger was increased until erosion of the base material in compartment B was noticed. This point is defined as the critical hydraulic gradient (i_{crit}). A parallel gradient was achieved by sealing the top of compartment B and a perpendicular gradient could be achieved by sealing compartment C from compartment B. A plate was designed to apply a surcharge on the base material increasing the effective stress at the filter base interface. This plate is permeable to ensure there is no influence on the pore pressures. A numerical model based on the potential flow equation and Darcy's law was programmed to understand the flow within the physical model.

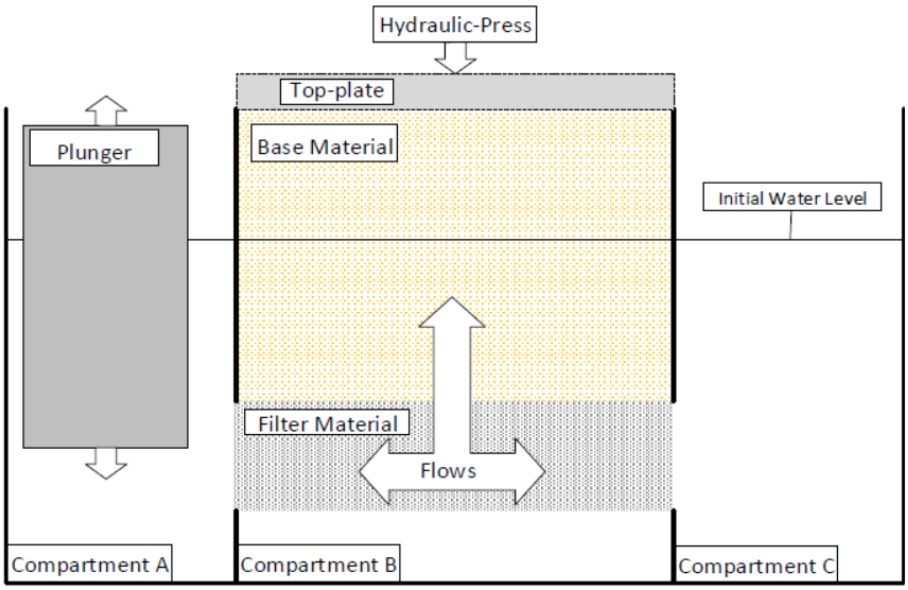

Figure 2: A schematic of the physical model used in this study.

The following results were determined using the models.

- A significant $i_{\perp}$ was observed in all tests in the parallel configuration. This hydraulic gradient is present due to the leaking of the top seal. The top seal leaked in all of the parallel configuration tests throughout the research line. Thus all of the parallel configuration tests throughout the research line are unsuitable for determining the $i_{\parallel,crit}$.
- Analysis of the the distribution of the pressure within the base material using the numerical model, determined that the $i_{\perp}$ is not constant along the filter-base interface for the combined configuration. The maximum value of $i_{\perp}$ which is critical for the stability was found to be located closest to compartment A. The maximum magnitude of the $i_{\perp}$ is four times larger than in the centre of the filter-base interface where it was measured. For the perpendicular configuration the $i_{\perp}$ was uniform across the filter-base interface and usable for determining the $i_{\perp,crit}$.
- It was determined that the $i_{\perp,crit}$ was likely the cause for erosion in all tests performed. The $i_{\perp}$ was also determined to likely be governing for this application.
- A negative correlation was found between SR and $i_{\perp,crit}$, the results were fitted to a hyperbolic function.
- Tests with surcharge have shown that this leads to an increased $i_{\perp,crit}$. With an effective stress of 150 kPa at the filter interface which is equivalent to 7.5m of sand cover, the $i_{\perp,crit}$ doubles, and seems to rise linearly.
- It was found that after erosion had occurred a stable interface could be reformed and as such design for the single largest wave is not necessary.
- No definitive conclusions could be formed about the influence of the angularity of the base material, as the more angular material tested seemed to have a lower critical gradient.

The results were applied to a case study of a typical rubble mound land reclamation, as formulated by Van de Ven (2019) and shown in Figure 1. Van de Ven (2019) determined the hydraulic gradients present in the filter-backfill interface. These hydraulic gradients present in the case study were compared to the results of the current study. From this comparison the main conclusion of this study could be made. This is as follows: *Under certain conditions a geometrically open, but hydraulically closed filter can be applied to prevent the erosion of backfill material from a rubble mound land reclamation structure.*

Contents

1

Problem Description and Analysis

1.1. Context

Coastal areas have 40% of the world's population and most of the rapidly growing mega-cities (Creel, 2003). Within many of these cities, there is a shortage of land area. In the Netherlands sea levels are expected to rise by up to 80cm by 2100 (Koninklijk Nederlands Meteorologisch Instituut, 2021). This further reduces the available land for expansion, making land reclamation and flood defences vitally important.

A widely used method for land reclamation consists of a rubble mound breakwater, of which the inner core interface is lined with a geotextile. The reclaimed land is raised with a backfill consisting of sand. The rubble mound breakwater can provide effective protection against hydraulic loads. Sand is a suitable material for use as a fill. It compacts easily, is easily transported and is widely available. The interface between sand and the quarry run core of a breakwater is not stable, hydraulic loads can travel through the permeable core of the breakwater eroding the sand through the breakwater. This can cause excessive settlements of the reclaimed land. A geotextile secures this interface preventing erosion.

This is a highly effective method but has one major drawback. The geotextile core-backfill interface is not only difficult and thus expensive to place, but it also introduces a man-made material into the natural environment. This study investigates the possibilities of replacing the geotextile with a filter constructed of gravel, a so-called granular filter. This will be easier to construct and therefore more cost-effective.

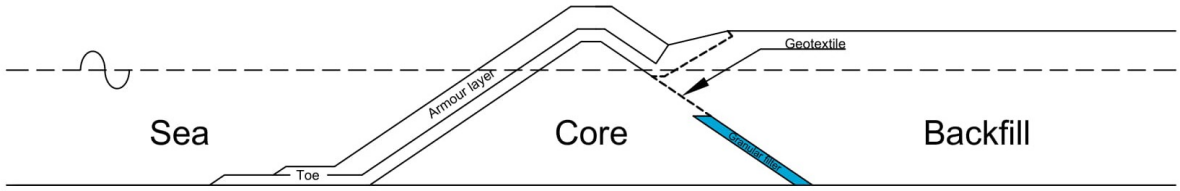

Figure 1.1: Cross-section of a rubble mound land reclamation with a granular filter securing the core-backfill interface.

Filters The function of the filter in this construction is to protect the sand against erosion through the core of the breakwater while allowing water to pass through (Schiereck and Verhagen, 2019). A granular filter is examined in this study, which just requires a layer of gravel. This also ensures no foreign materials are placed deep underground which will need removal in the decommissioning stage of a project.

Classification of Granular Filters Granular filters can be classified into three types depending on the mechanism of protection. There are filters where the largest particles of the sand (referred to as the

base material) are unable to fit through the pores between particles in the filter layer, thus preventing the loss of material. These filters are called geometrically closed and require precise placement of multiple layers of filter material with decreasing grain size. This is a complicated process.

A geometrically open filter requires fewer layers and is therefore attractive. A geometrically open filter can be made hydraulically closed. This means that even though the base particle could physically pass through the filter layer, the hydraulic loads remain below a threshold value where the base material starts to erode. This is defined as the critical hydraulic gradient for the filter. The strength of such a filter is due to the so-called arching of the base material.

If the hydraulic loads exceed the threshold this results in a hydraulically open filter. This means that some erosion of sand will occur. A filter can be designed to be hydraulically open above the design conditions only if it is able to restore a stable condition if the hydraulic leads decrease again

Arching of Base Material Arching of the base material is the mechanism that leads to the strength of an open filter. This is when multiple base particles interlock to close off the pores within the filter material leading to a stable interface.
Arching is influenced by the following Parameters:

- **Stability Ratio** The stability ratio describes the relative size of the base particles that need to form an arch to the size of the pores that need to be arched across.
- **Effective stress at the filter-base interface** The effective stress affects the friction between the base particles in an arch.
- **Angularity of Base Material** The angularity of the base material also influences the friction between the base particles in an arch.

Geometrically Open Hydraulically Closed Filter in a Rubble Mound Land Reclamation In this thesis, a geometrically open filter at the interface between the core of the rubble mound of the breakwater and the sand backfill of the land reclamation will be studied. This filter has characteristics that distinguish it from similar filters in different settings. These are the following:

- The filter construction is inverted, in traditional filters, the base material is located below the filter material. In this case, it is inverted with the base material above the filter material.
- This filter layer is located underground, which leads to an increased superposed load on the filter.
- The filter-base interface is at an incline compared to the traditional horizontal.
- The loading is a cyclic combination of parallel and perpendicular hydraulic gradients.

1.2. Research Line

Three previous studies have analysed this core back-fill interface as an MSc thesis at the TU Delft.
The initial study by Tutein Nolthenius (2018) used a scale model to investigate the effect of the removal of the geotextile at the landward side of the breakwater core. When a conventional particle size ratio was used between the back-fill and the core material, there was a significant amount of sand penetrating into the core of the breakwater. As such, it was concluded that the removal of the geotextile is not an option. Reducing the stability ratio of the interface lead to promising results. This lead to the conclusion that replacing the geotextile with an open filter could be an attractive solution.

Continuing on this research Van de Ven (2019) developed a numerical model in OpenFOAM of a rubble mound breakwater protecting a sand land reclamation. This model was used to determine the order of magnitude of the hydraulic gradient in the filter layer at the rear side of the breakwater. An initial experimental setup was designed and then used to test five different filter-base combinations to determine parallel and perpendicular critical gradients.

Boersma (2020) carried out further tests using the same experimental setup. The tests were expanded to different stability ratios and also included tests where a combination of parallel and perpendicular gradients was applied. It was discovered that initial saturation of sand in the filter layer lead to base material being present at the bottom of the model at a lower hydraulic gradient. It is unclear whether this is due to a reduced critical hydraulic gradient or that this is purely the sand that was initially

present in the filter layer being washed out. A new experimental set-up (see Figure 1.2) at a larger scale was also developed which allows for tests with a surcharge and/or under an angle. This setup will be used for the research in the current study.

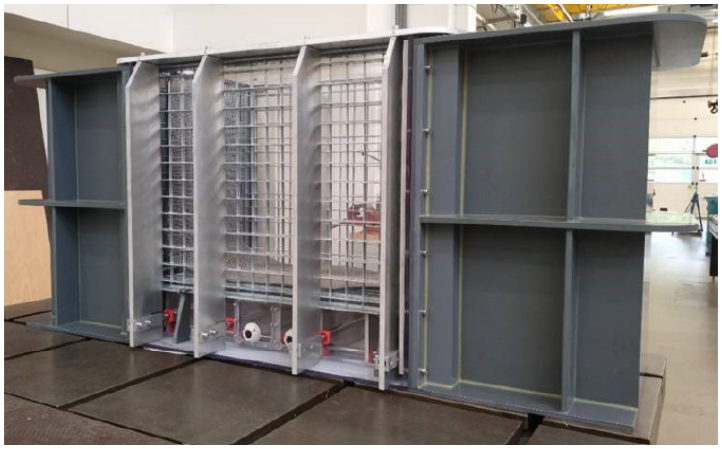

Figure 1.2: Experimental setup designed by Boersma (2020)

1.3. Problem Statement

This research line has produced a number of interesting results. However, there is still a knowledge gap about certain aspects of an open inverted filter. The aspects which need further investigating are:

- The influence of the effective stress at the filter-base interface on the critical hydraulic gradient is unknown.
- The influence of the angularity of the base material on the critical hydraulic gradient is unknown.
- There is limited knowledge about critical perpendicular hydraulic gradients.
- There is a limited understanding of the porous flow within the experimental setup.

1.4. Objective

The objective of this study is to extend the knowledge on the sand retention ability of an inverted geometrically open granular filter layer. This will enable the practical use of these filters. This is presented in the following research question:

"Is an inverted geometrically open granular filter, able to retain the sand backfill in a rubble mound land reclamation with cyclic hydraulic gradients due to wave loading?"

This question will be analysed with the following sub-questions:

1. What is the influence of the model configuration on the spatial distribution of the hydraulic gradient within the base layer in the experimental setup.
2. What is the influence of increased effective stress in the filter base interface on the critical hydraulic gradient in an inverted geometrically open filter layer?
3. How does the stability ratio influence the critical hydraulic gradient?
4. Does the first instance of erosion influence the sand retention ability at lower hydraulic gradients?
5. Does the combination of perpendicular and parallel hydraulic gradients influence the critical hydraulic gradient?
6. Does the angularity of the base material influence the critical hydraulic gradient?

1.5. Hypothesis

It is expected that a stable situation can be found for certain combinations of stability ratio and hydraulic load.

It is expected that increased effective stress will increase the strength of the arches. Therefore higher critical hydraulic gradients are expected for all load cases.

Higher stability ratios mean larger arches are required. Larger arches are easier to break. Therefore this is expected to lead to lower critical hydraulic gradients.

It is expected that like many granular filters there is a healing effect that allows arches to reform after damage.

The combination of a parallel and perpendicular gradient will likely increase the force on a particle and thus likely reduce the critical gradient.

The increased angularity of the base material will likely increase the critical hydraulic gradient as this increases the strength of the arches. This effect should be magnified with higher surcharges.

1.6. Conventions Used

The same axis system used by Van de Ven (2019) and Boersma (2020) is used in this study. The perpendicular hydraulic gradient is perpendicular to the filter-base interface and is significant only in the base material. The parallel hydraulic gradient is parallel to the filter-base interface and located in both the filter material and base material. The positive directions are shown in Figure 1.3.

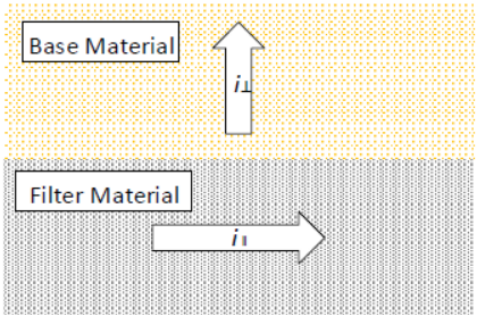

Figure 1.3: The positive direction of the perpendicular hydraulic gradient ($i_\perp$) and the parallel hydraulic gradient ($i_\parallel$) as defined in this study.

1.7. Structure of Document

The findings of this study are presented in this report in the order that the study was performed. First, a literature review presents the current state of knowledge on open inverted filters and explains key concepts which are relevant to this study (Chapter 2). Next, the physical modelling setup used to determine the critical gradients is described (Chapter 3). The numerical model used to calculate the flow within the physical model is then explained (Chapter 4). Following that the flow and hydraulic gradients present in the experimental setup are analysed (Chapter 5). The results of the tests to determine the critical gradients are presented (Chapter 6). These results are then discussed (Chapter 7). After which conclusions and recommendations are made (Chapter 8).

2

Literature Study

This chapter addresses the theoretical background and previous research into filter constructions. In general, when designing a construction the strength must be larger than the load. This also applies to open inverted filters. These properties are explained first. The strength of a filter is determined by the properties of the granular material. The loads on the filter are due to the porous flow through the granular material. This is explained next. When the load exceeds the strength erosion occurs. This is addressed next. After this, the current level of knowledge on preventing erosion with a granular filter is summarised. Arching is then examined in more detail as this is a key mechanism for the strength of an open filter. Finally, the key conclusions from the literature review will be summarised.

2.1. Properties of Granular Materials

Gravel and sand which make up the filter and base materials are granular materials. Within a granular material, the grains independently have properties and the material as a whole has properties. Both of these will be discussed in this section.

2.1.1. Grain Size

The size of particles is commonly defined by their diameter (d). In some cases, the diameter is not known or unpractical to measure. If the mass is known a nominal diameter (d_n) can be calculated, based on the shape and mass of the particles. The median nominal diameter and median diameter can be related to each other using the shape factor (F_s). This is commonly between 0.7 and 0.9 (Verhagen and Jansen, 2014).

$$d_{n,50} = F_s \cdot d_{50} \tag{2.1}$$

Sand particles have a diameter between 0.063mm and 2mm and gravel has a diameter between 2mm and 63mm. If the size of all the particles (or a representative selection) in a mixture is measured, it is possible to plot a cumulative grain size distribution (CSD). From the grain size distributions, it is possible to determine what type of grading it is. Sand with all similar size particles has a uniform or narrow grading. When there is a large difference between the large and small particles this is a wide grading. A wide grading where all intermediate particle sizes are represented is considered a well-graded soil. If intermediate particle sizes are missing it is a gap-graded sand. The Rock Manual (van Gent et al., 2017) defines the following definitions for gradings:

Grading Classification	$d_{85}/\ d_{15}$
Narrow	≤ 1.5
Wide	1.5 - 2.5
Very Wide	2.5 - 5

Table 2.1: Grading widths according to CIRIA et al. (2007).

2.1.2. Bulk Properties of Granular Materials

Granular materials consist of particles surrounded by air and water. There are standard parameters that describe the material as a whole, these are bulk properties.

Porosity Porosity (n) describes the ratio between the volume of the pores and the total volume. This is defined as follows:

$$n = \frac{V_p}{V} \tag{2.2}$$

The porosity is dependant on the parameters of the particles such as the grain size distribution and shape of the particles. In a wider graded material, the relative difference in size allows smaller particles to fit in the voids between larger particles. It is also dependent on the placement of the particles. Particles that are loosely packed have more space between them and thus a higher porosity (Verruijt and Broere, 2011).

Saturation The saturation of a soil describes the amount of water in the pores. If the saturation and the density of the particles and water is known we can calculate the total density.

Angularity Sand particles can be rounded or have sharp edges, a particle with sharp edges is considered angular while a particle with rounded edges is rounded. A classification scale to describe the angularity was developed by Powers (1953). It is also possible to determine the angularity based on the porosity in a loose state (ASTM, 2017). More angular materials have a higher porosity in a loose state. The angle of repose of a material is the angle of a natural slope, this depends among other things on the angularity, the fall height and the water content of a material (Van Burkalow, 1945). As such the angle of repose could also be used to determine the angularity.

The most reliable method to determine the angularity of a granular material is through visual observation (Muszynski and Vitton, 2012). As such in this study, a visual observation will be used to determine the angularity of the materials.

Permeability The permeability of soil is mostly determined by the size of the smallest particles in the granular material. Two common formulas to determine permeability are the Hazen (2013) formula and the Carman (1938); Kozeny (1927) formula. The Hanzen formula is based on uniformly graded filters and thus only suitable for this application whilst, the Kozeny-Carman Formula has wider applicability but requires more parameters of the soil than just the d_{10} (Carrier III, 2003). The current study will focus on uniformly graded filter material and thus the Hazen formula is suitable for use.

2.1.3. Stresses

Stresses in granular materials are built up of two components. These are pore pressures and effective stresses. Pore pressures are the stress in the fluid between the particles. This is a pressure and thus acts equally in all directions. The remaining stresses are at the interfaces between grains and are referred to as 'effective stresses'. The difference between vertical and horizontal stresses, and shear stresses are a result of effective stress (Terzaghi, 1948).

2.1.4. Strength

Granular materials have limited contact interfaces where the grains touch each other. When a compressive load is applied, this results in normal stresses at the contact interfaces (Figure 2.1a). This is a strong configuration and will fail when the grains themselves fail. The stresses required for this are orders of magnitude larger than relevant in this study. When a tensile-load is applied there is nothing preventing the grains from being pulled apart (Figure 2.1b), as such there is no tensile strength. When a shear-load is applied this results in shear stresses at the particle interfaces (Figure 2.1c). These shear stresses depend on the friction between particles at the interfaces. The maximum amount of friction depends on the roughness or angularity of the particles and the normal stresses between these particles. Exceeding the friction available will cause particles to slip with respect to each other, this is the defining failure mode for granular materials (Verruijt and Broere, 2011).

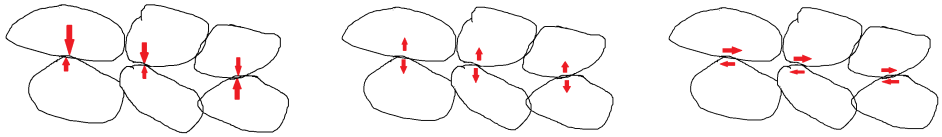

(a) Particles in compression. (b) Particles in tension. (c) Particles in shear.

Figure 2.1: Interface forces in a granular material.

The most basic model that can describe the shear strength of a soil is the Couloumb critical shear stress (τ_f), defined in equation 2.3. In this model an analogy is made between a block on an inclined plane (Verruijt and Broere, 2011).

$$\tau_f = c + \sigma' \tan \phi \tag{2.3}$$

The first term is the cohesion (c), in granular materials with little to no fines this is negligible as such this term will be set to zero Lambe and Whitman (1991). The second term represents the friction, this term depends on the normal effective stress (σ') and the internal angle of friction (ϕ). The normal effective stress is the normal stress between the interfaces of particles averaged over an area. The internal angle of friction is used to represent the roughness of the particles. For sands, this is typically between 27° and 35°, and for gravel typical values are between 30° and 37.5° (NEN, 2017).

2.2. Flow in Porous Media

This section describes the flow process in a porous medium. First, the principles of the flow are explained from the mechanics. Second, the specifics of the flow in the studied application of the filter are presented.

2.2.1. Fluid Mechanics

The Navier-Stokes equation can describe all different forms of flow. For example sea waves, tides and river flow. If the location of all pores and participles is known and taken into account this is will work for flow though a porous medium. This is not a practical approach. It is possible to average the velocity over both the pores and the particles, the resultant average velocity is defined as the filter velocity (u_f). When written in terms filter velocity three terms are used to represent the Navier-Stokes equations. It is common to combine all linear terms with a linear friction term. This is largely dependant on the laminar flow resistance. The quadratic terms are combined in a quadratic friction term, largely dependant on turbulence. This results in the classic Forchheimer-equation, which is applicable for steady flow. For oscillatory flow this equation can further be extended which results in the extended Forchheimer-equation. For this the additional inertial term is required (Schiereck and Verhagen, 2019).

$$\frac{1}{\rho_w g}\frac{\partial p}{\partial x} = i = a u_f + b u_f |u_f| + c\frac{\partial u_f}{\partial t}$$

(2.4)

The left hand side of this equation is equal to the hydraulic gradient (i). Values for the coefficients (a , b and c) where summarised by Van Gent (1995). Terms in this equation can be neglected depending on the size of the particles and flow velocities involved. This is described by two dimensionless numbers the Reynolds number and the Keulegan–Carpenter number. The Reynolds number determines the relative influence of turbulence and laminar resistance on the flow. The Keulegan-Carpenter (KC) number represents the relative influence of inertial and laminar resistance (Van Gent, 1995).

In cases where the laminar resistance is dominant, the Forchheimer equation reduces to:

$$q = -ki \tag{2.5}$$

This equation is known as Darcy's law and k is equal to the inverse of $-a$ in Equation 2.2.1.

2.2.2. Specifics of Flow Through Breakwater

Polidoro et al. (2015) studied the propagation of flow through a breakwater used in a rubble mound land reclamation. The situation studied is shown in Figure 2.2.

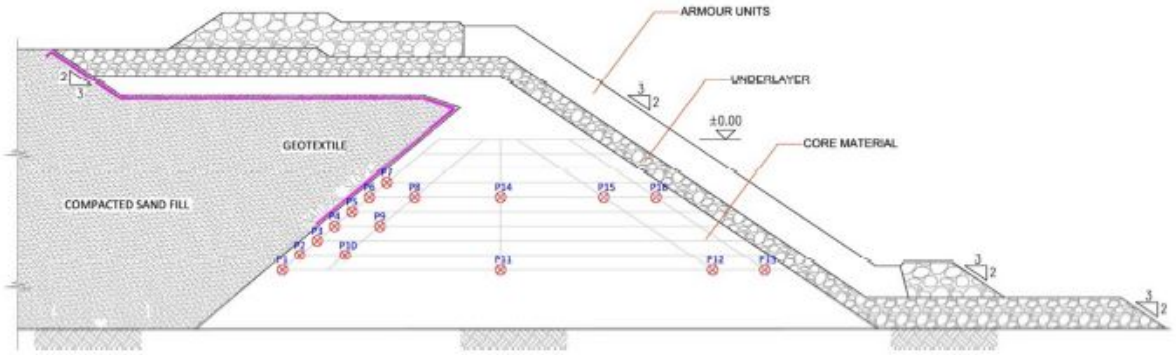

Figure 2.2: Situation studied by Polidoro et al. (2015).

For this specific situation, the hydraulic gradient in the breakwater core was determined. It was found that the hydraulic gradient at the end of the geotextile did not exceed 0.03 in 98% of the peaks. However the hydraulic gradient in the backfill was not determined. The perpendicular component of the hydraulic gradient is significantly larger in the less permeable backfill material. The gradient in the backfill needs to be known to design an open filter for this interface.

Van de Ven (2019) developed a numerical model for a similar land reclamation in OpenFOAM. This land reclamation has both an open granular filter and a textile. The situation modelled is shown in Figure 2.3.

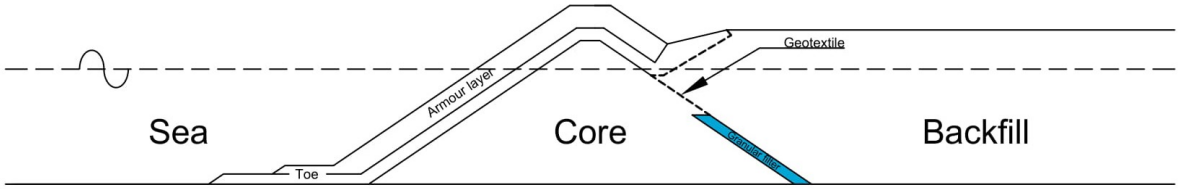

Figure 2.3: Land reclamation modelled by Van de Ven (2019).

Using this model the magnitude of the parallel and perpendicular hydraulic gradients in the backfill at the rear of the breakwater were determined. These are presented in Figure 2.4.

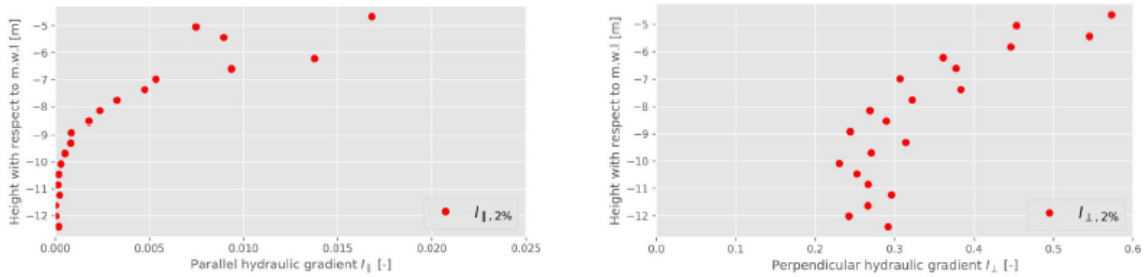

Figure 2.4: Gradients at rear of breakwater as determined by Van de Ven (2019).

The hydraulic gradients shown above are in the backfill thus are governing for the stability of the filter backfill interface.

Other Hydraulic Loads Storm surge set up or heavy rainfall lead to an increased groundwater level (Wilson et al., 2011). This may lead to constant flow out of the land reclamation into the breakwater

core. This needs to be considered in combination with the cyclic loading due to waves determined by Van de Ven (2019).

2.3. Erosion of Material

Erosion occurs when there is an inbalance of forces allowing a particle to move. The forces acting on a particle are from the flow of water, contact with other particles or due to gravity. A particle within a layer has other particles surrounding it, all the surrounding particles exert normal forces preventing the particle from moving. At the edge of a layer (e.g. a river or sea bed) or at the interface of two layers of different sizes, a particle is not fully surrounded by other particles. If the forces due to flow become high enough the particle will erode.

2.3.1. Erosion from a Bed

Erosion of material from the surface of a cohesionless material has been well studied. A relation between the velocity of the flow and the size of the particles to determine the first movement of particles was determined by Izbash (Schiereck and Verhagen, 2019). Another approach was used by Shields, in this a shear velocity at was calculated at the bed (Shields, 1936). This was then related to movement of the particles in a diagram presented in Figure 2.5. It should be noted that the critical shields parameter corresponds to the continuous movement of grains at all locations.

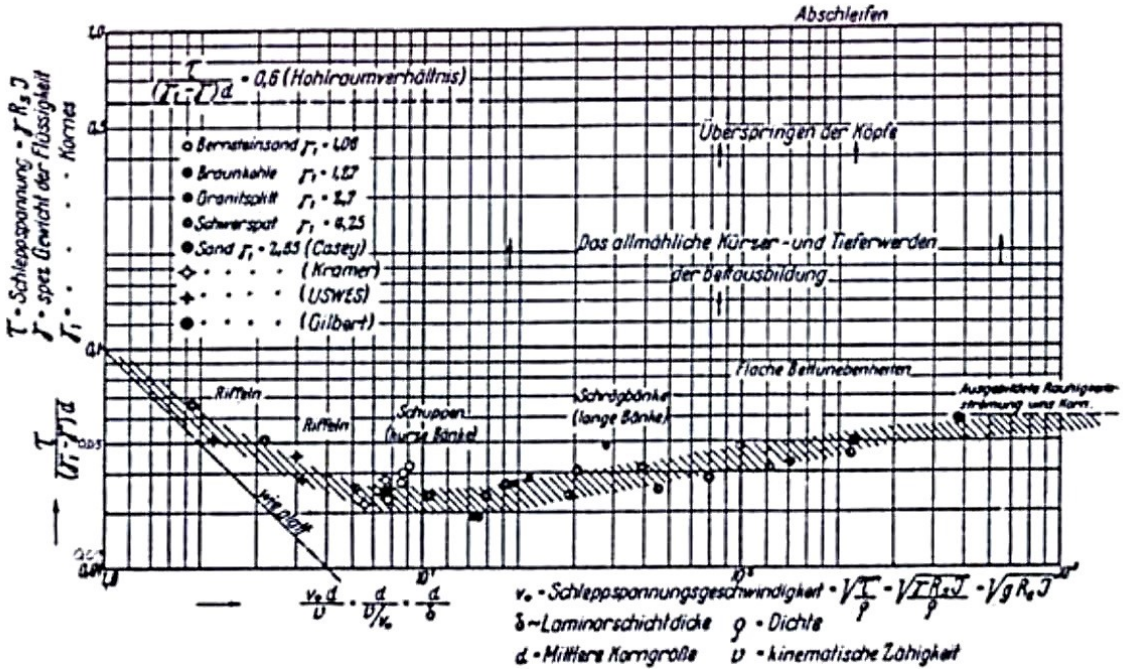

Figure 2.5: The relation between the critical bed shear stress and Shields parameter from Shields (1936)

Liu and Chiew (2012) studied erosion of a sand bed and determined that seepage can have an effect on the critical critical shear stress. Seepage into the sand has a stabilising effect, while seepage out of the sand has a destabilising effect. Another phenomenon that has been observed in the erosion of sand beds is the armouring effect. This is when the finer particles are eroded out of a material, which leaves a stable layer of coarser particles (James et al., 2010).

2.3.2. Erosion within a Granular Material

The hydraulic forces in a granular material are the main loading on the filter which can break the arches. There are two main types of hydraulic loads on a particle within a granular material, these are the hydrostatic forces and the forces due to flow. Two force components are most significant within a granular filter. The force due to a different pressure on both sides of a particle and the drag force due to the flow around a particle (Nguyen et al., 2013). The difference in pressure is represented by the hydraulic gradient and the flow velocity depends on the permeability of the soil and the hydraulic gradient.

2.4. Granular Filters

This section highlights the current state of research on filters. The majority of this research is based on filters with a traditional configuration where the filter material is located on top of the base material. This is a key difference meaning that the findings by these studies cannot be applied directly however the concepts and mechanisms behind the functioning of these filters is highly similar. Geometrically open and and geometrically closed filters will be addressed separately.

2.4.1. Load Cases

There are four different base load cases of flow direction as defined by De Graauw et al. (1984). These are either parallel flow or perpendicular flow and either cyclic or steady flow. These load cases are shown in Figure 2.6.

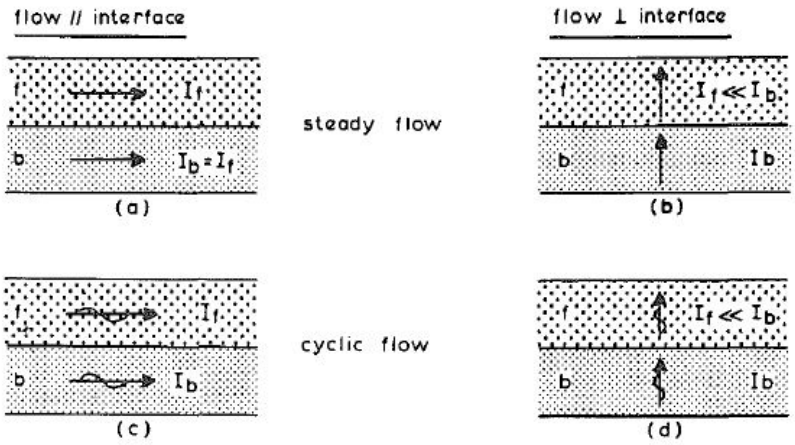

Figure 2.6: The four base load cases as defined by De Graauw et al. (1984).

2.4.2. Closed Granular filters

Geometrically closed granular filters are based on the idea that the particles in the base layer are not physically able to go through the gaps in the filter layer. These designs are generally based on the stability ratio (SR):

$$SR = \frac{d_{f15}}{d_{b85}} \tag{2.6}$$

In which d_f15 is the diameter of the filter of which 15% of the particles by mass are smaller. d_{b85} is the size where 85% of the base particles by mass are smaller. Various different authors determined design criteria based on the ratio. The coefficient of uniformity is defined as follows.

$$C_U = \frac{d_{60}}{d_{10}} \tag{2.7}$$

Terzaghi (1948) specified that the stability ratio must be below 4, this is valid for materials with a C_U below 2. The US Army Corps of Engineers (1984) accepts an SR of 5 for a C_U below 10. The Rock Manual uses a SR of 5 with a $C_U \leq 10$ (CIRIA et al., 2007). Differences in the coefficient of uniformity have been included the guidelines developed by Ziems (1969) (from (Heibaum, 2004)). In this the

design graph presented in Figure 2.7a was produced.Heerten and Wittmann (1985) compared these filter guidelines to that of Terzaghi. This is shown in Figure 2.7b.

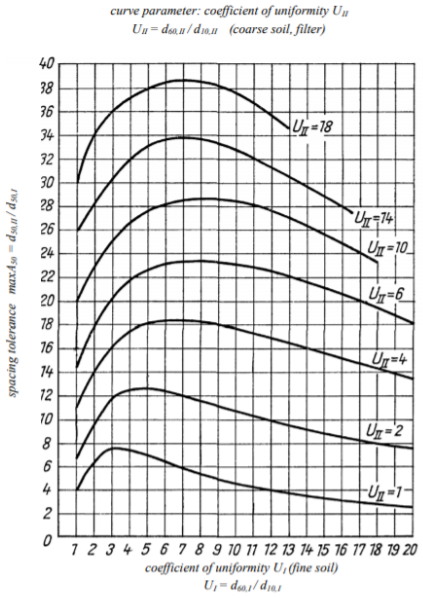

(a) Filter guidelines developed by Ziems (1969)

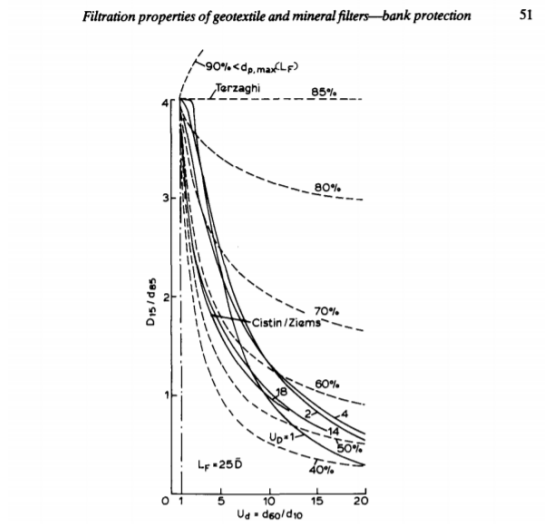

(b) Filter guidelines developed by Ziems (1969) compared to Terzaghi (1948) by Heerten and Wittmann (1985)

Figure 2.7: Influence of the width of a grading on the stability of a filter.

The failure of a filter with an uniform soil is a sudden destabilisation however in wide graded soil, failure occurs along with a change in permeability. This happens as the fine particles are washed out and is more difficult to predict Sugii et al. (2016). From this the conclusion can be made that a narrow graded filter has a more predictable failure and thus is better to study. Furthermore for the studying of an open filter the stability ratio should be at least 5.

2.4.3. Open Granular Filters

An open filter is designed to work within specific hydraulic conditions. Research about the stability of the filter in specific cases has been been done by various authors (Belyashevskii et al., 1972; De Graauw et al., 1984; Schürenkamp et al., 2016).

De Graauw et al. (1984) tested perpendicular and parallel hydraulic gradients separately. These tests were done in both unidirectional flow and cyclic flow. In all of these tests the filter material was placed above the base material. All tests show a decreased critical gradient for an increased stability ratio. These tests also showed an effect of the particle size of the base material. Smaller particles with the same stability ratio would lead to a higher critical gradient. This is likely due to higher flow velocities within the more permeable coarser material. Boersma (2020) however found no significant difference between two different particle sizes at the same stability ratio.

Wave Loading van Gent and Wolters (2015) investigated the wave loading of rock slope with an open filter underlayer. Accepting minimal transport of sediment it is possible to construct a filter with a significantly reduced cost compared to traditional geometrically closed filters. In van Gent et al. (2017) the hydraulic gradients in the filter layer where calculated. It was found that in areas of erosion a net outward hydraulic gradient was present. Further studies on the effect of storm duration and the effect of oblique waves found that after 25000 waves a stable condition was reached. An increased angle of the waves lead to a reduced amount of erosion (van Gent and Wolters, 2018).

Parallel Loading For parallel flow De Graauw et al. (1984) noted initial differences in the critical hydraulic gradient between cyclic flow and unidirectional flow tests. For cyclic flow there was an initial compaction of the filter material. This compaction lead to an increase in critical hydraulic gradient so that after some time the critical hydraulic gradient is equal for both steady and oscillating flow.

Wörman (1989) determined that is was possible to protect the sand around a bridge pier using only a thicker armour layer and removing the standard filter layer. In many cases this layer was thinner than the combination of an amour layer and geometrically closed filter layers. Further research by Bakker et al. (1994) resulted in guidelines for replacing the geometrically closed filters beneath the armour layer with a single geometrically open filter layer. A further optimisation was carried out. The design guidelines were optimised so that there will be a simultaneous erosion of all layers (Verheij et al., 2012).

Perpendicular loading For perpendicular flow De Graauw et al. (1984) noticed there was always a critical gradient present no matter the stability ratio. This is due to the fact that the filter layer is located above the base layer and sand must be transported upwards against gravity. This is a crucial difference with this current research as gravity now counteracts the stability of the sand. As such it would not be expected that there is a minimum hydraulic gradient.

De Graauw et al. (1984) also observed that there was decrease in critical gradient for an oscillating flow compared to an unidirectional flow. This matches with the experience of Schürenkamp et al. (2016) in this study the hydraulic gradients that were stable with unidirectional flow lead to continuous settlement of the top with an oscillating flow. The reason for this difference is that arching is presumed to be the main mechanism preventing erosion in an open filter with unidirectional flow. Oscillating flow could disrupt these arches more easily leading to a reduced critical gradient.

Belyashevskii et al. (1972) and Schürenkamp et al. (2016) performed tests remaining at the the same hydraulic gradient at which erosion was detected. These tests showed that for some cases near to the critical gradient there was initial erosion of the base material, this however stabilised after some time and no further erosion occurred. In other cases however there was still continuous erosion of the base material with the same hydraulic gradient.

Combined Loading In the research by De Graauw et al. (1984) also unidirectional flow tests were performed where the two directions of hydraulic gradients were combined. In this it was found that the presence of an additional hydraulic gradient in another direct did not have significant effect until both hydraulic gradients are close to their respective critical values. Furthermore it was found that the critical perpendicular hydraulic gradient is approximately twice as large as the critical parallel hydraulic gradient.

Filter Thickness The length a particle must travel through a filter has influence on the ability of the filter to function. This effect however diminishes asymptotically with increasing filter length. With filters thicker than 100 times the d_{f50} the effect of increasing the thickness further are negligible (Wittmann et al., 1980) (from (Heerten and Wittmann, 1985)).

Boersma (2020) tested two filters of different thicknesses: $25d_{f50}$ and $50d_{f50}$. Similar critical hydraulic gradients were found.

Chew et al. (2003) investigated the effect of holes in geotextile filter. It was found that it is possible to retain sand when there is an open filter ratio between the base and filter material if the holes in the geotextile do not become to large.

2.4.4. Open Inverted Filters

This section will summarise the relevant research into open inverted filters.

Combined Flow Boersma (2020) also investigated the effect of combining the flow patterns for an inverted filter. These were oscillating flow tests where the amplitude of both the the perpendicular and parallel gradient where increased. With these tests a lower critical gradient parallel gradient was found when compared to the parallel tests. No perpendicular tests were performed therefore the influence of additional parallel flow on the critical perpendicular hydraulic gradient could not be determined.

Van de Ven (2019) however carried out a perpendicular test with a similar stability ratio to one of these tests using the same physical model. For these tests the critical perpendicular gradients were similar to the perpendicular hydraulic gradients in the combined tests by Boersma (2020). Thus it could be that combining the flow directions reduces the critical gradient, however it also be that the combined tests failed due a governing perpendicular hydraulic gradient.

Application to Rubble Mound Land Reclamation Allsop and Williams (1991) determined a critical perpendicular hydraulic gradient for a internally unstable material. This was determined using experiments with unidirectional upward flow. This critical gradient was then applied to determine that a core-backfill interface could be stable. The hydraulic gradients in the core were used (Polidoro et al., 2015). However the hydraulic gradients in the backfill which will likely be governing were not determined or taken into account.

2.4.5. Surcharge

The effect of surcharge on a filter construction has also been investigated. A surcharge leads to an increased effective stress in the filter layer. De Graauw et al. (1984) tested the effect of this on an unidirectional perpendicular flow. Arching was found to be present between when the size ratio is upto six times larger than the criteria for a closed. This is upto a stability ratio of 30. It was noted that for stability ratios in which arching was believed to be present, there was an up to 8 fold increase in critical perpendicular hydraulic gradient due to the increased effective stress.
In a study of punctured geotextiles it was found that an increase of surcharge from 0 to 25kPa lead to a significant increase instability, however a further increase to 100kPa lead to no further increase in stability (Chew et al., 2003). From this appears there may be an upper limit to the benefit of superimposed load.

2.4.6. Constriction Based Design

Within the literature there is also a different approach to filter design. This is not based on stability ratio but on a calculation of the constriction sizes in filter material. This works as follows. For erosion to occur the base material must travel through between the pores in the filter material. The narrowest point between two voids is considered a constriction, particles that are eroded must pass through this. The size of these constrictions is dependent on the particle size distribution, particle shape and relative density of the filter layer.

In traditional filter design guidelines are based on the ratios between specific particle sizes in the base and filter material. Sjah and Vincens (2013) suggest that the cumulative constriction size distribution of the filter layer and particle size distribution of the base layer determine if a filter layer can be successful. Raut and Indraratna (2008) suggest the use of a constriction based design criteria has more physical significance than a particle sized based criteria.

Constriction Size Distribution The constriction sizes within a material can be determined based on inscribed circles. This is based on round particles and the constriction size is determined for each particle size. Three touching particles is the densest configuration and four is the loosest. The constriction size distribution can then be determined based on the particle size distribution for the both states. The a weighed average is then determined based on the relative density of the soil.

Indraratna et al. (2007) present a design criteria based on the constrictions of a filter material and the particle sizes of the base material. Locke et al. (2001) developed an analytical method to determine the time dependent erosion of base material into a filter. The resulting movement of particles into the layer create a new layer at the interface where the particles of the base and filter layer mix, the model predicts if the resulting filter is stable. These considerations result in the following design criteria proposed by Raut and Indraratna (2008):

$$\frac{d_{f;c35}}{d_{b;sa85}} \leq 1 \tag{2.8}$$

The $d_{f;c35}$ is the constriction size not exceeded by 35% of the constrictions in the filter material. $d_{b;sa85}$ is the particle size not exceeded by 85% of the particles of the base material when ordered by surface area. From this we can conclude that relative density and angularity of the base material are elements not considered in traditional filter design which may be of influence.

Computational Modelling of Constrictions Various authors have developed finite element method and computational fluid dynamics based numerical models to simulate base material passing through the constrictions in a filter (Abdelhamid and El Shamy, 2016; Hu et al., 2019; Nguyen et al., 2013). With this model many granular filters have been analysed. These studies determined that the most

significant loading forces due to flow on a base particle are the hydrostatic pressure difference and the drag force.

Relevance of this Approach These approaches are highly detailed and takes into account many more parameters than is traditionally done. This makes this method more cumbersome than normal. The improved accuracy of the method is predominately when using widely graded materials. As this study uses narrow graded filters the benefits are minimal. Therefore this guideline will not be evaluated further in this study.

2.5. Arching

An arch is a shape where a distributed load can be transferred to two supports with an optimum use of material. This shape has been used in construction for thousands of years from use in ancient Roman aqueducts to the use in modern bridges (Editors of Encyclopaedia Britannica, 2008). An investigation into the loads on buried pipelines after collapses in the United States in the early 1900s lead to discovery that the soil pressure my be less than the weight of the soil above. This was attributed to transfer of the load to the sides by arching within the soil (McKelvey, 1994).

2.5.1. Relevance for Open Filters

Arching is relevant for open filter design as this is thought to be the main mechanism providing resistance against erosion of the base material. Within an open filter arching is when multiple base particles interlock to close off the pores within the filter material leading to a stable interface.

2.5.2. Soil Mechanics

This effect was first investigated in granular materials by Terzaghi. Tests where performed where a trapdoor located at the bottom of a box filled with sand was lowered. Lowering the trapdoor resulted in a reduced soil pressure on the trapdoor. The results of this setup are shown in Figure 2.8b.

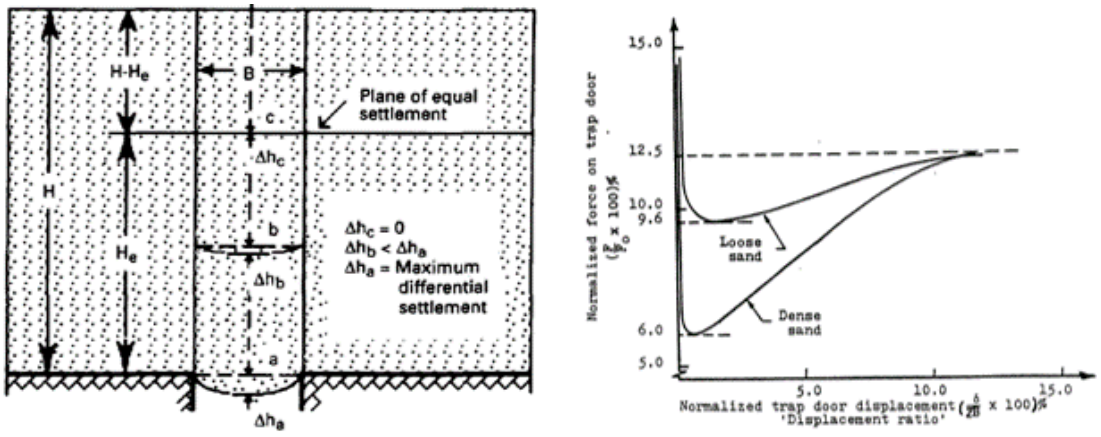

(a) Geometry of arching within soil from McKelvey (1994)

(b) Influence of soil state on ability to form arches Terzaghi (1948)

Figure 2.8: Trapdoor tests by Terzaghi (1948)

At the initial displacement (Lowering the trapdoor 1% of it's width.) this was less than 10% of the initial pressure. This reduction is dependant on soil state and can be seen in Figure 2.8b. At displacements of 10% of the width of the trapdoor or greater a constant pressure of 12.5% of the initial pressure was achieved (Terzaghi, 1936). This reduced pressure on the trapdoor is caused by a temporary arrangement of the particles due to the yielding based displacement of the soil above the trapdoor. This leads to increased shear stresses (Tien, 1996). These induced shear stresses rotate the principle stress to form an arch. This effect extends a height of 2.5 times the width of the trapdoor up into the soil. Shown as the plane of equal settlement in Figure 2.8a. The sand located above this is unaffected (Terzaghi, 1948). In cohesionless soil the arch very rarely caries the full load of the above soil, there is most often the formation of an inverted arch, which must be partially supported to be stable McKelvey (1994).

2.5.3. Influence of the Flow of Water

In the petroleum industry the amount of sand extracted alongside oil is dependent on the strength of the arching. In this context arching combined with outward flow has been extensively studied. Relevant results will be presented below.

Bratli et al. (1981) studied a sand filled container with a single hole at the bottom. The amount of downward flow and superimposed load were varied and the sand flowing out of the container was measured. First based on a theoretical approach using the Mohr-Coulomnb failure criteria two failure modes of the sand arches where identified. These two failure modes are either a collapse of an inner arch, or the total collapse of the arching system. These findings where later validated with experiments. Flow rates were increased until a small volume of sand left the container. This was the collapse of an inner arch. The new arch formed after the collapse of an inner arch was found to be stable up to a higher flow rate. Flow rates could be varied down to zero and up to the past maximum and continued for several hours without effect on the stability of the new arch. In sands the total collapse mode of failure occurred when arching zone encounters a physical constraint the top of the sand layer or an adjacent arch.

(Miller, 1994) also investigated the effect arching with similar tests. In this case it was found that increased effective stress in the sand, increased the flow rate required to break the arches, this increase continued with further increase of the effective stress until grain crushing occurred. This is in contrast with the results of Chew et al. (2003) where the there is a limit to the increase in strength with much lower effective stresses.

2.5.4. Angularity

The cases in which full arching can be formed are dependent on the angularity of the sand and the size of the opening. Miller (1994) found that there is a minimum requirement of angularity within a soil for arching to occur. In a soil where no arching was present, no amount of surcharge could induce arching.

2.6. Conclusion

From the literature study the following conclusions can be made:

- Porous flow can be described by Darcy's equation when turbulent and inertia resistance is insignificant when compared to laminar resistance. The relative influences can be calculated using Reynolds number and the Keulegan–Carpenter number.
- When constructing a granular open filter the primary loading parameter is the hydraulic gradient, the point at which erosion starts to occur is the critical hydraulic gradient. Both the perpendicular and parallel can cause erosion separately and influence each other only when both are close to the critical value.
- Arching is the main mechanism which stabilises an open filter. The main influencing parameters on arching are: stability ratio, effective stress, packing of materials and angularity of materials.
- Stability ratio is the main parameter used to describe the strength of an open filter this has an inverse relation with the critical hydraulic gradient.
- A self repairing or armouring effect leading to similar or greater critical hydraulic gradients is noticed in many types of filters.
- Magnitudes of the critical hydraulic gradients for specific open inverted filters have been found by Boersma (2020) and Van de Ven (2019).
- The primary loading on an open filter is due to hydraulic forces. The most significant are the hydrostatic pressure difference and the drag force. Both are proportional to the hydraulic gradient and the drag force is also related to the particle size via the permeability.

3

Description of Experimental Setup

This chapter describes the experimental setup used to conduct tests on the inverted geometrically open filter structure. The container for the experimental setup was designed by Boersma (2020). In order to perform the desired test modifications were made to the setup.

3.1. Test Setup

This section describes the experimental setup by explaining the different components.

3.1.1. Compartments of Test Setup

The experimental setup consists of a waterproof container with three compartments separated by a geotextile which allows water to pass through but retains the base and filter material. The setup is illustrated in Figure 3.1.

The three compartments within the setup contain:

- **Compartment A:** A plunger that controls the water level in this compartment and a laser that measures this water level.
- **Compartment B:** A sand base layer located above a gravel filter layer supported by a wire mesh.

  Within these layers, water level differences lead to hydraulic gradients. The hydraulic gradients are increased until erosion occurs. When this occurs base material passes through the filter layer and wire mesh to be observed in the bottom cells.

  On top of this container, there is a plate is used to increase the effective stress within the base and filter material. This is done by applying a surcharge.
- **Compartment C:** A laser that measures the water level.

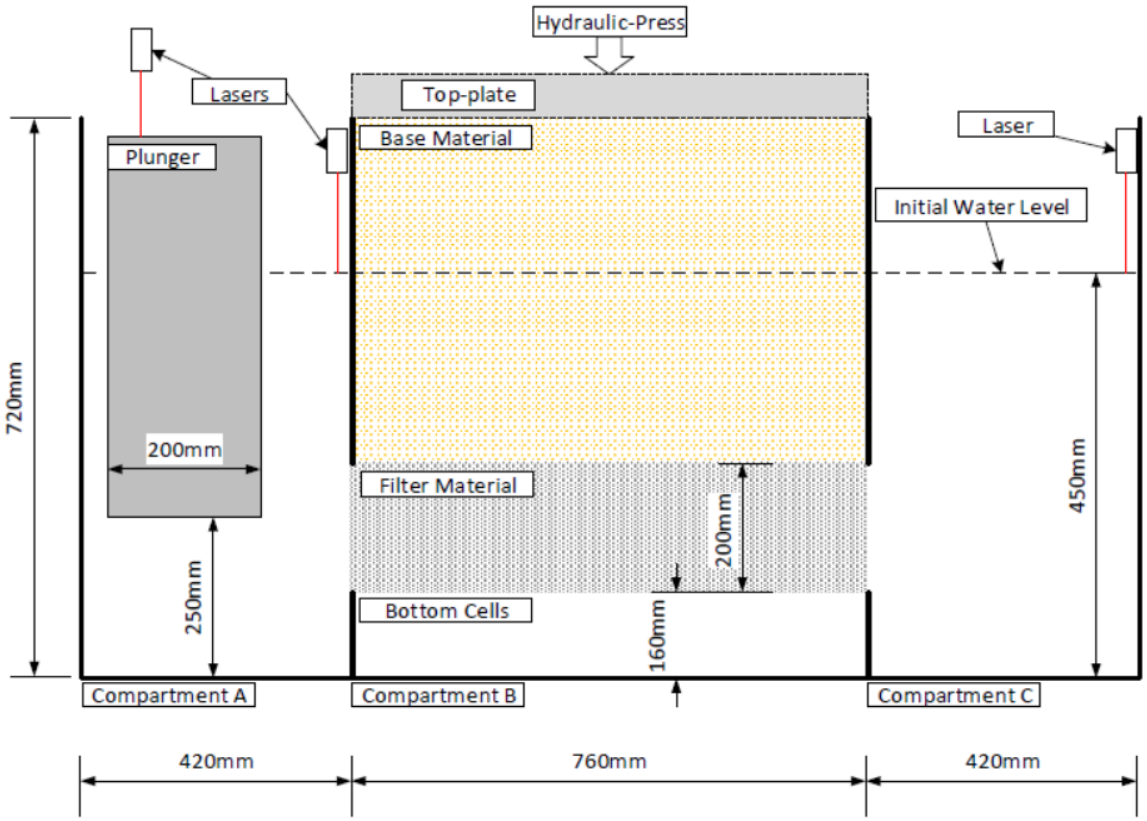

Figure 3.1: The Physical Model used for testing in this study.

3.1.2. Plunger

A plunger is used to control the water level in compartment A. The plunger is a hollow box partially filled with water. It has an amplitude of 20mm and is filled in such a manner that it balances in the middle of its amplitude. Changes in the water level of compartment A lead to water level differences and thus induce a hydraulic gradient in the filter construction. This plunger is attached to a servo to control the plunger. The period is varied by adjusting the speed of the servo. The position of the plunger is recorded using a laser.

3.1.3. Hydraulic press

In a portion of the tests, a surcharge is applied to the top of the sand base material. This is done to mimic the weight of the sand above the base soil. This load is applied using a hydraulic press. During the test, the load is applied in a force-controlled manner. This means that throughout the test the pressure within the soil is kept constant. To distribute this load a plate has been designed. The main requirements for the design of the plate were that the plate is strong enough to handle the load from the press and stiff enough to distribute the point load evenly across the sand. A detailed description of the design can be found in Appendix A. The position of the top-plate and force applied by the hydraulic press were measured using built-in sensors. The position of the top-plate corresponds with the settlement of the base material which can be either due to erosion of base material or due to compaction of one or both of the layers.

3.1.4. Lasers

The water levels in the different compartments are used to induce the hydraulic gradients. Therefore it is important to know the water levels. The water levels in the different compartments will be measured using a laser and floater construction.A laser is attached to the model. This laser reflects on paper floating on the surface of the water. This paper has been coated in grease to waterproof the paper to ensure that it stays afloat. This is shown in Figure 3.2.

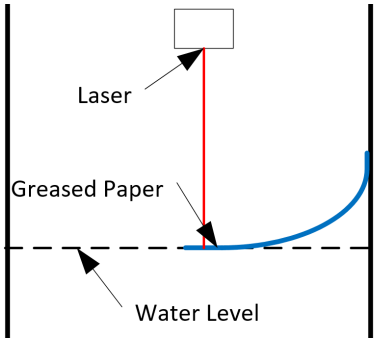

Figure 3.2: Laser floater system used to determine the water levels in the different compartments.

3.1.5. Pressure Sensors

The objective of the research is to determine the effect of changing various parameters on the critical hydraulic gradient. In all tests both the parallel and perpendicular hydraulic gradients were measured. The hydraulic gradients were measured using pressure sensors. This was done by measuring the pressure at two points. The hydraulic gradient is the difference in the pressure divided by the distance between the pressure sensors. The locations and distance between the sensors are shown in Figure 3.3.

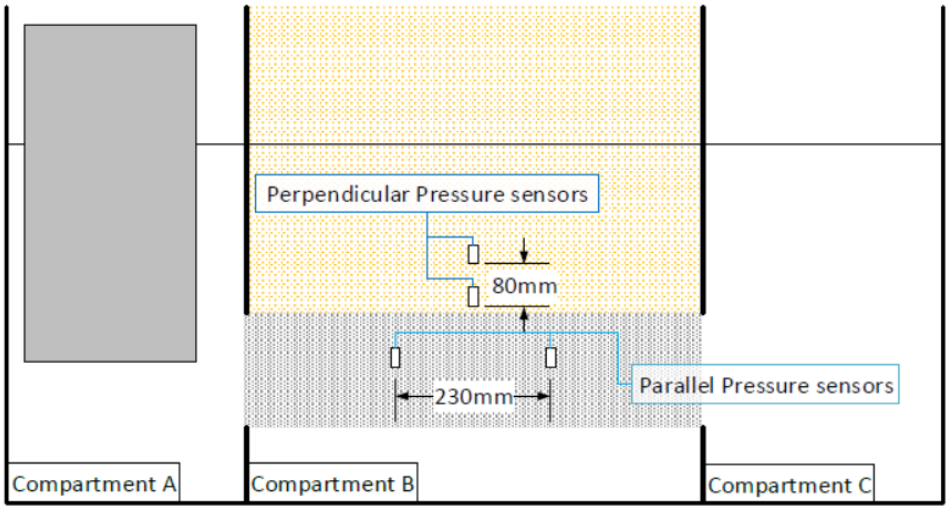

(a) Side view.

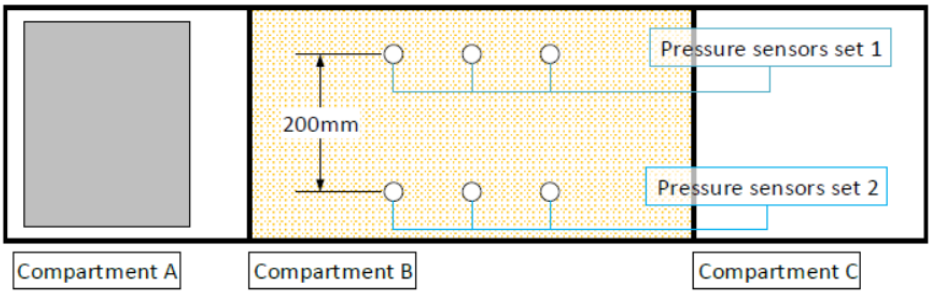

(b) Top view.

Figure 3.3: A diagram showing the layout of the pressure sensors within the model. The opening of the sensor where the hydraulic head is measured is located at the centre bottom of the sensor.

The pressure sensors used were vented gauges which determine the difference between the atmospheric pressure and water pressure, this is the hydraulic head. The distance between the sensors was fixed using a rack. The sensor casing was coated in a resin to ensure the waterproofing of the sensor.

3.1.6. Cameras and Tent

The point at which erosion starts to occur is important to determine the critical hydraulic gradient. Two Logitech c920 HD stream webcams were used to record a time-lapse of the bottom cells using the software Sky Studio Pro. The time-lapse recorded one frame per second. A tent was placed over the entire model setup and LED construction lights are used to light up the model. This was done in order to keep lighting conditions constant.

3.2. Model Configurations

The experimental setup had three base configurations which could be used for testing. These configurations were parallel, perpendicular and combined.

3.2.1. Parallel

For the parallel configuration the top of compartment B was sealed. The expectation was that this would lead to a porous flow through the filter layer between compartment A and compartment C. This would lead to only parallel hydraulic gradients. This is shown in Figure 3.4.

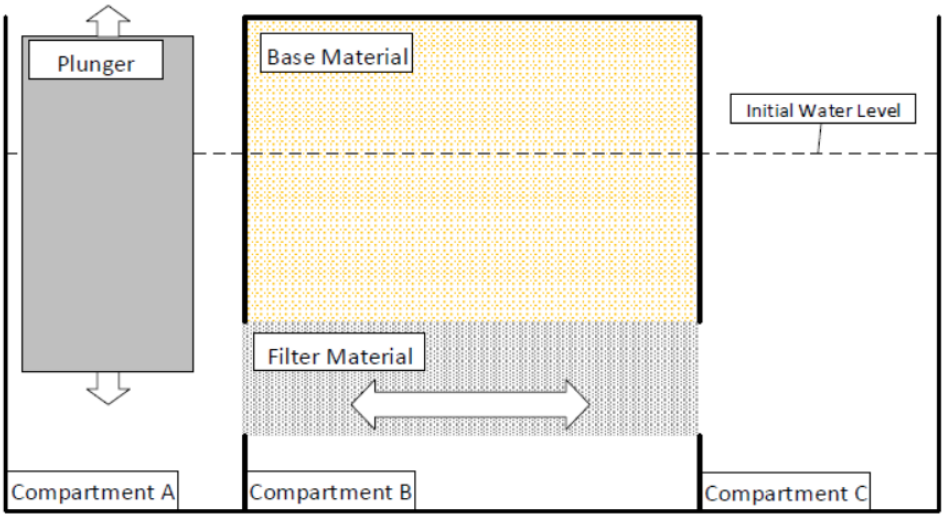

Figure 3.4: Schematic diagram of the parallel configuration used in this study.

3.2.2. Perpendicular

For the perpendicular configuration, the connection between compartment B and compartment C was sealed, as shown in Figure 3.5. The flow within the setup is from compartment A into the filter and then into the base material. The permeability of the base material is orders of magnitude lower than the filter material and the specific discharge is the same. Therefore the hydraulic gradients present in the base material are orders of magnitude larger than the hydraulic gradients in the filter material. The hydraulic gradients within this configuration are located in the base material and are perpendicular to the filter-base interface.

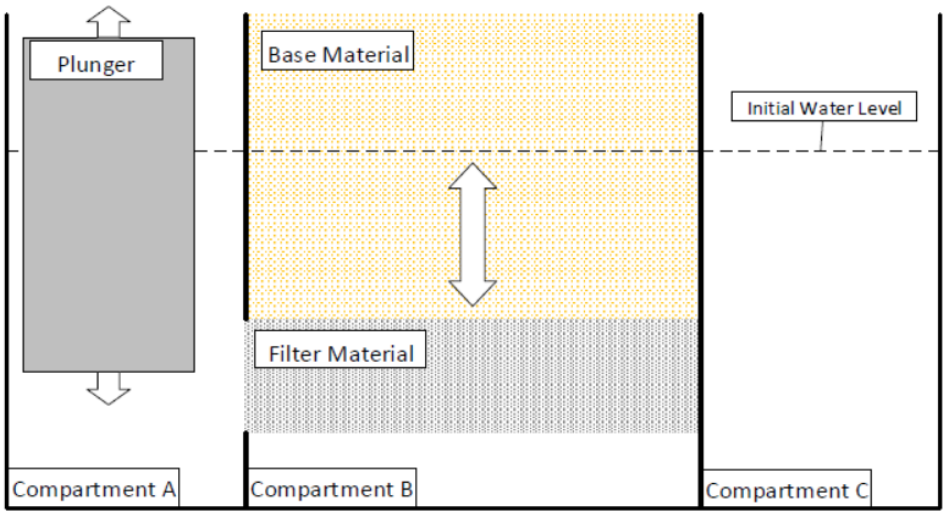

Figure 3.5: Schematic diagram of the perpendicular setup used in this study.

3.2.3. Combined

For the combined configuration both a vertical flow in the base material and a horizontal flow in the filter material were present. This configuration is illustrated in Figure 3.6.

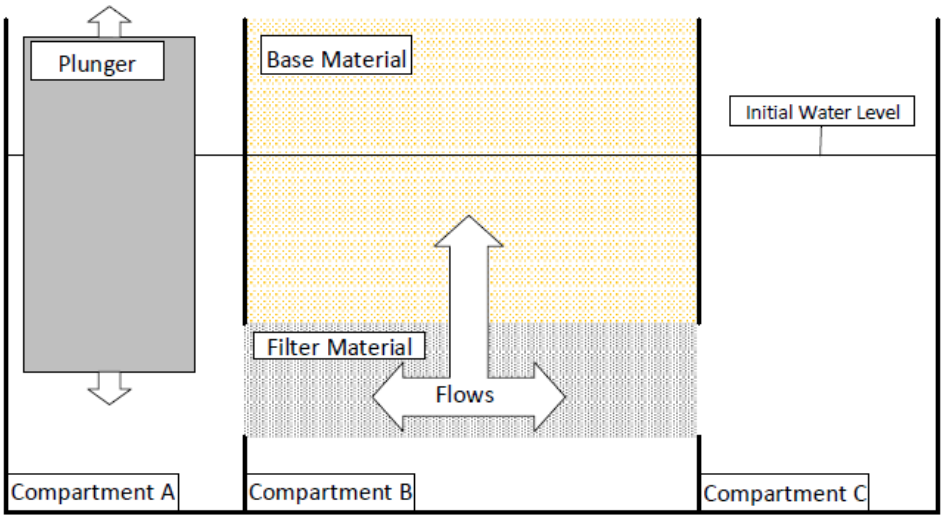

Figure 3.6: Schematic diagram of the combined setup used in this study.

3.3. Granular Material

Different granular materials have been used within the model for different tests. Sands were used for the base material and gravel was used as the granular filter. The gravel used required preparation. Furthermore important parameters of the granular materials have been identified which have influence on the functioning of the filter. These are the particle size distribution of both the filter and base material and the angularity of specifically the base material. The particle size distribution has influence on the stability ratio which will be varied between tests and the wideness of the grading which will be controlled throughout tests as only narrow graded filters will be used. The angularity of a material has influence on the ability of arches to form and will thus be determined for the base material where arches will form. This section will address the preparation of the filter material, the determination of the angularity, the particle size distribution and summarise the key parameters of each material.

3.3.1. Preparation of Filter Material

For each test new washed gravel was used. Washed gravel ensured the water was clear for visual observations. New gravel ensured there was no sand mixed in with the gravel. This prevented possible filter saturation effects as identified by Boersma (2020). With filter saturation the pores of the filter material are partly filled with the base material when placing the filter. This is thought to reduce the critical hydraulic gradient of a filter.

3.3.2. Angularity of the Sand

The expected mechanism stabilising the filter is the arching of the sand across the gaps in the filter layer. As the extent to which arches can form is dependant on the angularity of the material this is an important factor to determine. As such the angularity of the base material (sand) is determined. As there will be no arching action of the filter material its angularity is less relevant.

An analysis of the angularity was performed by visual observation of 30 grains of sand for the three types of sand. This was done under a microscope. The roundness and sphericity of the sand was then visually compared with the chart shown in Figure 3.7a from Powers (1953). The results of this analysis are shown in Figure 3.7b. A joint distribution is plotted with the roundness on the x-axis and sphericity on the y-axis. The marginal distributions are also shown on each axis respectively. A different colour is used for each base material.

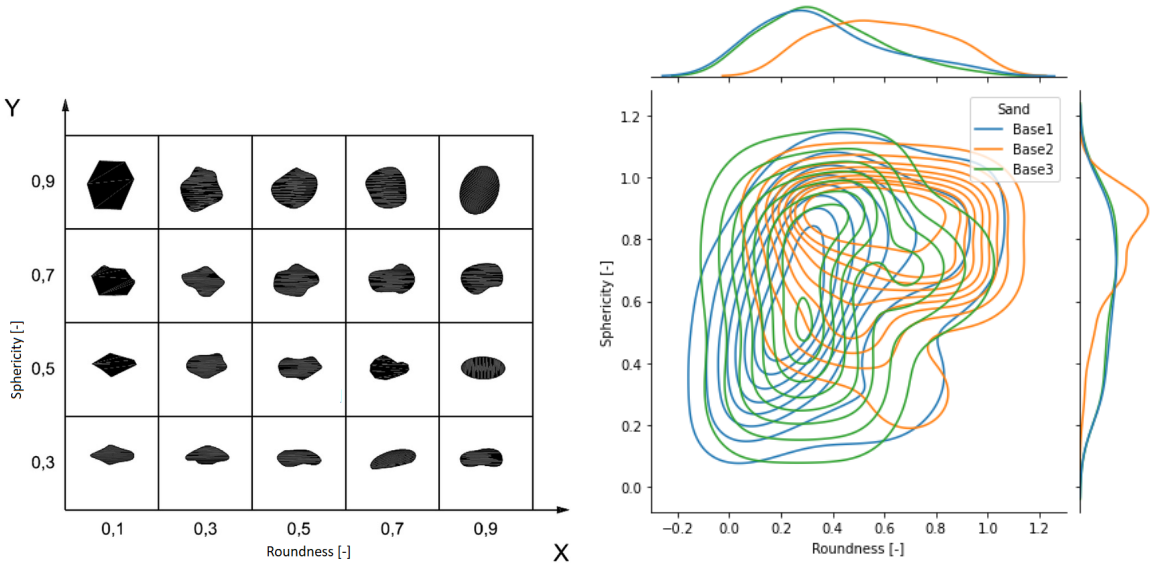

(a) Chart used for comparison with the particles (Powers, 1953).

(b) Chart showing the sphericity and roundness of the base material

Figure 3.7: Analysis of the angularity of the base material

Base materials 1 and 3 closely match in both roundness and sphericity but differ significantly from base material 2. Base materials one and three are sourced from marine sediment deposits, either current or past seabeds. Base material 2 is sourced from a river bed and shows a significantly higher angularity both in roundness and sphericity. As such for investigating the influence of angularity a comparison can be made between the less angular Base 2 and the more angular Base 1 and Base 3.

3.3.3. Particle Size Distribution

The particle size distributions of the sand base layers were determined with a sieve analysis of a sample of each material. The mass fraction that is smaller than a specific sieve is plotted as a cross in Figure 3.8. For the filter layers a sample of minimum 100 pieces was weighed and converted to the particles sizes. The mass fraction smaller than a specific size is shown as a point in Figure 3.8. Using these points a log-normal distribution was fitted using the SciPy package Optimise, to determine a continuous function for the particle size distribution. This result is plotted as a line in Figure 3.8.

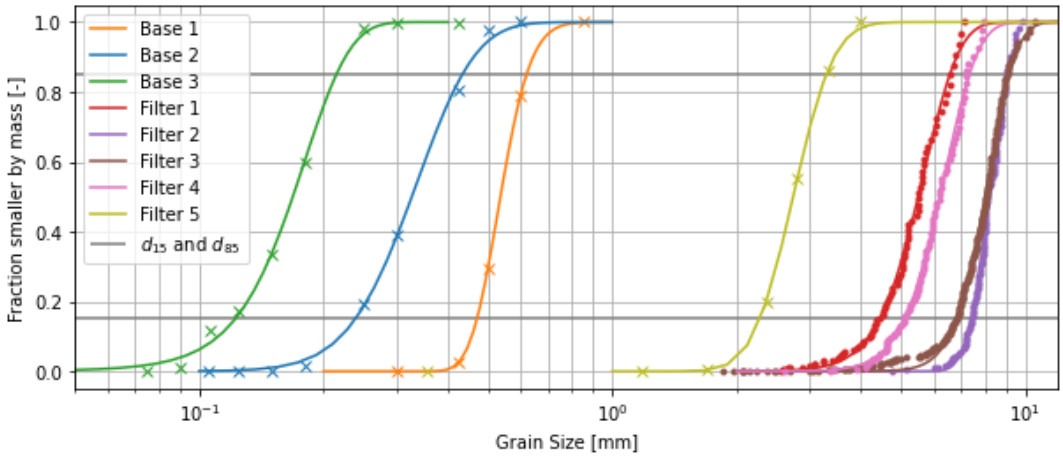

Figure 3.8: Particle size distribution of filter and base materials.

3.3.4. Summary of Properties

The most relevant parameters of the filter and base materials are presented in the tables below:

Name	Roundness	Sphericity	d_{15} [mm]	d_{50} [mm]	d_{85} [mm]	CU (d_{60}/d_{10})
Base 1	0.36	0.63	0.47	0.53	0.61	1.2
Base 2	0.59	0.77	0.24	0.32	0.42	1.6
Base 3	0.36	0.64	0.12	0.17	0.21	1.7

Table 3.1: This table highlights the properties of the base materials used in this study.

Name	d_{15} [mm]	d_{50} [mm]	d_{85} [mm]	d_{85}/d_{15}
Filter 1	4.4	5.5	6.6	1.5
Filter 2	7.4	8.1	9.0	1.2
Filter 3	6.8	8.1	9.1	1.3
Filter 4	5.1	6.2	7.2	1.4
Filter 5	2.2	2.7	3.2	1.5

Table 3.2: This table highlights the properties of the filter materials used in this study.

3.4. Model effects

The physical model introduces effects do not occur in reality, these model effects. How these are dealt with will be discussed in this section.

3.4.1. Wall Effects

The wall of the model is completely flat and this leads to larger pore openings than within the centre of the filter layer. The base material can bypass the filter through these openings. To minimise this affect the walls of the model are lined with bubble plastic.

3.4.2. Placement of Sensors

The placement of the sensors within the filter and base materials leads to object that are located within the model that would not be present in the application. These could lead to channelling alongside the sensors or cables. To minimise this effect the cables are guided horizontally to the front and back of the model in the shortest distance and then once behind the bubble plastic they are guided into the left compartment where they can leave the setup.

At the locations that the cables went behind the plastic the small slits needed to be taped closed to prevent base material bypassing the filter on the back of the sand. The first test failed as a result of the sand passing through this slit.

3.4.3. In and Outflow Effects

Inflow and outflow of water into the filter can effect the flow and thus hydraulic gradients near the entrance and exit. To minimise this the cells closet to the entrance and exit will be ignored when detecting erosion.

3.5. Testing Procedure

In this section the execution of a test will be described. This consists of three parts preparation, execution and after a test.

3.5.1. Preparation of a test

The steps for the preparation of a test are presented below. Figure 3.9 is a legend for the installation diagrams.

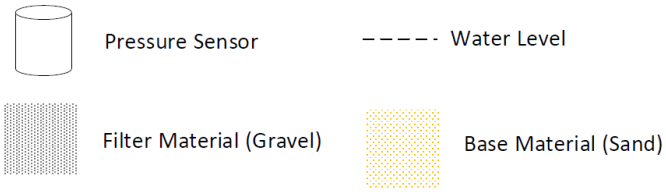

Figure 3.9: Legend for installation steps.

1. The preparation of a test started with a dry and clean model. In this the mesh grid and geotextile to contain the filter and base material was placed. Then the bottom 50mm of filter layer was placed and the water level raised to 50mm above the top of the filter layer. On top of this the rack for the pressure sensors was placed. The bottom six pressures sensors were injected with water to remove air bubbles and placed.

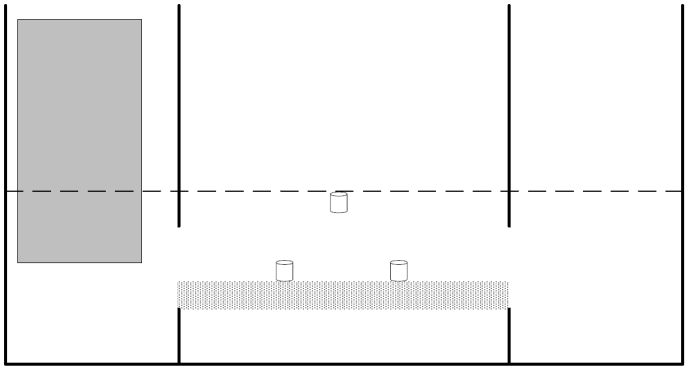

Figure 3.10: Installation step 1.

2. The remaining 50mm of filter layer and initial 50mm of base material were placed. The water level was raised above the level of the top two pressure sensors. These sensors were injected with water and placed in the rack.

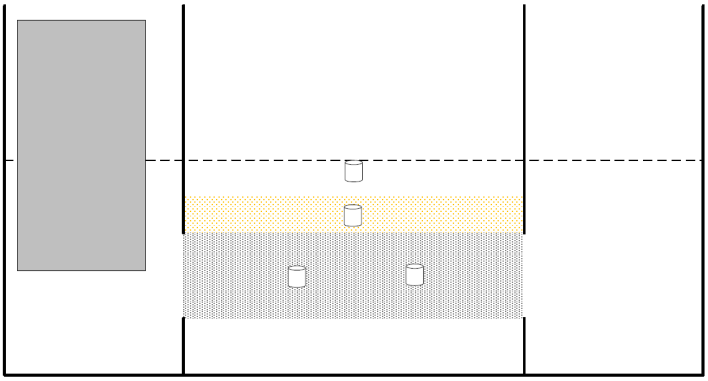

Figure 3.11: Installation step 2.

3. The rest of the model was then filled with the base material and the water level raised to 450mm.

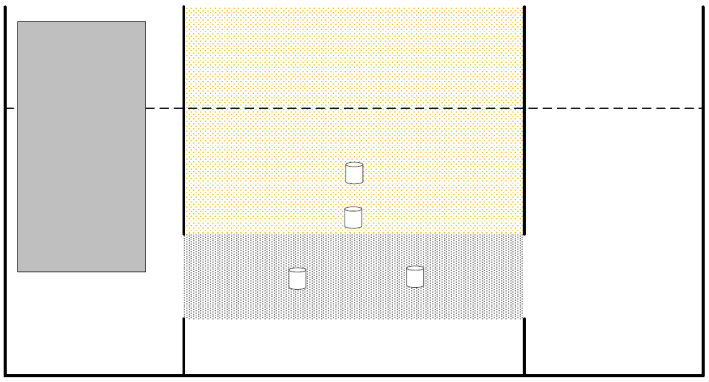

Figure 3.12: Installation step 3.

4. The floaters for the lasers were placed.
5. (Parallel tests only) Sealing of the top of the model.
6. (Tests with a surcharge only) Placement of top-plate for applying a surcharge. Transport to under the hydraulic press.
7. The tent and cameras were placed and the time lapse was started.
8. The recording of all sensors was started.
9. (Tests with a surcharge only) The load was applied using the hydraulic press.

After these steps the setup was ready for testing.

3.5.2. Execution of a test

The testing was then started by starting the plunger. The tests were carried out in segments with a fixed plunger velocity. Between segments the plunger velocity was increased reducing the period of the forcing. Each test phase started with a calibration of 6 minutes, after this the plunger continued with the same period for an hour. The test was complete when the after 8 steps of increasing the hydraulic gradient. The period of the plunger was decreased from 120 seconds to 12 seconds during these 8 steps.

3.5.3. After a test

After completion of a test, the recording of data and time lapse was stopped and the tent was removed. The setup was dismantled by reversing the preparation of an experiment. The container was then emptied and cleaned for the next test.

3.6. Analysis

This section describes the post processing of the data recorded by the sensors. The sensors were calibrated and the pressure sensor data was filtered.

3.6.1. Calibration sensors

The model setup contained sensors which require periodic calibration to function properly. These sensors are the lasers, pressure sensors and load cell in the hydraulic press.

Lasers The lasers were calibrated once. This is was done by measuring the water level manually and comparing this to reading of the sensor. The paper floating on the water level in the containers was effected by the speed at which the water level changed when this was done quickly the paper would lag behind and overshoot afterwards. The paper would however settle after some time. This makes this setup usable for the calibration of the pressure sensors.

The repeated movement of the plunger disturbed the paper too much. Therefore determining the hydraulic gradients using the lasers was not possible.

Differential Pressure Sensors The pressure sensors were calibrated before increasing the hydraulic gradient for each step. To calibrate these sensors the plunger was held at a fixed location until the water level in the model could equalise. This constant water level in the model was used to set the hydraulic head of the pressure sensors to the water level measured by the lasers. This was done for the top and bottom of the stroke of the plunger. The results of the calibration can be seen in Figure 3.13.

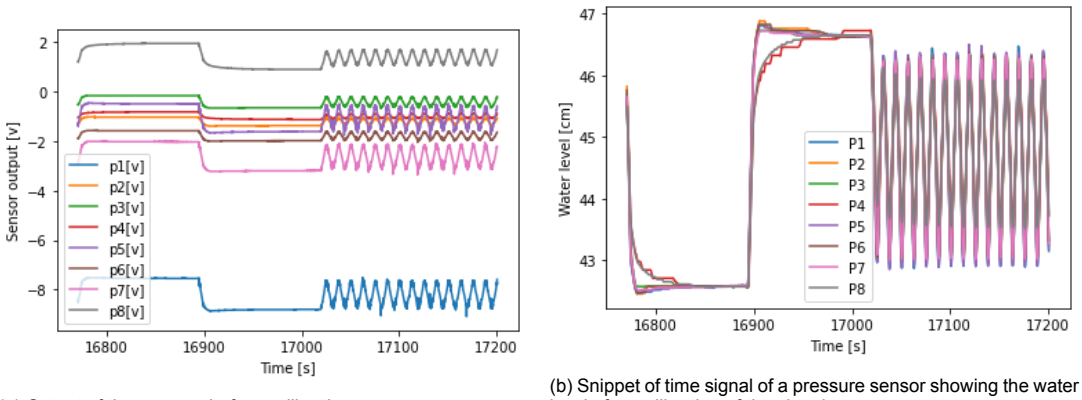

(a) Output of the sensors before calibration.

(b) Snippet of time signal of a pressure sensor showing the water level after calibration of the signal

Figure 3.13: The effect of calibration on the output of the pressure sensors during test 6, showing before and after calibration of the results. This process was performed for each segment of the test for all the tests. P1 to P8 represent each pressure sensor.

In Figure 3.13a the output of the pressure sensors is shown. The periods where the water level is allowed to equalise can been seen where the output of the sensors remains constant. The last 10 seconds of these periods are used for the calibration. The output measured by the pressure sensor is set to equal to the hydraulic head determined by the lasers. Using these known points a linear regression is made between the sensor output and the hydraulic head.

These pressure sensors have an accuracy of 0.001psi which corresponds to being able to determine the hydraulic head with an accuracy of 0.7mm.

Load Cell Hydraulic Press The load cell in the hydraulic press is calibrated periodically by the lab technicians and thus was properly calibrated during the experiments performed.

3.6.2. Filtering of Pressure Signals

The data collected by the pressure sensors showed significant oscillations with a time scale that was orders of magnitude smaller than the forcing of the plunger. These short scale oscillations are likely due to vibrations and have been filtered out of the signal. The effect of filtering the signal can be seen in Figure 3.14b, where the blue line shows an unfiltered signal and the orange line shows a filtered signal.

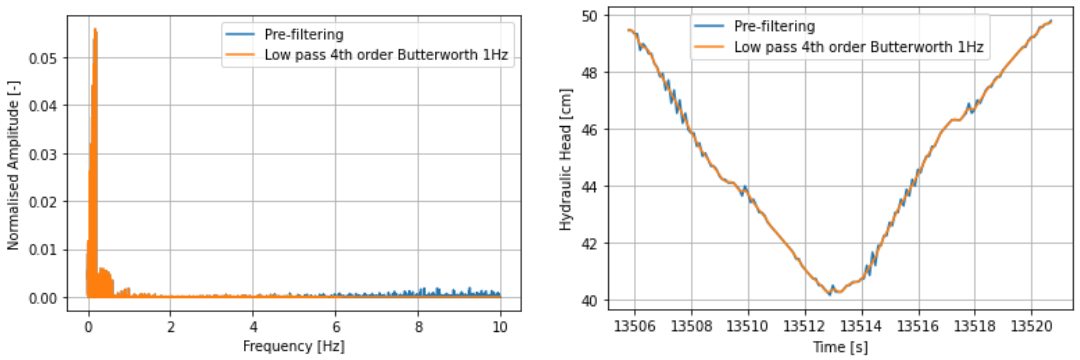

(a) Fast Fourier Transform to show amplitude-frequency spectrum of a pressure signal before and after filtering of the data.

(b) Snippet of the time signal of a pressure sensor showing the effect of filtering the pressure signal.

Figure 3.14: The effect of filtering pressure sensor 2 during test 2, shown as an example of the effect of the same filtering performed on all pressure sensors during all tests.

The filter applied to the pressure sensors was a low-pass fourth order Butterworth filter. The Butterworth filter was selected as a Butterworth filter has very limited influence on the amplitude of passing frequencies. A fourth order filter was chosen. For this filter a cut-off frequency of 1Hz was chosen as this is an order of magnitude higher than the smallest period of forcing (10s) and lower than the sampling rate of 10Hz. The effect of the filtering on the amplitude response can be seen in Figure 3.14a. In this figure it can be seen that the unfiltered blue spectrum shows a significant amount above the nyquist frequency of 5Hz. This is removed in the filtered signal shown in orange.

3.6.3. Determination of the Hydraulic Gradients

From the hydraulic head signals measured by the differential pressure sensors and the water levels in containers A and C measured by the lasers the hydraulic gradients are calculated using the pressure difference and distance between the points. For the pressure sensors the distance between the sensors is used to determine the hydraulic gradients. From the water levels the length of the filter is used as the distance. The Hydraulic gradients present in a cycle are not constant during a cycle of the plunger but have a peak value. The positive and negative peak value of the hydraulic gradient per cycle were found using the Argrelextrema function from the SciPy Signal Python package. These values where collected and the mean value of the peaks is determined to be the hydraulic for the test segment. As mentioned above the differential pressure sensors have a limited accuracy this also influences the precision of the hydraulic gradients which can be determined. For the perpendicular hydraulic gradient this is 0.00875 and for the parallel hydraulic gradient this is 0.003. This difference is due to the difference in distance between the differential pressure sensors.

3.7. Test Program

This section describes the experimental program that was used for this study. The objective of the experiments will be highlighted. The parameters most relevant to the stability of the filter will be highlighted and all performed tests will be presented.

3.7.1. Objective of Tests

The objective of the physical model tests is to gain more knowledge about how the key strength (arching of the base material) and load mechanism (the flow of water) influence the stability of an open inverted filter. This is done by determining the influence of key parameters which influence the stability of an open inverted filter.

3.7.2. Key Parameters

Key parameters for these tests are the following:

- **Angularity of base material** The influence of angularity can be investigated when the other parameters are kept constant. Tests 14, 16 and 20 can be used to compare the influence of the difference in angularity between Base 1 and Base 2 at 100 kPa surcharge.
- **Stability ratio** In different tests different filter-base are used leading to different stability ratios. The influence of the stability ratio can be determined by comparing tests where other parameters are constant. This is the parallel test without surcharge and the perpendicular tests without surcharge.
- **Hydraulic gradient** The hydraulic gradient is increased in steps throughout a test. This way the step where erosion occurs is the relevant critical hydraulic gradient.
- **Surcharge** The applied surcharge was changed between tests. The surcharge directly determines the effective stress in the base material, which influences the strength of the arches.

3.7.3. Tests Performed

The configurations for the tests performed for this study were the following:

Test	Configuration	SR [-]	Surcharge [kPa]	Base-Filter Combination
1*	Parallel	7.2	0	Base 1 & Filter 1
2	Parallel	7.2	0	Base 1 & Filter 1
3	Parallel	7.2	0	Base 1 & Filter 1
4	Parallel	7.2	0	Base 1 & Filter 1
5*	Parallel	10.5	0	Base 2 & Filter 1
6	Parallel	10.5	0	Base 2 & Filter 1
7	Combined	7.2	0	Base 1 & Filter 1
8	Combined	7.2	0	Base 1 & Filter 1
9	Perpendicular	7.2	0	Base 1 & Filter 1
10	Perpendicular	10.5	0	Base 2 & Filter 1
11	Perpendicular	10.5	0	Base 2 & Filter 1
12	Perpendicular	12.2	0	Base 1 & Filter 2
13	Perpendicular	10.5	0	Base 3 & Filter 5
14	Perpendicular	12.2	100	Base 1 & Filter 2
15*	Perpendicular	12.2	200	Base 1 & Filter 2
16	Perpendicular	12.2	100	Base 1 & Filter 2
17	Perpendicular	10.5	100	Base 2 & Filter 1
18	Combined	7.2	100	Base 1 & Filter 1
19	Combined	7.2	200	Base 1 & Filter 1
20	Perpendicular	12.1	100	Base 2 & Filter 4
21	Perpendicular	12.1	200	Base 2 & Filter 4
22	Perpendicular	11.2	100	Base 1 & Filter 3
23	Perpendicular	11.2	200	Base 1 & Filter 3
24	Parallel reduced height	12.2	0	Base 1 & Filter 2

Table 3.3: Setup of all model tests performed. Test 1, 5 & 15 failed due to failure of a component of the experimental setup. These tests were repeated at a later time and received a new number.

4

Numerical Modelling of the Porous Flow within the Physical Model

An objective of this thesis is to gain a deeper understanding of the flow processes within the physical experimental setup. A numerical model was developed to assist with this understanding. This is explained in this chapter. The 1D numerical model developed by Boersma (2020) was used as a starting point and was expanded to meet the objectives of this study. First the objectives of the numerical model are addressed. Then the model created by Boersma (2020) will be briefly summarised (for a full derivation of this model see Boersma (2020)). Next the 2D expansion of the model will be explained. Finally the coupling between the expanded model (2D) and the original model (1D) will be highlighted. The compressibility of air was also included in the model. However, as this turned out not to be directly relevant for this study it is included in Appendix B.

4.1. Objective of Numerical Model

The numerical model is used to help with the understanding of the flow processes that occur within the experimental setup during a test. As such, the numerical model needs to calculate the pressure distribution within the base material during a cycle of the plunger.

4.2. 1D Model

The starting point for the numerical model is the model developed by Boersma (2020). This model calculates the water levels in the different compartments during a cycle of the plunger. This is calculated using a numerical application of a volume balance and Darcy's law. The full model for the combined situation which consists of parallel and perpendicular flows is explained. For the parallel situation perpendicular flows and gradients are neglected. For the perpendicular situation flows to compartment C are neglected.

Model Description The numerical model represents the experimental setup, the parameters used to describe this are shown in Figure 4.1 and are listed below.

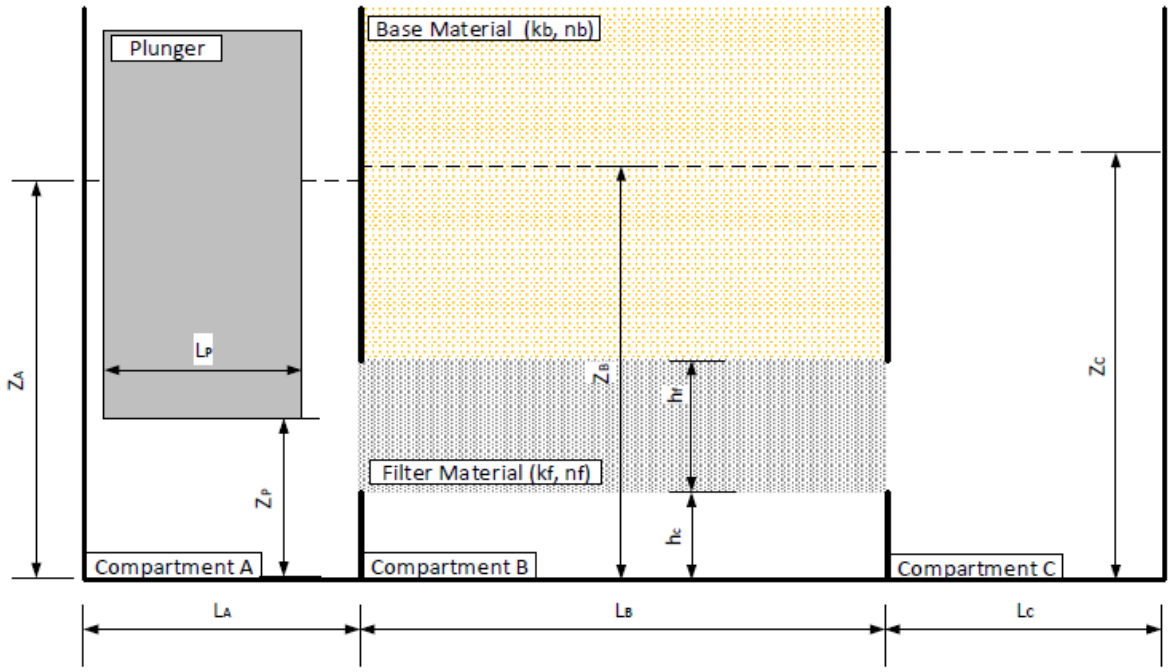

Figure 4.1: Parameters in the numerical description of the experimental setup.

The parameters :

- z_A: Water level in compartment A [mm]
- z_B: Groundwater level in compartment B [mm]
- z_C: Water level in compartment C [mm]
- z_p: Level of bottom of plunger [mm]
- h_f: Filter layer thickness [mm]
- h_bc: Bottom cells height [mm]
- L_A: Length of compartment A [mm]
- L_B: Length of compartment B [mm]
- L_C: Length of compartment C [mm]
- L_p: Length of the plunger (2D representation of the area blocked in Comp. A) [mm]
- k_b: Permeability of the base layer [m/s]
- n_b: Porosity of the base layer [-]
- k_f: Permeability of the filter layer [m/s]
- n_f: Porosity of the filter layer [-]

Influence of the Plunger on the Water Level in Compartment A The oscillating of the plunger changes the submerged volume of the plunger. On the down-stroke of the plunger the submerged volume increases. Therefore the water level in compartment A rises proportionately. This is quantified using a volume balance. The volume of the water displaced by the plunger is equal to the volume of the water level rise. This results in the following equation, which describes the change in water level in compartment A due to the plunger:

$$z_A(t+1) = z_A(t) - \frac{\frac{d}{dt}z_p \cdot L_p}{L_A - L_p} \tag{4.1}$$

L_p is not the actual length of the plunger but a 2D representation of the plunger size. This is calculated as follows:

$$L_P = \frac{\text{Cross-sectional area of Plunger}}{\text{Area of Compartment B}} \cdot L_A \tag{4.2}$$

Hydraulic Gradients The hydraulic gradients within the model are calculated using the water levels in the different compartments and the distance over which the gradient is dissipated. For the parallel hydraulic gradient, the flow is between compartment A and compartment C. This is over the length of the filter. This results in the following equation:

$$i_{\parallel}(t) = \frac{z_C(t) - z_A(t)}{L_B} \tag{4.3}$$

For the perpendicular hydraulic gradients the gradient occurs both across the filter layer and the base layer. There is a permeability difference between the base and filter material. The filter material (gravel) has a significantly higher permeability than the base layer (sand) (Verruijt and Broere, 2011). Due to this permeability difference, the hydraulic gradient will be more significant in the base material. The hydraulic gradient over the filter is negligible and is thus neglected. The perpendicular hydraulic is modelled in the base material below the groundwater level in compartment B. There are two components to the perpendicular hydraulic gradient: (1) the part between compartment A & compartment B and (2) the part between compartment B & compartment C. This results in the following equations:

$$i_{A,\perp}(t) = \frac{z_B(t) - z_A(t)}{z_B(t) - h_f - h_c} \tag{4.4}$$

$$i_{C,\perp}(t) = \frac{z_B(t) - z_C(t)}{z_B(t) - h_f - h_c} \tag{4.5}$$

Flow Between Compartments The hydraulic gradient between the compartments is known. Therefore the specific discharge between the compartments can be calculated using Darcy's law. This specific discharge is converted to discharge using the dimensions of the layers.

$$q = -k \cdot i \tag{4.6}$$

The discharge consist of three components. A parallel discharge ($q_{\parallel}$) for the parallel flow and two perpendicular parts. One for the flow between compartment A and B ($q_{A,\perp}$) and the other for the flow between compartment C and B ($q_{C,\perp}$). The two perpendicular components can be added together using the superposition principle to determine the total perpendicular hydraulic gradient. The directions of the discharges are shown in Figure 4.2 and the magnitude is calculated using the equations below:

$$q_{\parallel}(t) = -k_f \cdot h_f \cdot i_{\parallel}(t) \tag{4.7}$$

$$q_{A,\perp}(t) = -k_s \cdot L_B \cdot i_{A,\perp}(t) \tag{4.8}$$

$$q_{C,\perp}(t) = -k_s \cdot L_B \cdot i_{C\perp}(t) \tag{4.9}$$

$$q_{\perp}(t) = -q_{C,\perp}(t) + q_{A,\perp}(t) \tag{4.10}$$

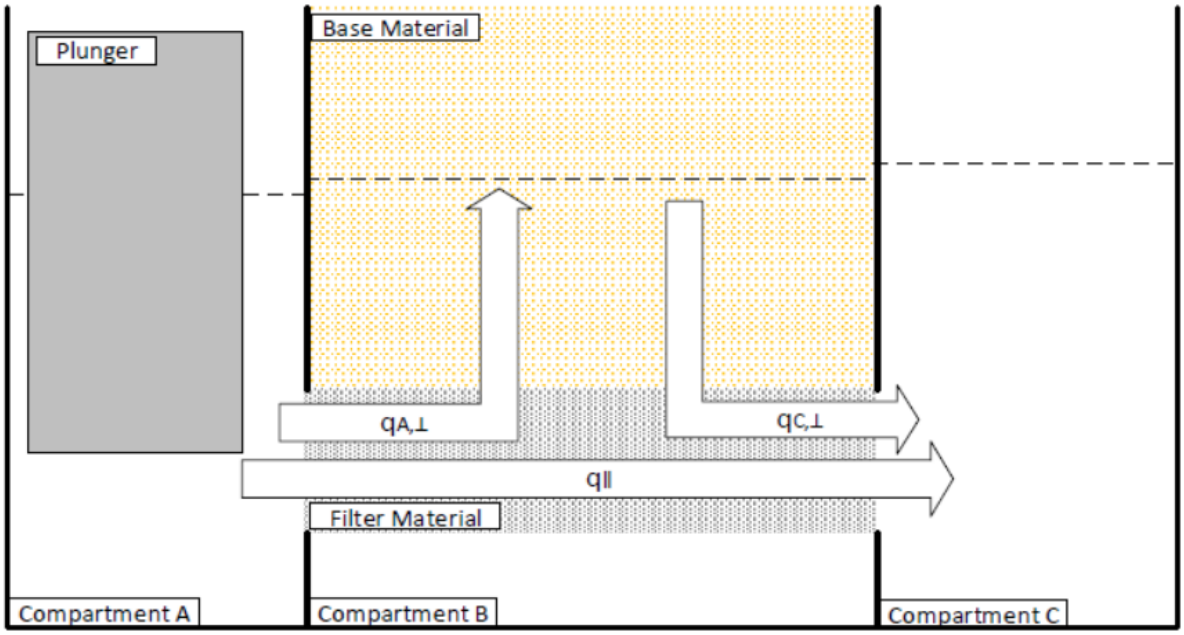

Figure 4.2: Discharges in the numerical description of the experimental setup.

Water Levels in Compartments For the water levels in the different compartments, a volume balance is derived. The change in water level is dependant on the water flowing in and out of the compartment.

$$\frac{d}{dt}z = \frac{q_{in} - q_{out}}{L} \tag{4.11}$$

An explicit Euler numerical scheme has been applied to this volume balance. To ensure stability and sufficient accuracy of the numerical solution a small step size must be used. A time step of 0.0001s was used. For compartment A the influence of the plunger is also included. Compartment B is already partially filled with the base material any water flowing into compartment B can only go into the pore space. The resulting equations for the water levels in a new time step are:

$$z_A(t+1) = z_A(t) - \frac{\frac{d}{dt}z_P \cdot L_p + q_{(\|} + q_{A,\perp}) \cdot \Delta t}{L_A - L_p} \tag{4.12}$$

$$z_B(t+1) = z_B(t) + \frac{(q_{A,\perp} - q_{C,\perp}) \cdot \Delta t}{L_B} \cdot \frac{1}{n_s} \tag{4.13}$$

$$z_C(t+1) = z_C(t) + \frac{(q_{\|} + q_{C,\perp}) \cdot \Delta t}{L_C} \tag{4.14}$$

Leaking of Air The model has also been expanded to include the effect of a trapped compartment of air. This would occur if there was a perfect seal at the top of compartment B in the parallel setup. As this seal leaked no pressure could be built up in the air pocket in compartment B. As such, this mechanism turned out not to be relevant for the current study. The explanation of this is included in Appendix B for future reference.

4.3. 2D Potential Flow Model

This section describes the model used to determine the pressure distribution within the base material. This model is based on the potential flow equation.

Model Description The flow within the base material is determined using the velocity potential of the fluid. Within the porous flow in the base material, the hydraulic head is the potential energy of the fluid. In order to equate the hydraulic head to potential energy the following assumptions are made:

- **2D flow field** Wall effects from the front and back of the container are neglected.
- **Incompressible flow** The fluid and base particles are assumed to be incompressible. This makes the mixture incompressible.
- **Laminar resistance is dominant** The effect of turbulence and inertia effects of changing boundary conditions are neglected. This means only laminar resistance is included.

Under these assumptions, the flow field can be solved by calculating the potential flow with the 2D-Laplace equation as presented below.

$$\frac{\partial \phi}{\partial x^2} + \frac{\partial \phi}{\partial y^2} = 0 \tag{4.15}$$

This equation is discretized and iteratively solved using central differences, resulting in the following algorithm:

$$P_{i,j} = \frac{dx^2 * (Pn_{i+1,j} + Pn_{i-1,j}) + dy^2 * (Pn_{i,j+1} + Pn_{i,j-1})}{2 * (dx^2 + dy^2)} \tag{4.16}$$

In this $P_{i,j}$ is the hydraulic head at a grid point in the current iteration. This is calculated from the hydraulic head in the adjacent grid points in the previous iteration ($Pn_{i\pm1,j\pm1}$). Iterations are repeated until the distribution of the hydraulic head no longer changes.

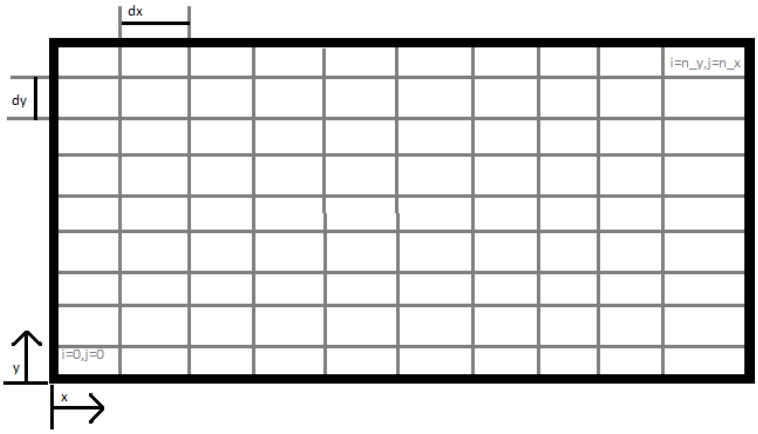

Figure 4.3: The Grid used for the numerical calculation of potential flow using the Laplace equation discretized with central differences.

Grid The grid used for the model is rectangular and covers the length of compartment B. The height is water level in compartment B. This includes the entire wet area of the base material. j indicates the number of the grid point in the x-direction and i indicates the number of the grid point in the y-direction. Outside the boundary, virtual grid points are used to compute the boundary conditions. In the application, a grid of 100 points by 100 points was used.

Boundary Conditions At the left and right wall of the base material, there is a closed boundary, there can be no flow into or out of the wall. As such the flow is set to zero using the following Neumann boundary condition:

$$\frac{\partial P}{\partial x} = 0 \tag{4.17}$$

The top boundary is open to the atmosphere, as such the hydraulic head is equal to the water level. This is defined with the following Dirichlet boundary condition:

$$P = z_B \tag{4.18}$$

The bottom boundary of the base material is to the filter material. On the left side, the hydraulic head is equal to the water level in compartment A, and at the right side, the hydraulic head is equal to the water level in container C. A linear interpolation is used in between. This is defined with the following Dirichlet boundary condition:

$$P = z_A * (x - L_B) + z_C * x \tag{4.19}$$

Hydraulic Gradients When the hydraulic head is calculated in all grid points the hydraulic gradients in each point are calculated. This is done by using the hydraulic head in the adjacent grid points as follows:

$$IVertical_{i,j} = \frac{Pi, j+1 - Pi, j-1}{2 * dy} \tag{4.20}$$

$$IHorizontal_{i,j} = \frac{Pi+1, j - Pi-1, j}{2 * dx} \tag{4.21}$$

Special Cases Two cases different to the combined set-up have also been modelled to determine the distribution of the hydraulic gradients within the base material. These cases are the perpendicular setup and the parallel setup with a leak located at a single point. To model the perpendicular situation the bottom boundary condition is adjusted. The hydraulic head here is equal to the water level in compartment B. This results in the following boundary condition:

$$P = z_A \tag{4.22}$$

During physical model testing, it was noticed that the parallel setup leaked air past the top seal. In order to determine the effect of this leak on the distribution of the hydraulic gradient, a situation with a leak has been modelled. The parallel setup with a leak is modelled by a closed boundary along the top. To include the leak at a single point, an open boundary will be imposed at the location of the leak. This results in the following boundary condition:

$$\frac{\partial P}{\partial y} = 0, \qquad for \qquad x \neq x_{Leak} \tag{4.23}$$

$$P = z_B, \qquad for \qquad x = x_{Leak} \tag{4.24}$$

4.4. Coupled Model

A coupled model was made which calculates the spatial distribution of the hydraulic gradient within the base material during a cycle of the plunger. A one-way coupling was made at each time step. Using the plunger position as input the 1D model determined the water levels within the different compartments. The water levels calculated by the 1D were then used as input for the 2D model. This produced the pressure distribution within the base material. The calculation process of the coupled model for a single time step can be seen in Figure 4.4.

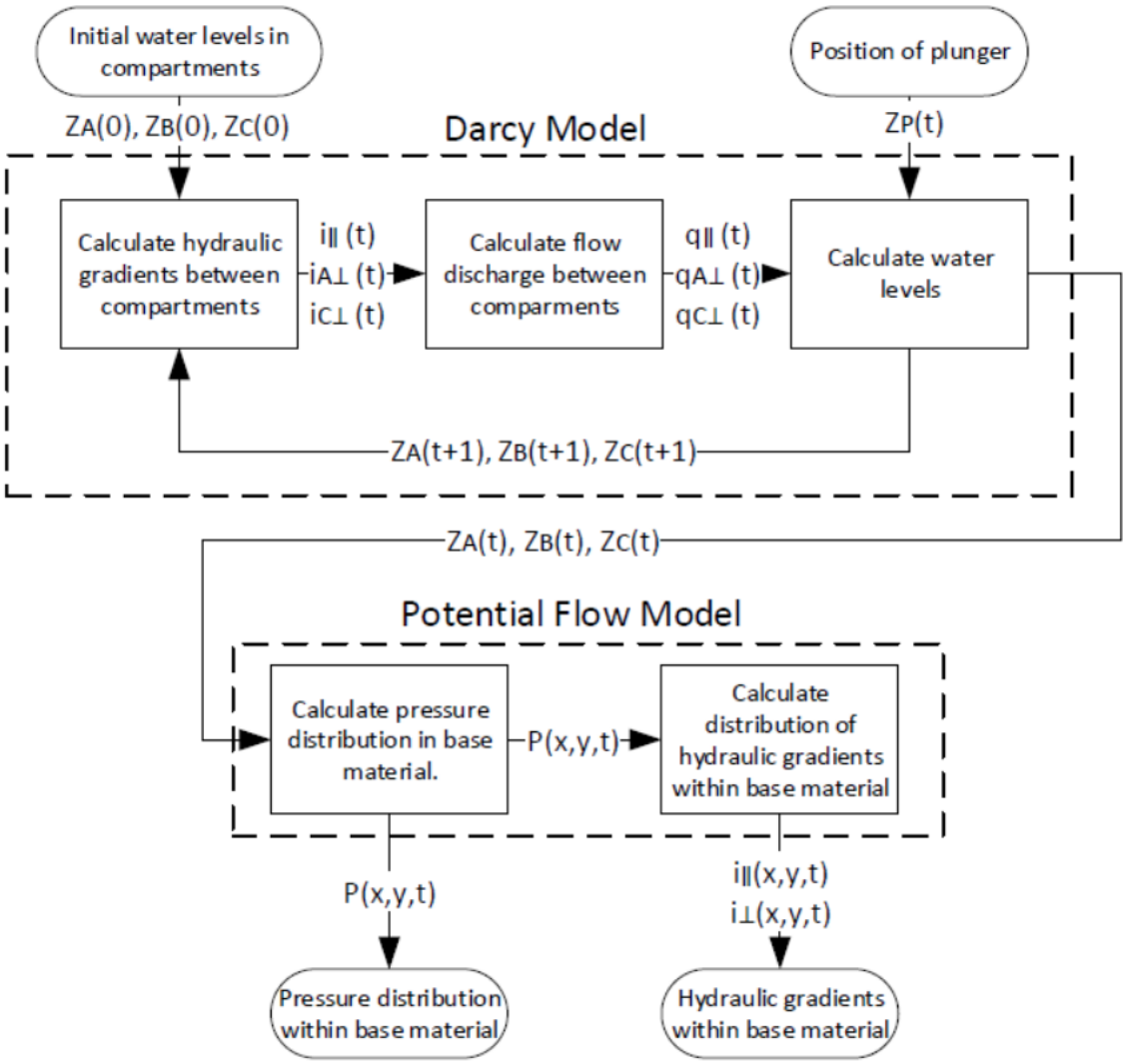

Figure 4.4: The process for the calculation of the pressure and hydraulic gradient distribution within the base material using the numerical model.

5

Analysis of Flow and Hydraulic Gradients

This chapter describes the hydraulic gradients that were measured in the physical model (described in chapter 3) for each model configuration. These measured hydraulic gradients are also compared to the results of the simulations using the numerical model described in chapter 4. The current chapter addresses the perpendicular, combined and parallel configurations.

5.1. Perpendicular Configuration

For the perpendicular tests the connection between compartment B and compartment C was sealed. The top of the base material in compartment B was left open. The expected flow for this configuration is a perpendicular flow in the base material. The configuration can be seen in Figure 5.1.

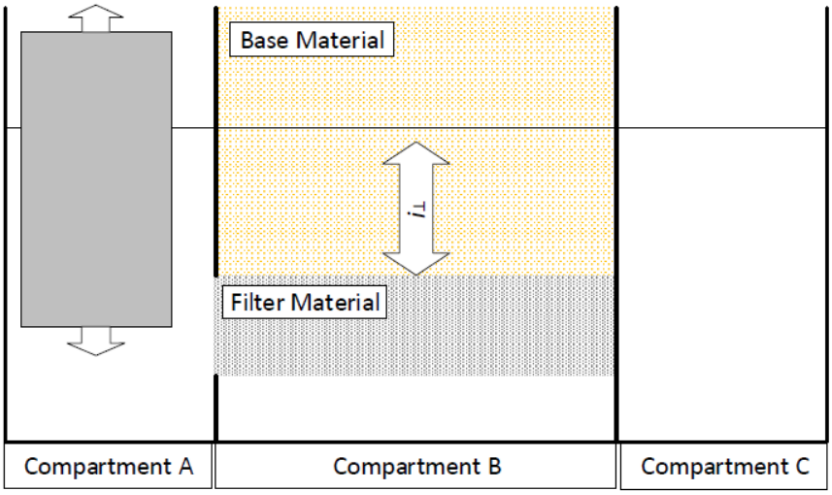

Figure 5.1: The expected flows for the perpendicular configuration.

This section describes the hydraulic gradients that were measured in the physical model and calculated using the numerical model for this configuration. Next the computed spatial distribution of the perpendicular hydraulic gradient is presented.

5.1.1. Measured Hydraulic Gradients

For the perpendicular configuration, only a perpendicular hydraulic gradient was detected using the pressure sensors. The results of the perpendicular hydraulic gradient during a perpendicular test are shown in Figure 5.2.

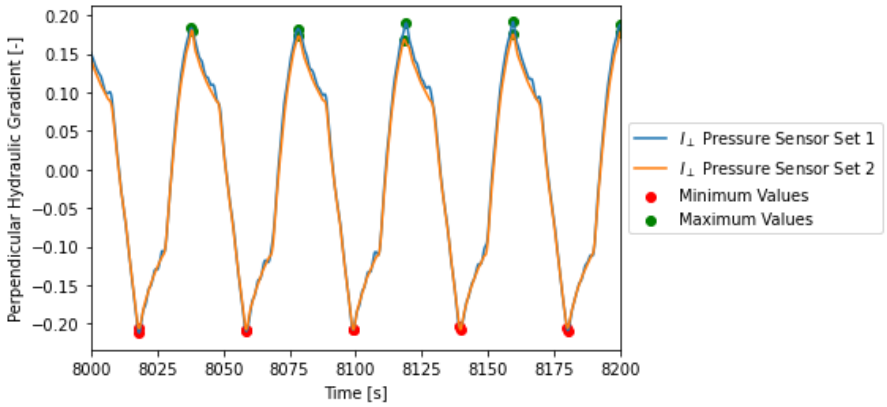

Figure 5.2: An excerpt from perpendicular test 10 showing the achieved hydraulic gradients as measured by the differential pressure sensors.

In Figure 5.2 we can see the perpendicular hydraulic gradient is consistent for each cycle. There are small variations between the two sets of pressure sensors. The variation in the hydraulic gradients measured by the two pressure sensor sets is mostly at the peaks of the signal. To minimise the influence of this variation, the hydraulic gradient for a test phase will be determined by averaging over multiple peak values.

5.1.2. Computed Spatial Distribution of the Hydraulic Gradients

The distribution of the hydraulic gradient within the base material has been analysed using the 2D numerical model. The results of this analysis are presented in Figure 5.3. Figure 5.3a shows the distribution of water pressure within the model expressed as a hydraulic head. Figure 5.3b and Figure 5.3c show the hydraulic gradients within the base material.

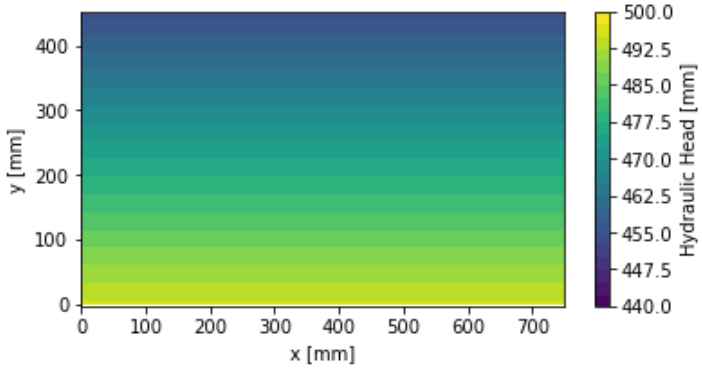

(a) Distribution of hydraulic head [mm]

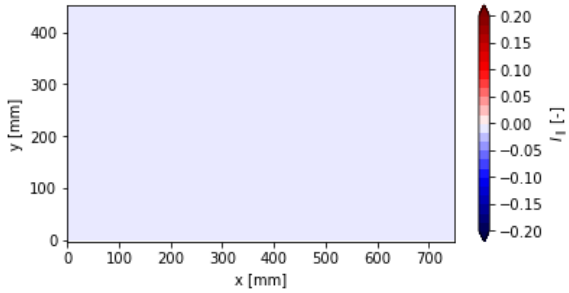

(b) Distribution of the horizontal hydraulic gradients within the base material.

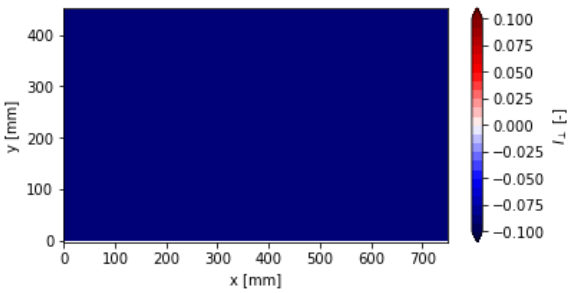

(c) Distribution of the vertical hydraulic gradients within the base material.

Figure 5.3: Numerical analysis of the flow within the base material using the Laplace equation.

Figure 5.3a shows that the hydraulic head within the base material is not constant. The hydraulic head is higher at the bottom of the base material (y=0mm) than the top of the base material (y=450mm). This leads to an upward flow. This can be seen in Figure 5.3c. This figure shows that the perpendicular hydraulic gradient is uniformly distributed and directed upwards. Figure 5.3b shows that there is no parallel hydraulic gradient present. This was expected.

From this analysis we can conclude that distribution of the hydraulic gradients corresponds well with the expectation. This means that the measured hydraulic gradients are representative for the entire filter base interface.

5.1.3. Comparison Measured and Computed Hydraulic Gradients

A comparison has been made between the measured hydraulic gradient during the experiments and the hydraulic gradient calculated using the 1D numerical model. The numerical model has been calibrated by adjusting the permeability of the sand so that the amplitude of the numerical result matches the amplitude of the experimental result.

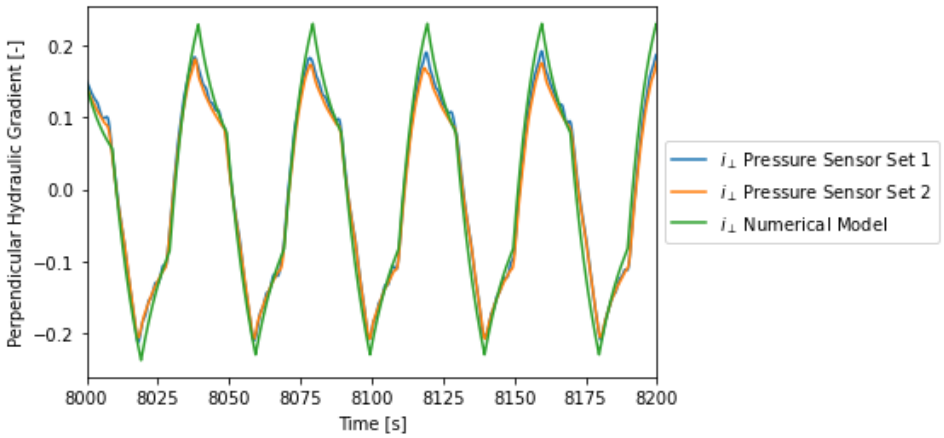

Figure 5.4: Comparison of the measured perpendicular hydraulic gradients and the perpendicular hydraulic gradient calculated by the 1D model. Permeability base = 4 mm/s and porosity base = 0.4

The comparison in Figure 5.4 shows a large correspondence between the hydraulic gradients calculated by the numerical model and the hydraulic gradients measured during the experiments. The permeability of the sand has been used as a tuning parameter. This explains why the magnitude is similar. The shape is also similar, meaning that the development of the hydraulic gradients in time is comparable.

5.2. Combined Configuration

For the combined configuration of the model, the sides of the filter layer and the top of compartment B are left open. The expected flow for this configuration was a combination of perpendicular and parallel flow. This can be seen in Figure 5.5.

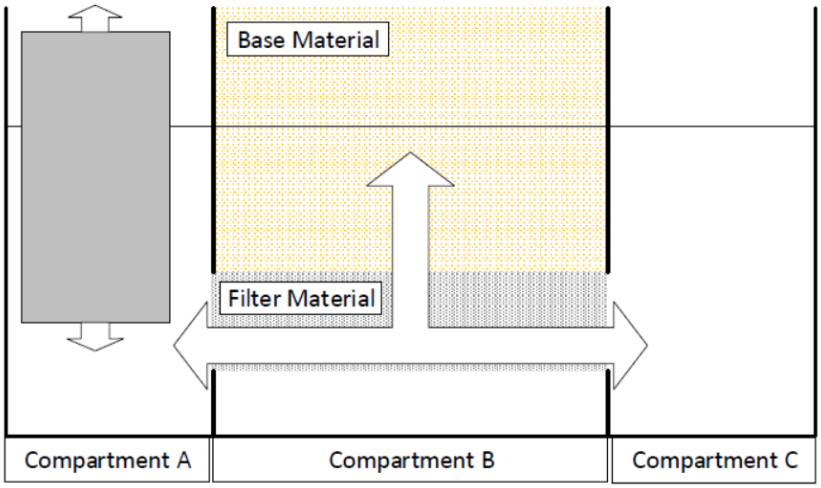

Figure 5.5: The expected flows for the combined model configuration.

This section describes the hydraulic gradients that were measured in the experiments and the hydraulic gradients that were calculated using the numerical model. Then the computed spatial distribution of these hydraulic gradients is presented.

5.2.1. Measured Hydraulic Gradients

The hydraulic gradients present during an experiment are presented in Figure 5.6. The water levels in compartments A and C (measured by the lasers) and hydraulic head within the filter construction (measured by the pressure sensors) were used to calculate the hydraulic gradients.

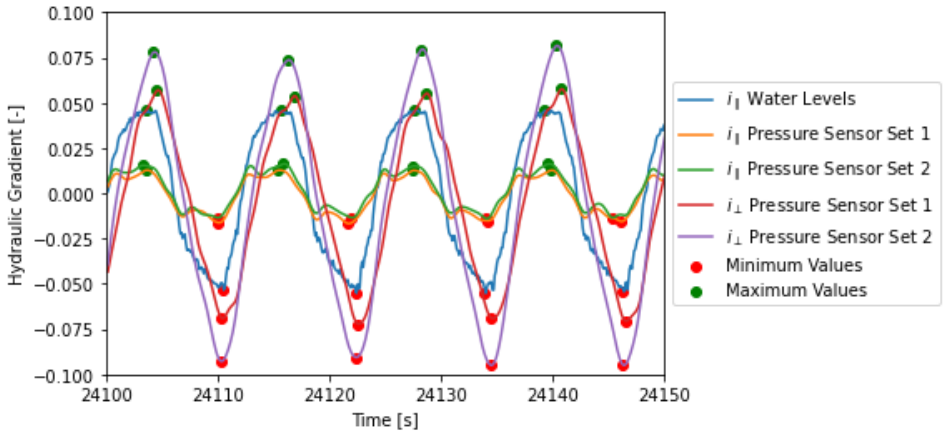

Figure 5.6: Excerpt from combined test 7 showing the achieved hydraulic gradients as measured by the differential pressure sensors or calculated from the water level difference between compartment A and C.

In Figure 5.6 there is a clear difference between the parallel hydraulic gradient measured by the pressure sensors and the parallel hydraulic gradient that is determined by the water level difference. This difference in hydraulic gradient can be explained by the presence of the geotextile at the ends of the filter.

There is a geotextile between each compartment. This geotextile also provides resistance to the flow. This means that the parallel hydraulic gradient determined by the water levels is also influenced

by the flow through the geotextile. As such, the water level difference will overestimate the parallel hydraulic gradient present in the filter.

The hydraulic gradient within the filter is measured directly by the pressure sensors present in the filter. This makes the hydraulic gradient measured by the pressure sensors a more accurate representation of the actual hydraulic gradient across the filter base interface. As such the parallel hydraulic gradient measured by the pressure sensors will be used further in this study.

5.2.2. Computed Distribution of Hydraulic Gradients

As seen in Figure 5.6, there is a combination of perpendicular and parallel hydraulic gradients present in the filter construction. The 2D numerical model explained in chapter 4 was used to simulate the flow within the base material. This was done for a point in time when the water level differences were maximal. The results of this analysis are presented in Figure 5.7. Figure 5.7a shows the distribution of water pressure within the base material. This is expressed as a hydraulic head. Figure 5.7b and Figure 5.7c show the hydraulic gradients within the base material.

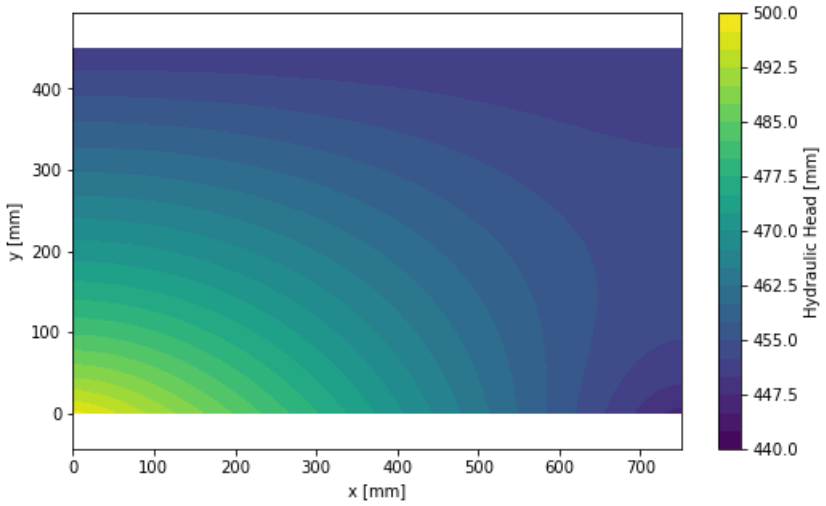

(a) Distribution of hydraulic head [mm]

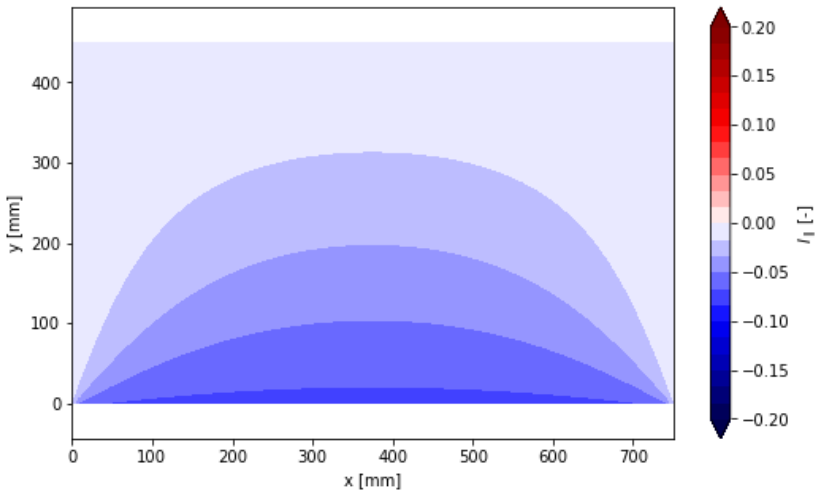

(b) Distribution of the horizontal hydraulic gradients within the base material.

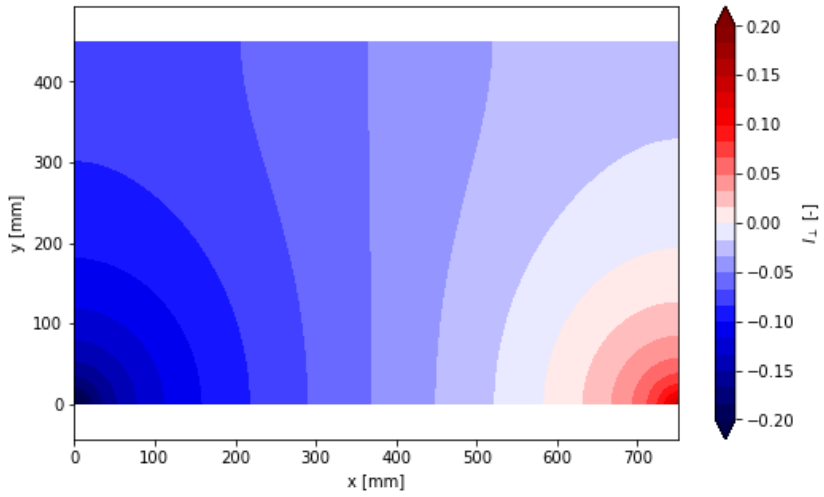

(c) Distribution of the vertical hydraulic gradients within the base material.

Figure 5.7: Combined configuration numerical model results. This is a numerical analysis of the flow within the base material using the Laplace equation.

There is a large difference in hydraulic gradient in different locations within the base material. Along the base filter interface erosion can occur. As such in this location the hydraulic gradient is most interesting.

The maximum amplitude of the perpendicular hydraulic gradient across the interface was closest to compartment A. Therefore, for a combined configuration test, erosion would be expected closest to compartment A. This is in line with the result of Test 7. This was the only combined test with erosion. During this test, the erosion occurred close to compartment A.

Figure 5.8 shows the perpendicular hydraulic gradients during one cycle of the plunger. Different ways of representing the perpendicular hydraulic gradient within the filter are shown.

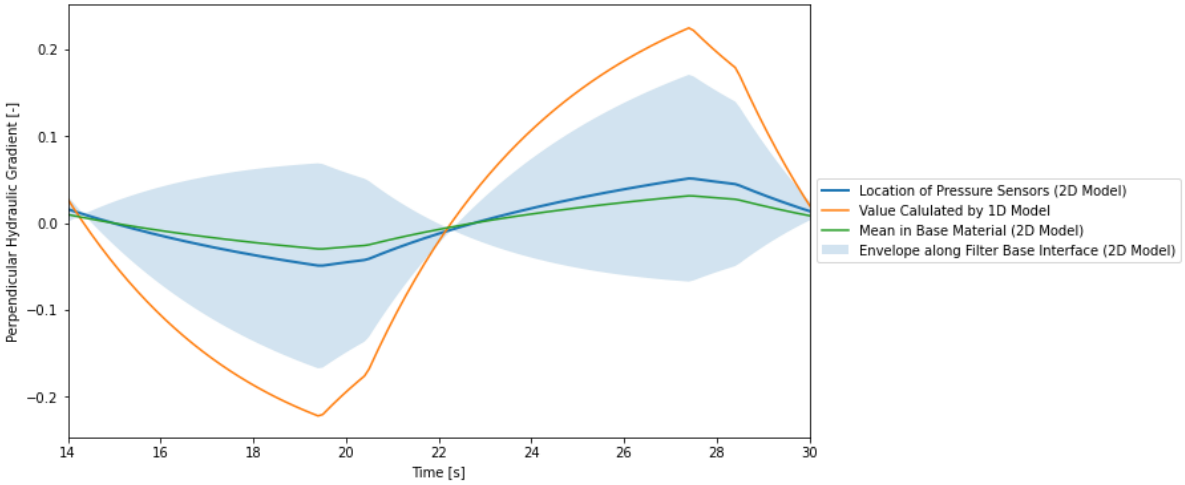

Figure 5.8: Magnitude of hydraulic gradients at different locations within the base material according to the numerical model during a single cycle of the plunger.

The following observations are made about Figure 5.8:

- The perpendicular hydraulic gradient at the location where the pressure sensors are, exactly matches the mean perpendicular hydraulic gradient across the filter base interface.
- The perpendicular hydraulic gradient averaged over the entire base material, is less than the perpendicular hydraulic gradient averaged across the base filter interface. This is due to a flow from compartment A to compartment C through the base material. This flow is neglected in the 1D numerical model.

- The value for the perpendicular hydraulic gradient calculated by the 1D numerical model should correspond with the mean perpendicular hydraulic gradient across the interface. Both of these values represent the total flow in and out of the base material. These values do not correspond with each other. This is likely due to an important component of the flow being neglected in the 1D model.
- The envelope of the perpendicular hydraulic gradient along the filter base interface has a magnitude four times larger than the value at the location of the pressure sensors. Erosion will occur due to the maximal value of the hydraulic gradient across the interface. As such the envelope of the hydraulic gradients is governing. This means that governing value for the perpendicular hydraulic gradient is four times larger than than the measured value. For the remainder of the report, the measured perpendicular hydraulic gradients in combined configuration tests will be increased by a factor of four to adjust for this difference.

5.2.3. Comparison Measured and Computed Hydraulic Gradients

A comparison is also made with the 1D numerical model see Figure 5.9.

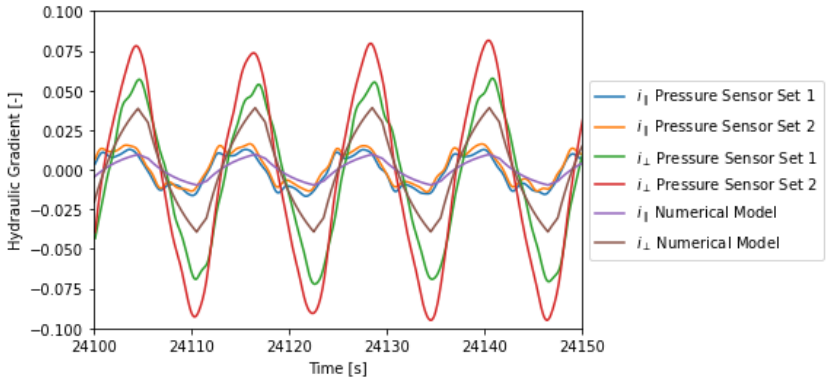

Figure 5.9: Comparison of the measured hydraulic gradients and the hydraulic gradients calculated using the 1D numerical model for test 7. The presence of the geotextile is neglected. Permeability filter = 300 mm/s, permeability base = 6 mm/s and porosity base = 0.4

From Figure 5.9 we can see that the numerically computed hydraulic gradients are significantly different in shape from the measured hydraulic gradients. The amplitudes of the hydraulic gradients are similar. However, this is what the numerical model is calibrated on. Therefore it is expected that the amplitudes are equal. The different shape then indicates that there is not a good correspondence between the numerical and physical models.

This poor correspondence could be expected for two reasons. (1) The inertial & turbulent flow effects are neglected within the numerical model. These processes are significant within the filter. This can be computed with the Keulegan–Carpenter number and Reynolds number. (2) The geotextile separating the compartments in not modelled. This geotextile has an effect on the flow within the filter construction.

5.3. Original Parallel Configuration

In the parallel test setup the top of compartment B was sealed and both sides of the filter open. This is shown in Figure 5.10. For this configuration, it was expected that there would be a parallel flow between compartments A and C through the filter layer.

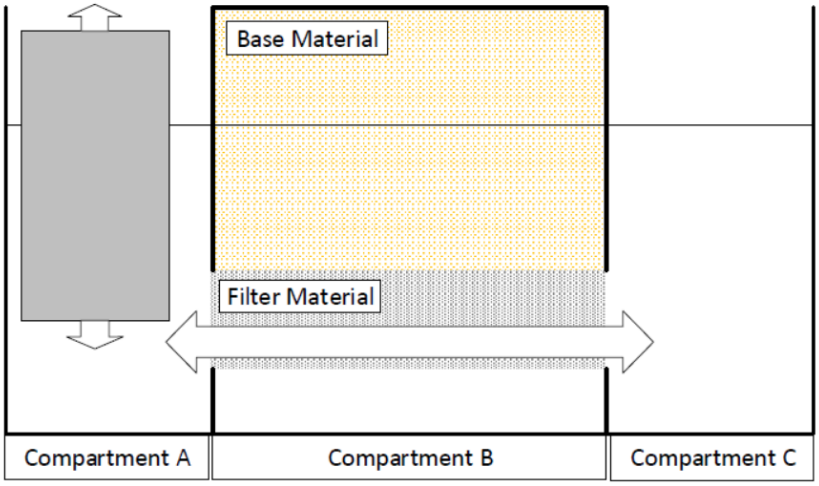

Figure 5.10: Expected flow within the experimental setup when this is in the parallel configuration.

This section will present the hydraulic gradients measured during the tests and present the analysis of the flow calculated using the numerical model.

5.3.1. Hydraulic Gradients Measured

The hydraulic gradients measured during a typical parallel test are presented in Figure 5.11. In this figure, the hydraulic gradients calculated from the pressure sensors and the water levels are shown. This is shown for a portion of a typical parallel configuration test (test 3).

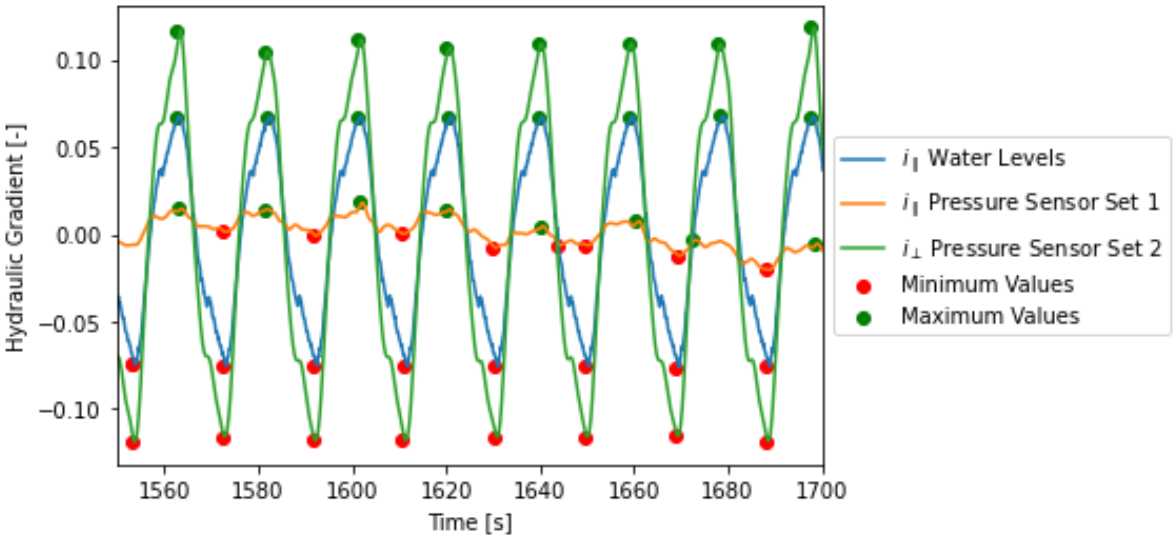

Figure 5.11: Excerpt of parallel test 3 showing the hydraulic gradients measured.

In Figure 5.11 it can be observed that there is a significant perpendicular hydraulic gradient as well as the expected parallel hydraulic gradient. This was the case in all parallel configuration tests.

Two options could explain the presence of the perpendicular flow. Both explanations relate to the air trapped in the base material. Either this area is not properly sealed and air leaks out of the model,

or the compression of this air pocket is relevant. For the compression of air, a build-up of pressure is required. If air can leak out of the model then no pressure can build up. As such, leaking of air is the most likely cause for the perpendicular hydraulic gradient during the parallel configuration tests.

It is also observed that there is a difference between the hydraulic gradient calculated from the water levels and the hydraulic gradient calculated from the pressure sensors. As explained in section 5.2, this is due to the effect of flow through the geotextile which separates the compartments. The hydraulic gradient calculated from the pressure sensors is representative of what happens within the filter layer. This hydraulic gradient will be used further in this study.

5.3.2. Distribution of Hydraulic Gradients

To gain insight the 2D numerical model has also been used to calculate the spatial distribution of the perpendicular hydraulic gradient within the base material if there is a leak at a single location. Two situations with a leak in different locations have been calculated. The results of these analyses are presented in Figure 5.12a and Figure 5.12b.

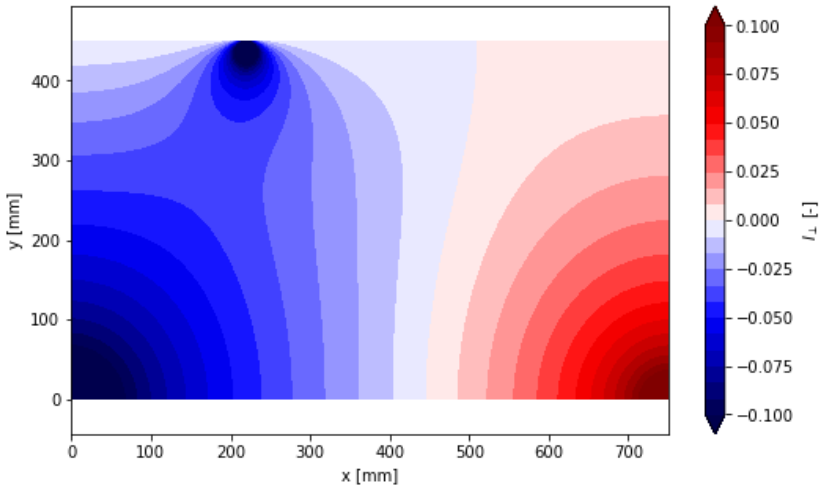

(a) For a situation with the leak at x=23cm.

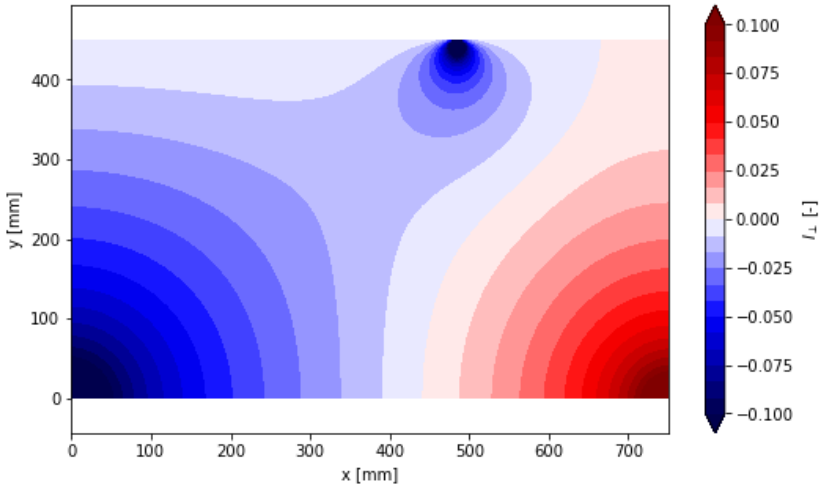

(b) For a situation with the leak at x=50cm.

Figure 5.12: 2D numerical model results for the distribution of the perpendicular hydraulic gradient ($I_\perp$) within the base material in a parallel setup with a leak.

In Figure 5.12 we can see that the location of the leak has a significant influence on the distribution of the hydraulic gradients within the model. The perpendicular hydraulic gradient was measured only in one location. Therefore we cannot reconstruct that flow pattern within the base material to determine the location of the leak. There is most likely leaking in more one location which is an extra unknown in

determining the distribution of the flow. This is likely further complicated due to 3D effects of the leak.

We must take note that the perpendicular hydraulic gradients present are an order of magnitude larger than the parallel hydraulic gradients present. Therefore the perpendicular hydraulic gradients are a significant part of the flow field in these parallel tests. This perpendicular hydraulic gradient cannot be ignored.

From this we can conclude that the results of the parallel tests are unreliable. This is because the determined perpendicular hydraulic gradient is inaccurate and is significant enough to possibly be governing. The parallel hydraulic gradient can be accurately determined. However, this likely is not governing.

5.4. Modified Parallel Configuration

A modified parallel configuration was made where the top seal is below the level of the water. This configuration was made to test whether the cause of the perpendicular hydraulic gradients in the parallel configuration is due to the leaking of air or due to the compression of the air present. The configuration is shown in Figure 5.13.

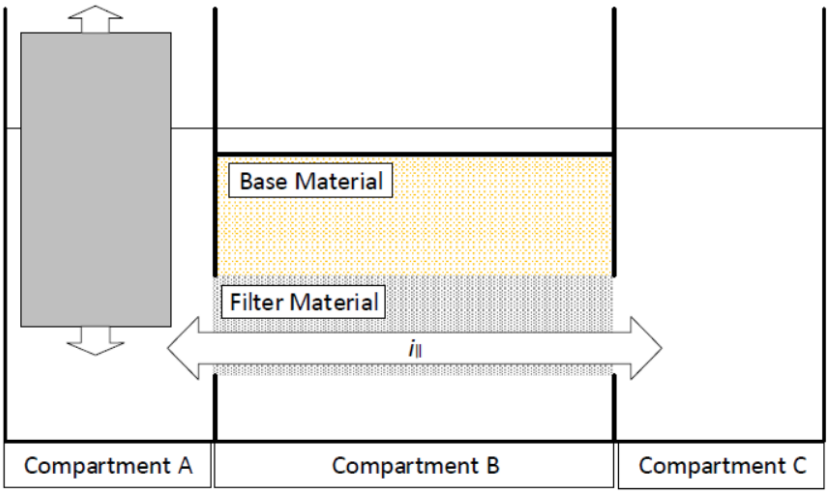

Figure 5.13: The expected flows for the modified parallel configuration.

As seen in Figure 5.13 there is now a seal below the water level. Due to the seal now being below the water level, there is no air to compress. If the model leaks this can be visually observed as water will now leak out of the model. The hydraulic gradients measured during this test are shown in Figure 5.14.

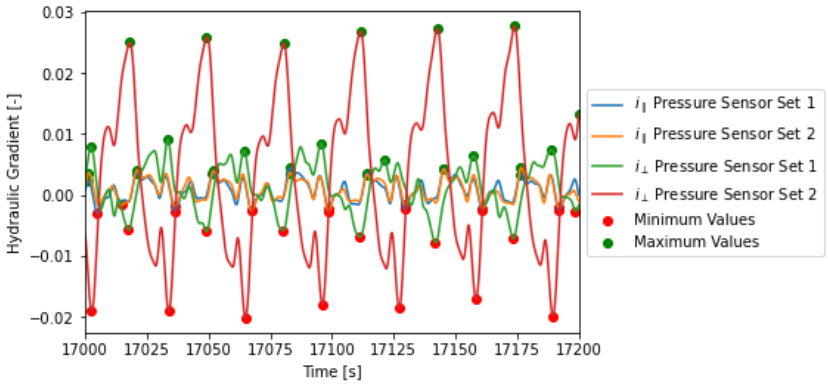

Figure 5.14: The hydraulic gradients measured in the model after it started leaking. This is test 24.

In Figure 5.14 a perpendicular hydraulic gradient is observed. This means that there was a leak in this configuration. This leak of water was also visually observed and developed over the first hour

of the test. The location(s) of the leak(s) is unknown. The distribution of the hydraulic gradient within the base material depends on the location of the leak. Therefore the distribution of the perpendicular hydraulic gradient is unknown.

5.5. Recommended Parallel Configuration

A further modified configuration has been analysed using the numerical model. In this configuration, the sides of the base material are also open for the flow of water. The configuration is shown in Figure 5.15.

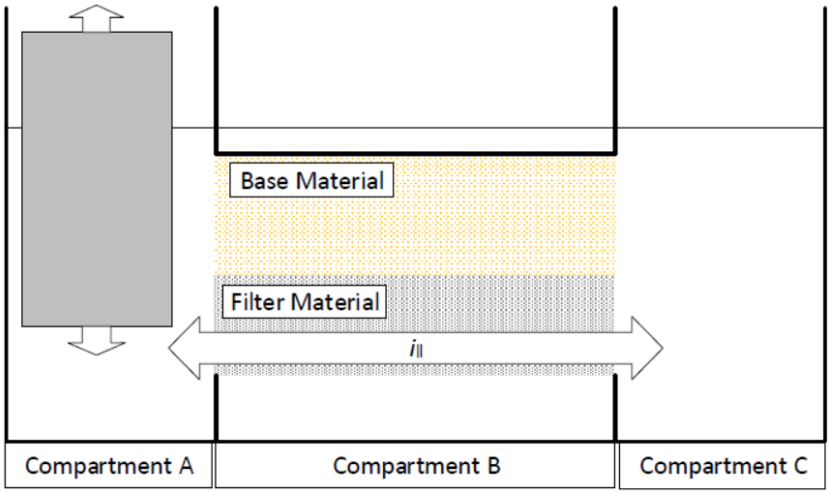

Figure 5.15: The expected flows for the recommended parallel configuration.

The setup shown above should be less sensitive to leaking. This has been analysed with the 2D numerical model. A leak was introduced at x=210mm. The resulting flows within the base material are shown in Figure 5.16. This figure shows a moment in time when the hydraulic gradients are maximal. Figure 5.16a shows the hydraulic head within the base material. Figure 5.16b shows the parallel hydraulic gradient within the base material. Figure 5.16c shows the perpendicular hydraulic gradient within the base material.

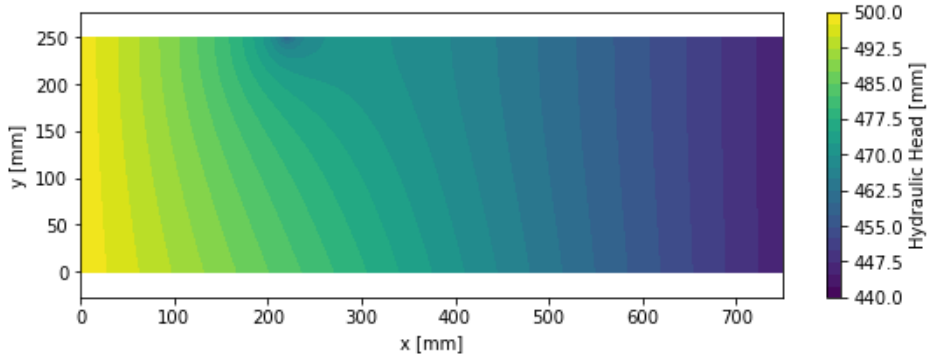

(a) Plot showing the distribution of the hydraulic head in mm within the base material.

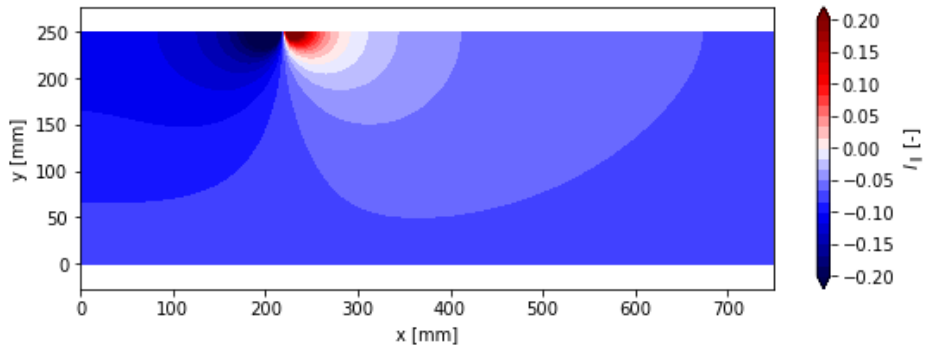

(b) Plot showing the distribution of the parallel hydraulic gradient within the base material.

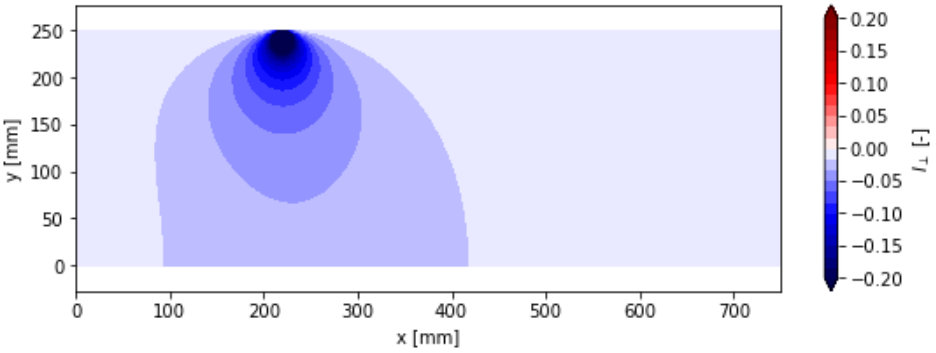

(c) Plot showing the distribution of the perpendicular hydraulic gradient within the base material.

Figure 5.16: Results of 2D numerical model for the recommended parallel setup when there is a leak in the top seal

From Figure 5.16 it is observed that even when there is a leak present, the parallel hydraulic gradient is an order of magnitude larger than the perpendicular hydraulic gradient. This is because the leak now minimally influences the perpendicular hydraulic gradient. This is in contrast with the results of experiments performed during this study, where the perpendicular hydraulic gradient was always larger than the parallel hydraulic gradient.

With the ratio of hydraulic gradients in the recommended configuration, a minimal influence of the perpendicular hydraulic gradient can be expected. As such, testing for a critical parallel hydraulic gradient is possible. As such this configuration is recommended for further research into the critical parallel hydraulic gradient.

5.6. Conclusions

From the analysis of the hydraulic gradients within the experimental setup the following can be concluded:

- The hydraulic gradients determined by the differential pressure sensors give the best and most reliable value for the hydraulic gradients within the physical model.
- In combined configuration tests, the maximum perpendicular hydraulic gradient was four times as large as the measured value. For the remainder of this report, the measured perpendicular critical hydraulic gradient during combined tests is corrected for with this factor in the presented results.
- For the perpendicular configuration the perpendicular hydraulic gradients are uniform within the model. Therefore, the measured value of perpendicular hydraulic gradient was representative for the entire filter base interface.
- Due to the leaking of the parallel configuration, the parallel configuration results cannot be used to determine the critical parallel hydraulic gradient.

6

Results of Physical Model Tests

This section describes the determination of the critical hydraulic gradients from the physical model tests. First, the critical hydraulic gradient is defined. Then the results of the 24 model tests are presented.

6.1. Definition of Critical Hydraulic Gradient for this Study

The critical hydraulic gradient is defined as the hydraulic gradient which is present when an open filter is no longer stable. In the tests performed in this study, the hydraulic gradient was increased in steps between the segments of each test. This study investigates the moment that erosion starts occurring. This is difficult to determine exactly. The criterion used to define this was: *As soon as there is a noticeable difference in the time-lapse images. This counts as erosion*.

If erosion occurred this test segment then became the erosional segment of the test. The hydraulic gradient present in this segment is considered the upper bound for the critical hydraulic gradient. The hydraulic gradient from the segment before is considered the lower bound for the critical hydraulic gradient.

If no erosion occurred during a test no upper bound could be found. The last segment (which had the highest hydraulic gradients present) was used as the lower bound for the critical hydraulic gradient.

6.2. Model Tests Performed

This section contains a summary of all the tests. The data files for each test are uploaded to the TU Delft education repository. Table 6.1 contains the setup of each test. Table 6.2 contains the results of each test.

Test	Configuration	SR [-]	Surcharge [kPa]	Base-Filter Combination
1	Parallel	7.2	0	Base 1& Filter 1
2	Parallel	7.2	0	Base 1& Filter 1
3	Parallel	7.2	0	Base 1& Filter 1
4	Parallel	7.2	0	Base 1& Filter 1
5	Parallel	10.5	0	Base 2& Filter 1
6	Parallel	10.5	0	Base 2& Filter 1
7	Combined	7.2	0	Base 1& Filter 1
8	Combined	7.2	0	Base 1& Filter 1
9	Perpendicular	7.2	0	Base 1& Filter 1
10	Perpendicular	10.5	0	Base 2& Filter 1
11	Perpendicular	10.5	0	Base 2& Filter 1
12	Perpendicular	12.2	0	Base 1& Filter 2
13	Perpendicular	10.5	0	Base 3& Filter 5
14	Perpendicular	12.2	100	Base 1& Filter 2
15	Perpendicular	12.2	200	Base 1& Filter 2
16	Perpendicular	12.2	100	Base 1& Filter 2
17	Perpendicular	10.5	100	Base 2& Filter 1
18	Combined	7.2	100	Base 1& Filter 1
19	Combined	7.2	200	Base 1& Filter 1
20	Perpendicular	12.1	100	Base 2& Filter 4
21	Perpendicular	12.1	200	Base 2& Filter 4
22	Perpendicular	11.2	100	Base 1& Filter 3
23	Perpendicular	11.2	200	Base 1& Filter 3
24	Parallel Reduced Height	12.2	0	Base 1& Filter 2

Table 6.1: Setup of all model tests performed.

Test	Notes	Result	LB $I_{\perp}$ [-]	UB $I_{\perp}$ [-]	LB $I_{\parallel}$ [-]	UB $I_{\parallel}$[-]
1		Test Failed				
2		Erosion after 4 hours	0.085	0.10	0.0067	0.0093
3	Long test	No Erosion	0.12		0.0067	
4		Erosion after 4.2 hours	0.05	0.051	0.0064	0.0065
5		Test Failed				
6		Erosion after 5.5 hours	0.065	0.054	0.0055	0.0069
7		Erosion after 6.5 hours	0.064	0.071	0.011	0.015
8	Long test	No Erosion	0.066		0.013	
9		No Erosion	0.29			
10		Erosion after 2.5 hours	0.12	0.19		
11	Long test	No Erosion	0.23			
12		Erosion after 2 hours	0.056	0.068		
13		Erosion after 4 hours	0.09	0.13		
14		Erosion after 4.5 hours	0.12	0.13		
15		Test Failed				
16		Erosion after 4.5 hours	0.10	0.12		
17		No Erosion	0.21			
18		No Erosion	0.058		0.0048	
19		No Erosion	0.07		0.005	
20		erosion after 4 hours	0.15	0.16		
21		No Erosion	0.19			
22		No Erosion	0.18			
23		No Erosion	0.24			
24		Erosion after 4.5 hours	0.015	0.015	0.0032	0.0039

Table 6.2: Results of all tests performed.

6.3. Effect of the Stability Ratio on the Critical Hydraulic Gradient

The effect of the stability ratio[1] on the critical hydraulic gradient of an open inverted filter has been investigated. In order to determine the influence of the stability ratio tests were performed without a surcharge where the stability ratio was varied. This section presents the found perpendicular critical hydraulic gradients and the parallel critical hydraulic gradients.

6.3.1. Perpendicular Hydraulic Gradients

This section presents the critical perpendicular hydraulic gradients found during testing in this study. It compares these results with the previous results in the research line and determines a trend between the stability ratio and the critical perpendicular hydraulic gradient.

Perpendicular Configuration Tests Figure 6.1 presents the results of the perpendicular tests. The x-axis shows the stability ratio. This is the primary strength parameter of the filter. A stability ratio below 5 complies with the filter rules defined by the Rock Manual (CIRIA et al., 2007) and thus is a closed filter. This is considered stable for all hydraulic gradients. The y-axis shows the perpendicular hydraulic gradient. This is the main loading parameter. Each test is plotted with an upper and a lower bound for the critical hydraulic gradient as described in section 6.1. The results of the perpendicular configuration tests are plotted in blue.

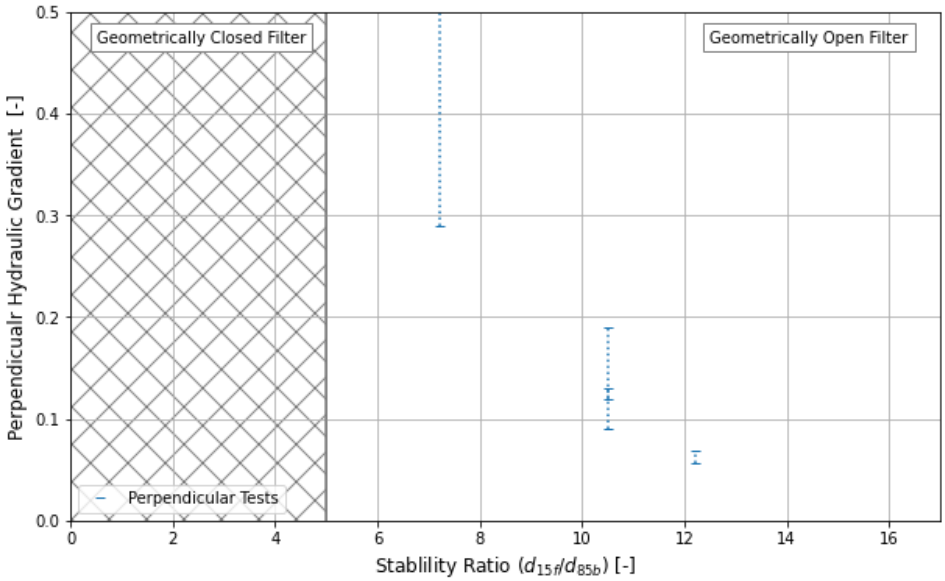

Figure 6.1: The critical hydraulic gradient for perpendicular flow with different stability ratios.

Figure 6.1 shows the results for four tests. In three of these tests, erosion was detected and a range for the critical perpendicular hydraulic gradient was found. For the test with a stability ratio of 7.2, no erosion was detected. Therefore only a lower bound was found.

These results indicate a clear negative correlation between the critical perpendicular hydraulic gradient and the stability ratio because tests with a higher stability ratio show a smaller critical perpendicular hydraulic gradient.

Combined Configuration Test Figure 6.2 shows the perpendicular hydraulic gradient from the combined test (test 7). This is plotted in orange. The combined test has been adjusted as the measured value has been increased by a factor of four to convert it to the maximum value of the perpendicular hydraulic gradient across the interface (see chapter 5).

[1] This is the ratio between the size of the exceeded by 15% of the base particles (by mass) and 85% of the filter particles (by mass).

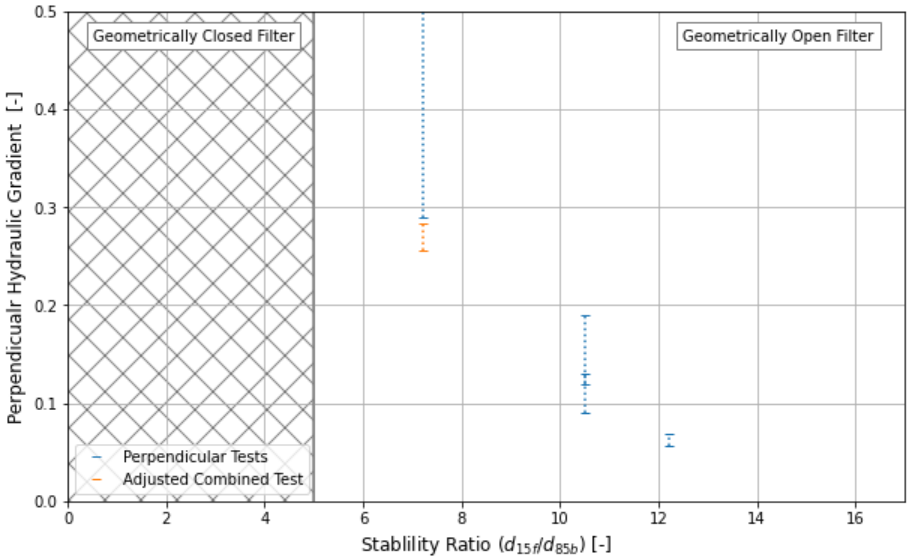

Figure 6.2: The critical perpendicular hydraulic gradient for perpendicular and combined flow with different stability ratios.

The adjusted perpendicular hydraulic gradient from the combined configuration test appears to be in line with the results of the perpendicular tests.

Comparison with Previous Studies in the Research Line Previous studies in this research line also determined a critical perpendicular hydraulic gradient for specific stability ratios. These results are shown along with the results of the current study in Figure 6.3.

Van de Ven (2019) performed perpendicular configuration tests. The critical perpendicular hydraulic gradient determined in these tests is plotted in green.

Boersma (2020) performed tests with a combined configuration. These results are plotted in pink. Like with the current study, the critical perpendicular hydraulic gradients found during the combined configuration tests by Boersma (2020) have been increased by a factor of four. This was done as the hydraulic gradient was not measured in the location where the maximum perpendicular hydraulic gradients occurred (see chapter 5).

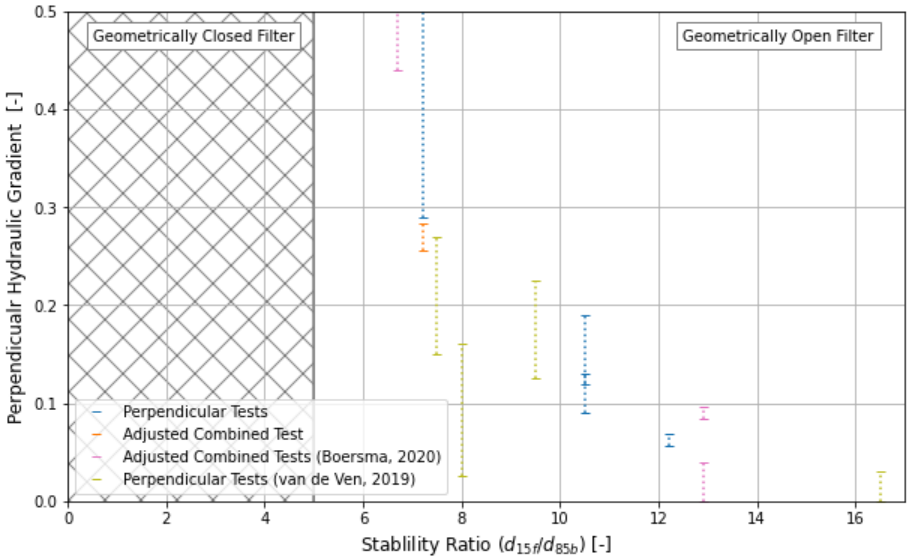

Figure 6.3: The critical perpendicular hydraulic gradient for perpendicular and combined model configurations with different stability ratios, compared with results from other studies in this research line.

The adjusted perpendicular hydraulic gradients in the combined configuration tests from Boersma (2020) appear to be in line with the trend of the results from the current study.

The critical perpendicular hydraulic gradients determined by Van de Ven (2019) do not all appear in line with the results from Boersma (2020) and the current study. In particular, the test by Van de Ven (2019) with a stability ratio of 8 especially has a lower critical perpendicular hydraulic gradient than the results in the other studies. Boersma (2020) found the results of Van de Ven (2019) to be influenced by an initial saturation of base material in the filter layer. This saturation resulted in a false indication of erosion before this occurred. This is likely why the critical perpendicular hydraulic gradients determined by Van de Ven (2019) are lower than the critical perpendicular hydraulic gradients determined by Boersma (2020) and in the current study.

Determination of Trend The relationship between stability ratio and critical perpendicular hydraulic gradient has two physical limits. (1) If the filter is geometrically closed, then there is an infinite critical hydraulic gradient. (2) The critical hydraulic gradient cannot be negative. To comply with these limits a hyperbolic equation is fitted for the relationship between the critical perpendicular hydraulic gradient and the stability ratio. For this the following equation is used:

$$i_{\perp,crit} = \frac{a}{SR - b} \tag{6.1}$$

Parameter a is a scale factor for the hyperbolic and parameter b is the vertical asymptote. The vertical asymptote describes when a filter becomes geometrically closed. The scale factor determines the critical gradient of the open filter. These parameters were fitted using a least-squares approach with the Curve_fit function from the SciPy package in Python.

This fitting used the critical perpendicular hydraulic gradients determined in the following tests: The perpendicular tests by Van de Ven (2019), the combined tests by Boersma (2020), the combined tests from this study, and the perpendicular tests from this study. Some of these tests are more reliable than others. In order to account for this a weighted fit was performed. The weights used are presented in Table 6.3.

Source of Result	Weight Applied
Perpendicular configuration	1
Combined configuration	1
Perpendicular configuration (Van de Ven, 2019)	0.25
Combined configuration (Boersma, 2020)	0.5

Table 6.3: Weights of test results used in fitting trend between stability ratio and the critical perpendicular hydraulic gradient.

The data points used for the fitting are plotted in Figure 6.4. The colour of the point shows from which type of test the result is. The shape indicates the result of the test. For tests where both an upper and lower bound have been determined the mean of these two values is used. This is shown on the plot as an ”X”. For tests where only a lower bound for the critical hydraulic gradient was determined, this value was used. This is plotted as a ”∇”.

The trend is plotted as a grey line in Figure 6.4. A 95% confidence interval[2] has been calculated. The confidence interval is plotted as the blue shaded region. The 95% prediction interval[3] has also been calculated. The upper and lower limit of the prediction interval is plotted as a dashed grey line.

[2] There is a 95% certainty that the trend lies within this region. The confidence interval is calculated using the student T distribution as the variance of the true critical gradient is unknown.

[3] This gives a 95% chance that a new data point will lie within this bounds.

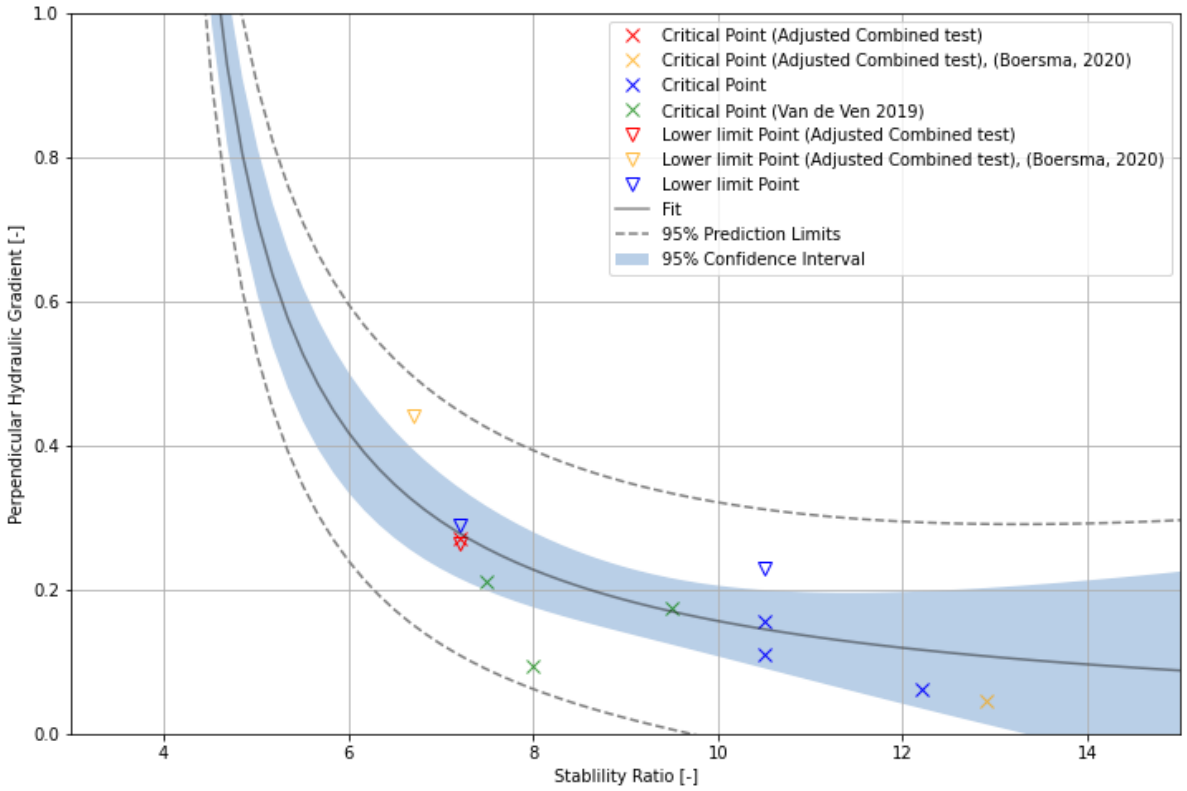

Figure 6.4: A determination of the trend between the stability ratio (SR) and the critical perpendicular hydraulic gradient. The uncertainties of the points can be seen in Figure 6.3.

The following observations were made about the fitting of the trend:

- The trend is negative. The uncertainty of the trend increases with an increasing stability ratio. For higher stability ratios this uncertainty is quite significant. This applies to the prediction limits and the confidence interval.
- The vertical asymptote of the fit is SR 3.6, which corresponds to a geometrically closed filter. This is significantly smaller than when a filter is generally considered geometrically closed.
- It is important to note that both the results with and without erosion were used. This means that critical hydraulic gradients and lower bounds for the critical have been included. Therefore the results of this fit may be more conservative than necessary.

6.3.2. Parallel Hydraulic Gradients

In this section, the critical parallel hydraulic gradient determined with the combined and parallel configuration tests are presented. The results from this study are presented, along with the results from Boersma (2020) and Van de Ven (2019). These results are presented in Figure 6.5. It is important to note that for each parallel test, a perpendicular hydraulic gradient was present. The magnitude of this perpendicular hydraulic gradients is unknown.

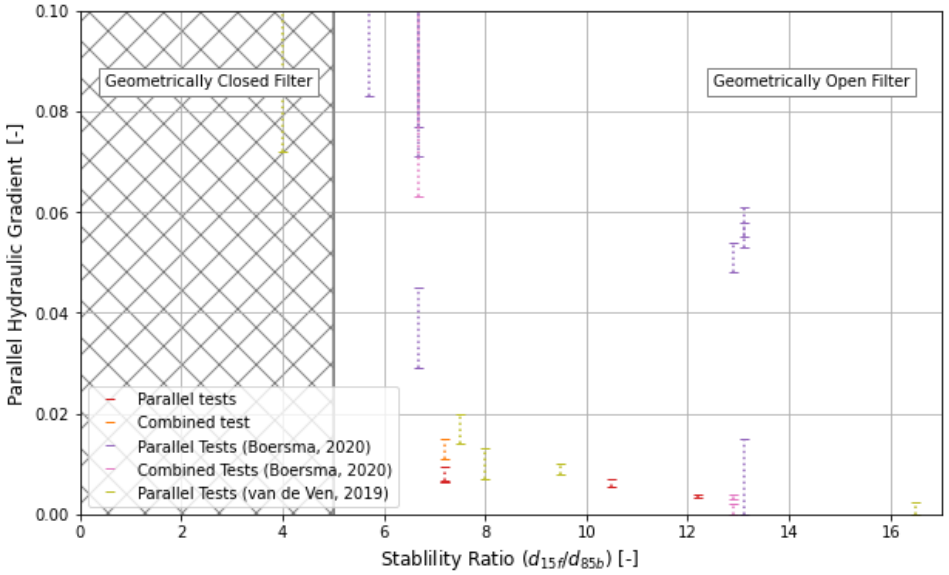

Figure 6.5: The critical parallel hydraulic gradient for parallel and combined flow with different stability ratios. Compared with previous results from this research line.

The following observations were made about critical parallel hydraulic gradients as shown in Figure 6.5:

- A large variation in the critical parallel hydraulic gradient was found in all tests. No clear trend can be determined.
- In all parallel tests in this research line there was leak,[4] which leads to perpendicular hydraulic gradients.
- All tests had a combination of perpendicular and parallel hydraulic gradients. There is a different ratio between perpendicular and parallel hydraulic gradients for each test.
- For all tests where the perpendicular component of the hydraulic gradient is known, this perpendicular component fits the trend found.

From these observations, it can be concluded that in all tested cases the perpendicular component of the hydraulic gradient is governing. It also can be concluded that, for these tests the parallel hydraulic gradient does not influence the critical perpendicular hydraulic gradient.

[4] Both Boersma (2020) and Van de Ven (2019) mention a visual observation of leaking in their recommendations chapter.

6.4. Influence of a Surcharge on the Critical Perpendicular Hydraulic Gradient

Arching within the base material is the main mechanism that explains the stabilisation of the interface between the base and filter material. The level of effective stress in the filter base interface influences the friction in the arches. Increased friction means an increased force is required to dislodge a particle form an arch. To quantify this influence, perpendicular tests with different levels of surcharge have been performed. The results are shown in Figure 6.6.

The blue markers are the perpendicular tests that were performed without surcharge from the hydraulic press. Green shows tests with a surcharge of 100kPa and magenta shows tests with a surcharge of 200kPa. Tests where erosion occurred are shown by both limits of the uncertainty. In the tests where no erosion occurred only the lower bound value is shown.

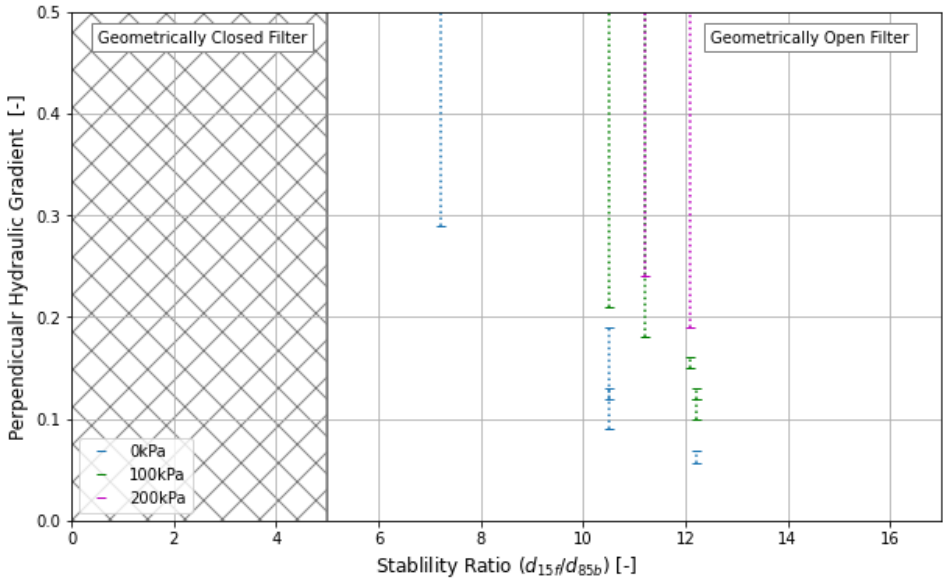

Figure 6.6: The critical hydraulic gradient for perpendicular flow with varying amounts of surcharge.

The following observations are made about Figure 6.6:

- A difference in the achieved maximum hydraulic gradient was observed. This is due to the slippage in the plunger mechanism, which increased throughout the study and caused the achievable hydraulic gradient to decrease during the study.
- In most tests no erosion was detected. A critical value was only found for the tests with a high stability ratio or a limited surcharge.
- Tests with a stability ratio of between 10 and 12 show a significant increase in the critical perpendicular hydraulic gradient.

Determination of a Trend The effect of an increased surcharge is also shown in Figure 6.7. In this figure the surcharge applied to the base material is shown on the x-axis. The y-axis shows the critical perpendicular hydraulic gradient relative to the tests without surcharge. The critical hydraulic gradient for a given stability ratio is taken from the trend determined in Figure 6.4.

A linear trend has been found using a least squares approach. This trend is shown with the grey line. The 95% confidence interval [5] for the mean has been determined. This is shown by the shaded region. The prediction limits shown by the grey dashed line give a 95% chance that a new value is within these bounds.

A point at which a critical gradient was determined is shown by a cross. A tests where no erosion was detected is shown with a triangle. This indicates a lower bound for the critical hydraulic gradient. The uncertainty of these values can be found in Figure 6.6.

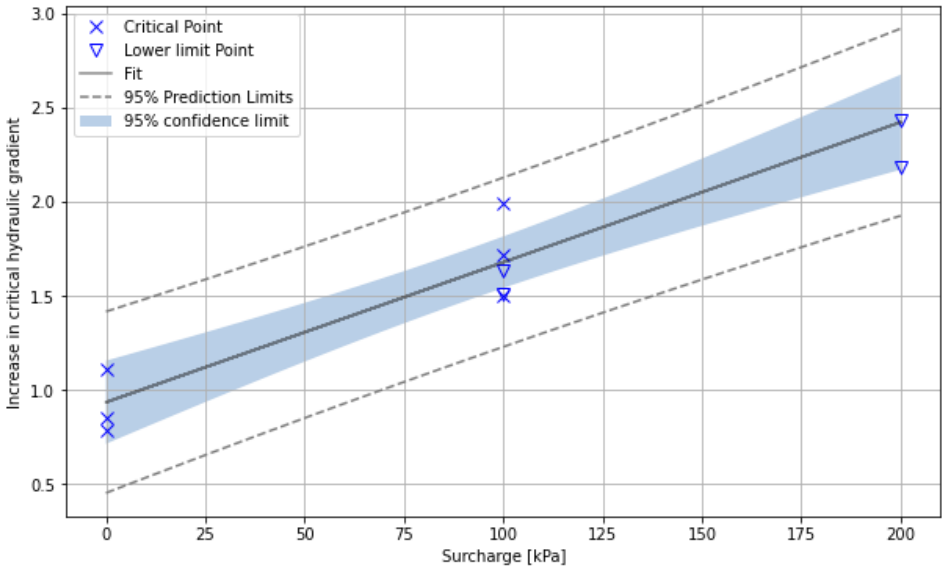

Figure 6.7: Determination of a trend for the factor that the effective stress in the filter base interface influences the critical perpendicular hydraulic gradient.

The following observations are made about Figure 6.7:

- When surcharge is applied to the filter construction, a positive trend is observed. This shows that an increased effective stress leads to a stabilising effect on the filter.
- Both critical and lower bound values have been included. With increasing surcharge there are more lower bound values. These values give an under estimation of the critical hydraulic gradient. Therefore this trend is likely conservative.
- The trend does not go through one with zero surcharge. This is a result of including the data points without surcharge in the fit. These data points do not correspond exactly to the determined relationship between SR and $i_{\perp,cr}$. To take this uncertainty into account these baseline tests are also included.
- The uncertainty of this trend is limited. The confidence limit shows only $\pm$10% at the the highest surcharge tested.

[5] There is a 95% certainty that the trend lies within this region. The confidence interval is calculated using the student T distribution as the variance of the true critical gradient is unknown.

6.5. Influence of the Angularity of the Base Material on the Critical Hydraulic Gradient

The angularity of the base material is a factor which is expected to influence the strength of the arching of the base material. It is hypothesised that more angular grains show a greater arching effect. This should become more pronounced with greater superimposed load. Tests with a similar stability ratio but a different angularity of the base material have been performed. The results of these tests are presented in Table 6.4.

Stability Ratio [-]	Erosional $i_{\perp}$ [-]	Angularity Base Material [-]	Permeability Base Material
12.2	0.13	high	high
12.2	0.12	high	high
12.1	0.16	low	low

Table 6.4: The test results used to determine the influence of the angularity of the base material.

These results show that tests with a lower angularity have a higher critical gradient. This is not what was expected. Therefore, the hypothesis that the angularity of the base material increases the critical hydraulic gradient cannot be confirmed.

The difference in critical hydraulic gradient in these tests is likely due to the difference in permeability between the two base materials. This influences the flow velocity and appears to be more important than the effect of angularity.

The tests with a lower critical gradient had a more permeable base material. The difference in permeability between the base materials is due to the size difference of the smallest particles. If these particles are larger the permeability of the material is also larger, due to the more permeable base material. Therefore the flow velocity within the pores is increased. Due to this the drag force on the base particles is increased for the same hydraulic gradient. Therefore there is a lower critical hydraulic gradient for more permeable base materials.

6.6. Influence of the First Instance of Erosion on the Future Stability of a Filter

One of the aspects investigated is if an occurrence of erosion influences the future stability of the filter. To investigate this, three sets of test were performed.

These tests were preformed on a setup that had already been used to determine a critical hydraulic gradient. The speed of the plunger was kept constant over a period of eight hours. The selected speed was one speed lower than what caused erosion in the original test.

No new erosion was detected in any of these tests. As such the filter was stable for the hydraulic gradient tested. The results of these tests are presented in Table 6.5.

Test Configuration	Stability Ratio	$I_{\perp}$ Erosion	$I_{\parallel}$ Erosion	$I_{\perp}$ Stable	$I_{\parallel}$ Stable
Parallel	7.2	0.10	0.0093	0.12	0.0067
Combined	7.2	0.071	0.015	0.066	0.013
Perpendicular	10.5	0.19	-	0.23	-

Table 6.5: Pairs of tests where a subcritical hydraulic gradient is applied for an extended period of 8 hours.

The following observations were made about the results:

- **Parallel configuration test:** The perpendicular hydraulic gradient observed was larger for the stable test than for the test where erosion was detected. This was unexpected. The parallel hydraulic gradient was lower in the test without erosion.

  An explanation for this is, the uncertainty of the perpendicular hydraulic gradient. As explained in section 5.3, the location and value of the maximum perpendicular hydraulic gradient across the filter-base interface is unknown in parallel tests. This also changed throughout a test. As such for this test, the true perpendicular hydraulic gradient is unknown.

- **Combined configuration test:** The hydraulic gradients achieved in the test with erosion are between 87% ($I_{\parallel}$) and 93% ($I_{\perp}$) of the critical values determined in the first portion of the test.

- **Perpendicular configuration test:** The perpendicular hydraulic gradient achieved in the test without erosion was higher than what was required to induce erosion in the first test. This was likely due the uncertainty in the programming of the plunger. After erosion occurred in the first part of the test the hydraulic gradient was further increased. During this further increase of hydraulic gradient erosion continued. The maximum hydraulic gradient achieved was higher than the hydraulic gradient in the following stable test.

- During all three tests no erosion occurred. Thus the filter is stable for the achieved hydraulic gradients.

These results indicate that a stable situation can be reformed after erosion has occurred. This erosion also does not seem to negatively affect the critical hydraulic gradient for the filter at a later stage. The perpendicular test indicates that the exposure to a higher hydraulic gradient could possibly increase the critical hydraulic gradient. This would be an armouring effect.

6.7. Context of Critical Gradients for Application to Case

In the previous sections the relationships between the stability ratio, superimposed load and the critical perpendicular hydraulic gradient have been determined. Furthermore it has been determined that the perpendicular hydraulic gradients appear to be governing if there is a combination of perpendicular and parallel gradients present. It was determined that the arches within the system can reform, this allows for a design for less strict design criteria.

Situation in the Case Study This section compares our findings to the hydraulic gradients present at the rear side of the breakwater that have been determined by Van de Ven (2019). The situation is shown in Figure 6.8. In this study there is 4,5m of sand present above the mean water level. The granular filter construction goes from -5m to a depth of 12m. The sand is assumed to be normally consolidated.

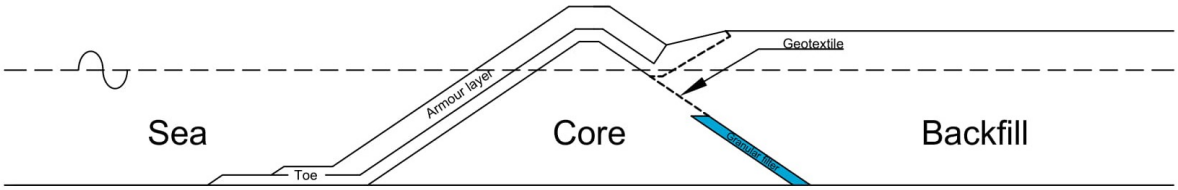

Figure 6.8: Location of the open filter in the application to the case.

Effective Stress at Filter Backfill Interface From the soil layers the vertical effective stress is calculated. The horizontal effective stress can be calculated using Equation 6.2 where K_0 is the coefficient of lateral earth pressure at rest.

$$\sigma'_h = \sigma'_v \cdot K_0 \tag{6.2}$$

As the sand is normally consolidated the primary principal effective stress (σ'_1) is the vertical effective stress (σ'_v) and the secondary principal effective stress (σ'_2) is the horizontal effective stress (σ'_v). The interface filter-backfill has a slope of 1:1.25. The effective normal stress on this plane is 76.5% of σ'_1. [6] The resulting effective normal stress in the filter backfill interface is shown in Figure 6.9.

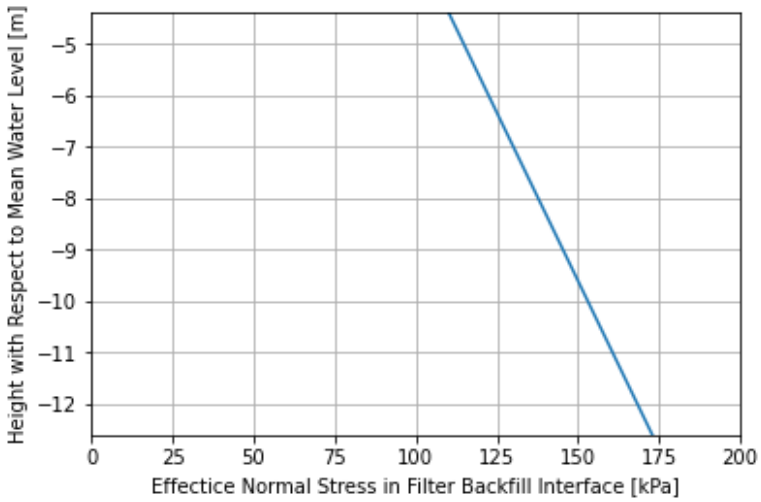

Figure 6.9: The effective normal stress in the filter backfill interface for the case study.

[6] This reduction was calculated using Mohr's circle. The ratio between the effective stress on this slope and the vertical effective stress is calculated. This ratio was 0.765:1.

Stability of Open Filters in the Case Study Using this soil pressure the depth-dependent critical hydraulic gradient can be calculated. This is done using the trends from Figure 6.4 and Figure 6.7. In Figure 6.10 the results of this are plotted for each stability ratio. The dots plotted are the perpendicular hydraulic gradients in the filter backfill interface which are exceeded by 2% of the waves during a design storm as determined by Van de Ven (2019). It should be noted that the determined relations for the critical perpendicular hydraulic gradient are conservative. Thus the result of this analysis is also conservative.

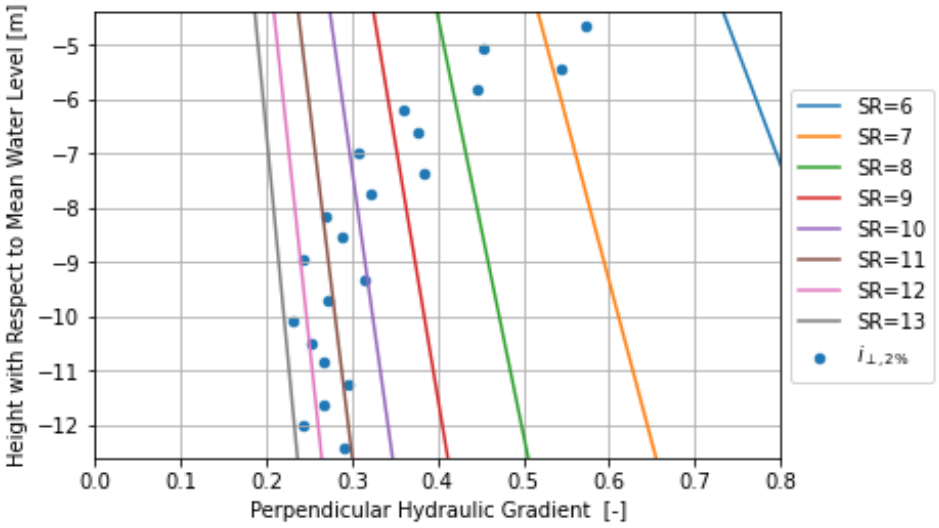

Figure 6.10: The comparison of the critical perpendicular hydraulic gradient for a specific stability ratio (SR), and the perpendicular hydraulic gradient exceeded by 2% of the waves during a design storm ($I_{\perp,2\%}$).

As seen in Figure 6.10 it is possible to construct a hydraulically closed geometrically open inverted filter for this specific case.

6.8. Conclusion from Results

In this section, the conclusions from the results of the physical model testing are summarised.

- For many filter base combinations no erosion could be induced using the experimental setup. Due to this only lower bound values for the critical hydraulic gradient were found for these tests.
- Arching is still the most likely mechanism to explain the stability of an open inverted filter.
- When there is a combination of perpendicular and parallel hydraulic gradients the perpendicular gradient appears to be governing.
- A negative relationship was found between the stability ratio and critical perpendicular hydraulic gradient. This is presented in Figure 6.4.
- A surcharge has a stabilising effect on the filter. A relationship is determined, which is presented in Figure 6.7.
- No conclusion could be made about the effect of the angularity of the base material on the stability of an open inverted filter. The permeability of the base material has been identified to also influence the critical hydraulic gradient.
- Arches can reform after damage therefore the design criteria do not need to be for the single largest wave expected. Instead, less conservative and therefore more cost-effective criteria can be used.
- The found relations are applied to the case study. It was found that below a certain depth an open filter could be designed.

7

Discussion

This chapter discusses the uncertainties and limitations in this study, the potential for the application of the knowledge, and compares the results found to the literature.

7.1. Uncertainties and Limitations in Modelling

Modelling is a representation of reality. In a model, simplifications are made. This can lead to the misrepresentations of processes and the introduction of other inaccuracies. This section will discuss the uncertainties and limitations of the physical and numerical model.

7.1.1. Physical Model

This section discusses the uncertainties that are introduced by the physical model.

Leakage of Top seal For the parallel configuration, the top was sealed to ensure that the hydraulic gradients present would be parallel. In this study it was discovered that for the present and previous studies(Boersma, 2020; Van de Ven, 2019), the seal along the top of the model leaked. This allowed for vertical flows within the base material. The exact locations of these leaks are unknown. The perpendicular hydraulic gradient was only measured at one location within the model. Furthermore, due to leaking the flow field becomes three dimensional. This makes it impossible to reconstruct the distribution of the perpendicular hydraulic gradients within the base material. Therefore there are perpendicular hydraulic gradients during parallel configuration tests, but the magnitude is unknown.

The parallel hydraulic gradients determined with these tests are accurately determined. These may or may not be governing. These are still usable as a lower bound for the critical parallel hydraulic gradient. In the parallel tests Boersma (2020) found critical parallel hydraulic gradients which where significantly larger than the 2% highest gradients determined by Van de Ven (2019) in the case study. Therefore, it can be concluded that the parallel component of the hydraulic gradient is likely not governing for this case.

Location of Sensors The pressure sensors were fixed in a rack which ensured that the relative distance between the sensors was constant during and between tests. This rack was not fixed within the model. As a result, there could be a slight variation in the location of the sensors between testes.

For combined tests, the magnitude of the perpendicular hydraulic gradient depends on the location within the filter base interface (see chapter 5). This means that uncertainty in the location the perpendicular hydraulic gradient is measured leads to an uncertainty in the maximum value of the hydraulic gradient.

For perpendicular configuration tests, the hydraulic gradients are uniformly distributed in space. Therefore uncertainty in the location that the hydraulic gradient is measured is not relevant.

For parallel tests, the location of the leak influences the distribution of the perpendicular hydraulic gradient. Therefore the distribution of the perpendicular hydraulic gradient is unknown. This makes the uncertainty of the location of the sensors is not relevant as the perpendicular hydraulic gradients cannot be reconstructed.

For all test configurations, the parallel hydraulic gradient is not location-dependent. Therefore the uncertainty of the location of the pressure sensors has a negligible influence on the results. The distance between the sensors is more important. This remains fixed due to the rack holding the sensors.

Plunger Mechanism The plunger mechanism had a so called 'play'. This means that the plunger could move differently from what it was programmed to do. This occurred because two axles within the model setup slipped relative to each other. This slipping happened at the same point in the stroke of the plunger each cycle. The amount of slippage that occurred slowly increased during the duration of this study. As a result the amplitude of the plunger slowly decreased and a flat step was introduced in the up and down movement of the plunger. This slowly increased throughout the study. As a result, the shape and amplitude of the cycle of the hydraulic gradients changed between tests. The hydraulic gradients are determined from the measured signal, this changed slightly between tests. However, the peak gradients which are likely governing for erosion and used in analysis are expected to be accurate within the measurement uncertainty.

The crank slider mechanism for the plunger also had a limited range. This limited range reduced the maximum hydraulic gradients possible. The maximum perpendicular hydraulic gradient that could be achieved was 0.29. From the determined relationships it would be expected that a filter with a stability ratio of 7 and a surcharge of 200kpa would need a perpendicular hydraulic gradient of at least 0.9 to be close to the critical value. Increasing the range of the plunger to 120mm will allow for this.

Compaction of Soil During a test with a surcharge, there was a permanent deformation of the soil. In tests where erosion occurred this is partly due to the base material leaving the filter construction. When no erosion occurred this is likely due to the rearranging of the particles in the sand layer. This leads to a reduced porosity of the base material. This change influences the strength of the sand. This is a possible effect on the critical hydraulic gradient which is separate from the increased effective stress.

Relocation of Model Tests without surcharge were carried out in the Hydraulic Engineering laboratory in Stevin III, whilst tests with a surcharge were performed in the laboratory Stevin II. This is a different location with slightly different ambient conditions. Different temperatures or vibrations could influence the testing. This influence is however likely to be very minor as both test locations were indoors in a similar laboratory. If this does have an influence, the use of two locations improves the reliability of the results. Two locations then reduces the significance of the external conditions as two different external conditions are used.

There was a difference in experimental procedure between the two laboratories: in Stevin III the tests were performed and prepared without moving the setup. In Stevin II the prepared test setup was transported underneath the hydraulic press using an electric pallet truck. This transport induced vibrations to the model which resulted in significantly more initial infall for the tests with a surcharge. As such it was more difficult to detect erosion in tests with a surcharge. This likely had an insignificant effect on the results as the time lapse images were taken from a fixed camera and under constant lighting conditions. This means any slight change in the amount of sand present was noticed in the time-lapse images. As such the critical hydraulic gradient could still be determined when there was surcharge present.

Distribution of Soil Pressure The true distribution of the effective stress (σ') in the soil due to the surcharge is unknown as this was not measured. In this study, the assumption has been made that there was a uniform distribution of the effective stress. Uneven stress distribution can influence the strength of the arches. This will occur both in the application and in the experiments. In some locations, the stress will be higher and in other locations the stress will be lower. Arches under lower stress have less additional strength. In that case, tests would be an underestimation of the beneficial effect of an increased effective stress at the filter base interface.

The soil layers in the experimental setup had a uniform thickness and a uniform load was applied to the top of the base material with a very stiff plate. This will lead to a minimal variation in the effective stress in the filter base interface in the experiment. This means that the this likely does not have a significant effect.

In the application, this uncertainty in the effective stress will mainly be dependent on the execution tolerances accepted in the design. A relevant margin of safety can be chosen based on these requirements.

7.1.2. Numerical Model

A numerical model was used to calculate the flow between compartments and the hydraulic gradients within the base material. The most important implications are discussed below.

Laminar Resistance The 1D numerical model used to determine the water levels in the different compartments is based on Darcy's law. Therefore only laminar flow is taken into account. For this the Reysnolds number must remain below 10 (Bear, 1972). For the flow in the base material, the laminar processes are dominant (Maximum RE=0.6). Therefore this simplification is valid. However for the flow through the filter material, the turbulent and inertial processes likely have an influence (Maximum RE=36). Therefore this schematisation is not entirely valid.

The flow field within the base material was calculated with the 2D numerical model. This uses the potential flow approach with the Laplace equation. This is valid if the flow can be described using Darcy's equation (Bear, 1972). As stated above a Darcy approach is valid for the base material. As such this calculation is valid for determining the flow in the base material.

Incomplete Coupling of the Models The two parts of the model have been used together to determine the pressure distribution within the base material. This was calculated for one cycle of the plunger. Using the 1D numerical model, the water levels in each compartment and hydraulic gradients between compartments were calculated. The water levels were used as input for the 2D numerical calculation of the pressure field within the base material. In turn the flows and hydraulic gradients were calculated from the pressure field. This is a one way coupling.

The perpendicular hydraulic gradients within the base material calculated in 1D and in 2D differ from each other. For the 1D application Flow in the base is modelled using Darcy as a result the nonlinear terms due to turbulent and inertial processes are not included. As this flow is has a Reynolds number of below 1 this is likely not the cause. The hydraulic gradients calculated using the 2D model also do not include the non linear terms, but do include 2D effects. As such the 2D effects are likely reason for the difference between the results.

The situation could be modelled using an existing numerical porous flow model, for example OpenFOAM. This way 2D effects, the influence of the interface, and the nonlinear resistance in the filter material could be taken into account.

7.2. Potential for the Application of the Knowledge

The situation modelled does not exactly represent reality the key differences which lead to limitations and uncertainties in the application of the results are presented below.

7.2.1. Inclination of the Filter

The filter tested in this study was horizontal. In the application to a land reclamation structure this filter will be under an angle. This possibly has an influence on the mechanics of the filter. There are two significant differences between the application and the situation tested. The direction of the gravitational force and the direction of the principal soil pressures.

The force due to gravity will act in a different direction. In the situation tested gravitational forces work perpendicular to the filter base interface. In reality the forces due to gravity work at an angle to the interface. This reduces the destabilising force. This could lead to additional strength of the filter.

In reality, the primary soil pressure is also no longer perpendicular to the filter base interface. This is taken into account by using the effective stress in the plane of the filter. There is limited knowledge about soil arching in an inclined plane. As such the true strength is unknown. This reduction may be a conservative approach as there is a higher level of stress present within the filter base interface.

7.2.2. Symmetry and Regularity of Gradients

The hydraulic gradients applied to the filter construction during this study were symmetrical and regular. The cycle of loading was the same throughout a test segment. When the filter is constructed in a land

reclamation the filter will be subject to loading by natural processes such as waves and tides. Due to natural processes, there is not a regular pattern of loading but an irregular wave field, which results in changing periods and amplitudes of loading. Tides or storm surges may lead to a period in time where there is a net flow in or out of the land reclamation. The effect of these factors is unknown, but likely minor. The amplitude of the hydraulic gradient determines the loads on the particles. An irregular wave field can be defined by a characteristic value for example the value exceed by 2% of the waves. When the value exceeds the design value damage may occur, however as arches can reform the majority of the time there will be a stable situation. Further research can confirm this.

7.3. Comparison to Literature

This study is not the only research done with relevant findings for the context of an open inverted granular filter used to retain sand back-fill in land reclamation. This section discusses the influence of the findings in this study on the results in previous studies in this research line. It also compares the main findings of this study to previous research relevant to the topics of arching or open filters.

7.3.1. Impact on the Research Line

The findings of this study have influenced the interpretation of the results in the previous studies within this research line. This section highlights which conclusions in the previous studies are no longer valid due to the findings of the current study.

Air Tightness Both describe the fact that the top seal is not airtight as they have visually observed air escaping along the top seal. The perpendicular hydraulic gradient was not measured during these previous studies. From the visual observation of leaking it can be concluded that there is also a unknown perpendicular hydraulic gradient present during parallel testing by Boersma (2020) and Van de Ven (2019). This means that it is uncertain if these tests failed due to the parallel hydraulic gradient. Therefore it is likely that the critical parallel gradient is higher than what was found within these previous studies.

Combined Gradients In the current study, tests in the combined configuration had a maximal perpendicular hydraulic gradient which was four times higher than measured. Boersma (2020) had a similar combined configuration. Therefore this is likely also the case for the tests in a combined configuration by Boersma (2020).

7.3.2. Comparison to Related Research

This subsection discusses the main findings of this study in the context of the previous research by other authors on related topics.

Effect of Surcharge This study found a positive effect of a surcharge on the critical perpendicular hydraulic gradient for all stability ratios tested. This was up to SR=12.2. This concurs with De Graauw et al. (1984) who found that, when arching was present, increasing the surcharge had a positive effect on the stability of the filter layer.

Arching stabilising a sand layer against the flow of water was analysed in different contexts by Miller (1994) and Chew et al. (2003). Both of these studies also concur that an increased surcharge increases the effectiveness of the arching. In contrast the study by Chew et al. (2003) found an upper limit of 25kPa after which extra soil pressure did not have any additional benefit. The current study disagrees with this finding, as an improvement in critical hydraulic gradient was found between 50kPa and 100kPa.

Stability Ratio This study found a decreased stability of the filter with a larger stability ratio. This matches the wider understanding of traditional open filter design where an increased ratio between the size of particles in the base and filter layers leads to a lower stability of the filter (Bakker et al., 1994; Belyashevskii et al., 1972; De Graauw et al., 1984; Schürenkamp et al., 2016).

This study found a filter to be theoretically geometrically closed when SR<3.6. Theoretically geometrically closed applies for an infinite hydraulic gradient, this cannot physically occur, as such studies define a practical guideline. Terzaghi (1948) found a filter to be geometrically closed when SR=4.De Graauw

et al. (1984) states that for strong oscillatory flow this may be need to be stricter than four. This corresponds well with the findings in the current study. The Rock Manual (CIRIA et al., 2007) uses SR<5. This difference in definition is likely due to testing with different hydraulic gradients.

Combined Flow This study found that the perpendicular hydraulic gradient is likely to be the governing gradient for this application in a rubble mound land reclamation. The perpendicular hydraulic gradient present was much higher than the parallel hydraulic gradient. A lower parallel hydraulic gradient could also be governing if this exceeds its own critical value. This did not appear to be the case.

The combination of both perpendicular and parallel hydraulic gradients did not appear to lead to a reduced critical perpendicular hydraulic gradient. De Graauw et al. (1984) found that the presence of another direction hydraulic gradient only leads to a decrease in the critical perpendicular gradient when both components of the gradient are close to their individual critical values. This was for steady flow on a traditional open filter.

De Graauw et al. (1984) also found that for specific filters, the parallel critical hydraulic gradient is approximately 40% of the perpendicular critical hydraulic gradient. In the current study, the parallel hydraulic gradient present is orders of magnitude smaller than the perpendicular hydraulic gradient. This means that the parallel hydraulic gradient was much smaller than its expected critical value. Therefore the perpendicular component of the hydraulic gradient was likely governing for the combined tests in the current study.

Reforming of Arches In this study, it was concluded that it is possible to reform a stable situation after erosion has occurred. From this, we can determine that once the arches are broken they are able to reform. The results also suggest that an armouring effect could be present, leading to a more stable situation. This concurs with the research by Bratli et al. (1981) who analysed the behaviour of a single sand arch. In the current study, new arches could reform after a collapse, these newly formed arches were more stable than the initial arches.

Belyashevskii et al. (1972) and Schürenkamp et al. (2016) studied non-inverted filters and had mixed results. They studied a filter using lower hydraulic gradients after erosion had occurred. In some cases, the filter would remain stable and in other cases, there would be continuous erosion. These studies had a much less strict definition of erosion. Erosion was defined when the filter layer started to settle. In order to cause settlement a significant transport of sand is needed. This requires hydraulic gradients well above the critical hydraulic gradient. Therefore reducing the hydraulic gradients might still result in gradients larger than the critical gradient. This difference in definition could explain the difference with the current study.

8

Conclusions and Recommendations

8.1. Conclusions

The objective of this study was to determine if a geometrically open granular filter can be used to retain the sand backfill in a rubble mound land reclamation. Arching is the mechanism that is believed to stabilise an open inverted granular filter. Many of the sub-questions address aspects of arching. This section will answer the main research question on a basis of the sub-questions.

8.1.1. Spatial Distribution of the Hydraulic Gradient in the Base Material

The first sub-question was as follows: *What is the influence of the model configuration on the spatial distribution of the hydraulic gradient within the base layer in the experimental setup.* To answer this sub-question, the spatial distribution of the hydraulic gradient in the base material was analysed using a numerical model. The conclusions for the performance of the three configurations of the experimental setup are presented below:

Perpendicular Configuration The perpendicular configuration leads to a uniformly distributed perpendicular hydraulic gradient within the base material. Therefore the measured hydraulic gradient is representative of the entire filter base interface. There was no parallel hydraulic gradient in these tests.

Combined Configuration There was a spatial distribution of the perpendicular hydraulic gradient within the base material during tests with the combined configuration. As a result, the maximum value of the perpendicular hydraulic gradient is four times larger than the value measured. The measured perpendicular hydraulic gradients are adjusted with a factor of four. This was done for all combined configuration tests in this research line.

The parallel hydraulic gradient was uniform across the filter base interface. Therefore the measured parallel gradients can be used directly.

Parallel Configuration A perpendicular hydraulic gradient was present when tests were performed in the parallel configuration. The perpendicular hydraulic gradients were caused by leaking at the top of the model. This also occurred for the parallel configuration tests by Van de Ven (2019) and Boersma (2020). The implication of this leaking is that the observed erosion was likely a result of the perpendicular hydraulic gradient and not a result of the parallel hydraulic gradient. Since only the parallel hydraulic gradients were measured in the aforementioned studies, those results cannot be used to determine the critical hydraulic gradient.

8.1.2. Influence of Stability Ratio

The stability ratio influences arching of the base material. This is the main strength mechanism of open inverted filters. A higher stability ratio is a larger ratio between the sizes, which leads to larger gaps within the filter relative to the size of the base particles. As such more base particles are required to

form a larger arch across the larger gaps. These larger arches with more particles are more fragile and thus the hypothesis is that increasing the stability ratio decreases the critical hydraulic gradients.

This hypothesis has been confirmed as this study has found that an increasing stability ratio decreases the critical hydraulic gradient. For the perpendicular hydraulic gradient a relation has been found. This is presented in Figure 8.1.

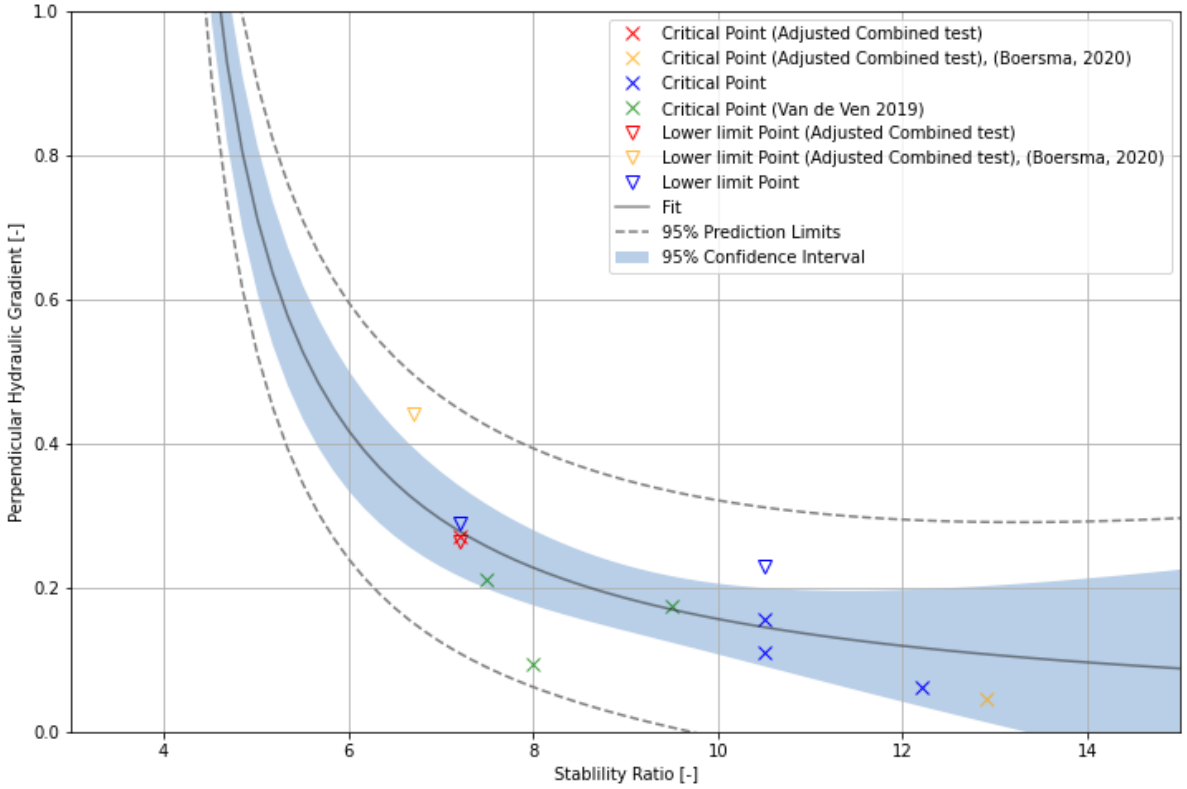

Figure 8.1: The determined trend between the stability ratio (SR) and the critical perpendicular hydraulic gradient. The uncertainty of each point can be seen in Figure 6.3.

8.1.3. Influence of the Effective Stress in the Filter Base Interface on the Critical Hydraulic Gradient

The main mechanism that ensures the stability of the open inverted filter is arching. The arches are held together by the friction between the base particles. This friction depends on the normal force between particles. Increasing the effective stress in the filter interface increases the normal force between the particles. Therefore the friction is also increased. The hypothesis was that the increased normal force leads to stronger arches. Therefore an increased critical hydraulic gradient was expected.

This hypothesis has been confirmed as it has been found that a surcharge positively affects the critical perpendicular hydraulic gradient. This influence has been quantified. The relationship is presented in Figure 8.2.

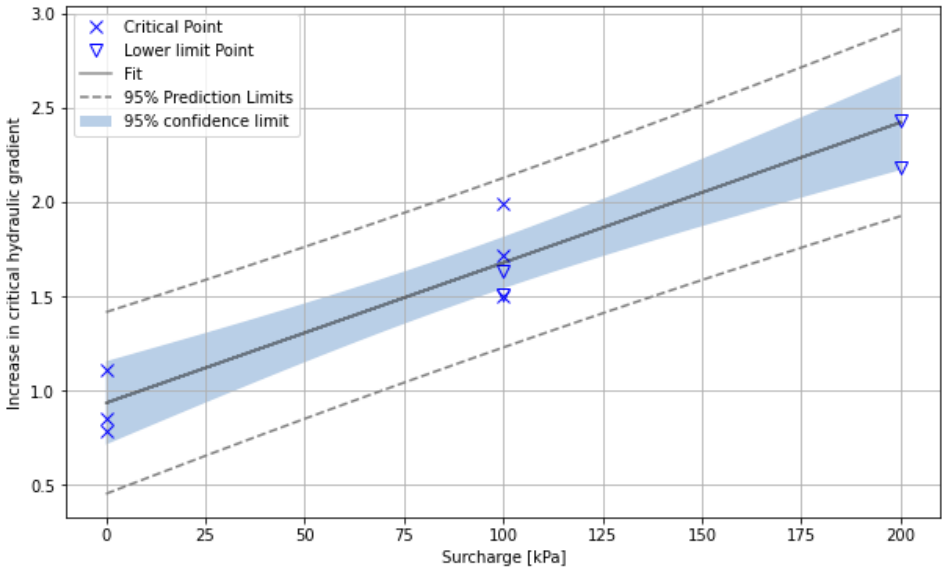

Figure 8.2: The trend that was determined for surcharge. It shows the factor that effective stress in the filter base interface influences the critical perpendicular hydraulic gradient.

8.1.4. Influence of the Angularity of the Base Material

The angularity of the base material also influences the arching, which is the main strength mechanism of open inverted filters. The angularity of the base material influences the friction in the arches. The hypothesis was that the increased angularity would lead to increased friction between the particles. This leads to an increased critical hydraulic gradient.

This study does not confirm this hypothesis it actually suggests the opposite. A possible explanation is that the difference in critical hydraulic gradient is likely due to the difference in permeability between the two base materials. The less permeable material had a higher critical gradient. This material has a decreased flow velocity for the same hydraulic gradient. This in turn reduces the drag force on the base particles. Therefore a less permeable material has a higher critical hydraulic gradient.

8.1.5. Influence of Erosion on Stability at Sub Critical Gradients.

This sub-question examined the stability of a filter after failure of the filter. This was done to determine if a storm exceeding the design criteria could cause irreversible damage.

When the critical gradient was exceeded, the arches of base material broke. Therefore, sand was transported through the filter. It was hypothesised that once these arches are broken, they can reform to regain a stable situation. This hypothesis has been confirmed. Stable situations have been found after erosion had occurred. This means that design criteria do not need to be based on the single largest wave. This allows for a less conservative design, which is a potential cost saving.

It was further found that some filters were stable for a higher hydraulic gradient than the initial critical hydraulic gradient. This indicates a possible armouring effect which occurs when broken arches reform to form a more stable configuration. This configuration then has a higher critical gradient. More work is needed to investigate this phenomena as this could lead to further cost-savings in the application.

8.1.6. Influence of the Combination of Parallel and Perpendicular flow

The influence of the combination of a perpendicular and a parallel flow on the critical hydraulic gradient has been researched. The hypothesis was that the combination of both a perpendicular and parallel gradient would increase the flow forces on the base particles. Therefore a combination of flows would reduce the critical hydraulic gradient.

This hypothesis has been disproven for the context of this study. For the filters tested the combination of a perpendicular and parallel hydraulic gradient does not seem to effect the critical perpendicular hydraulic gradient. The perpendicular hydraulic gradient was determined to be governing. The parallel hydraulic gradient did not appear to influence the critical value for the perpendicular hydraulic gradient.

This means that when designing an open inverted filter in land reclamation the perpendicular and

parallel components of the hydraulic gradient can be analysed separately to determine which is governing. The other component then can be ignored.

8.1.7. Main Question

The main objective of this study is to determine if an inverted geometrically open granular filter can be applied to retain the sand backfill in a rubble mound land reclamation. In line with the results of Boersma (2020) and Van de Ven (2019). This study confirms that the use of an open inverted filter in land reclamation is a valid alternative. Thus reducing the costs for these types of land reclamations dramatically.

This study found relationships which can determine the stability of an open inverted filter. These relationships can be compared to the hydraulic loads expected at filter-backfill interface in concept design. A suitable stability ratio for a filter in the concept land reclamation can be selected using this comparison.

A case study has been used as an example to demonstrate the process of designing an open inverted filter for a rubble mound land reclamation. The results of this case study are presented in Figure 8.3. The x-axis shows the perpendicular hydraulic gradient. The y-axis shows the location in the filter-backfill interface relative mean water level. The dots show the perpendicular hydraulic gradient exceeded by 2% of the waves during a design storm at that specific depth (These hydraulic gradients were calculated by Van de Ven (2019)). The lines show the critical perpendicular hydraulic gradient. The critical perpendicular hydraulic gradient is calculated for the location within this filter using the specific geometry of the case study.

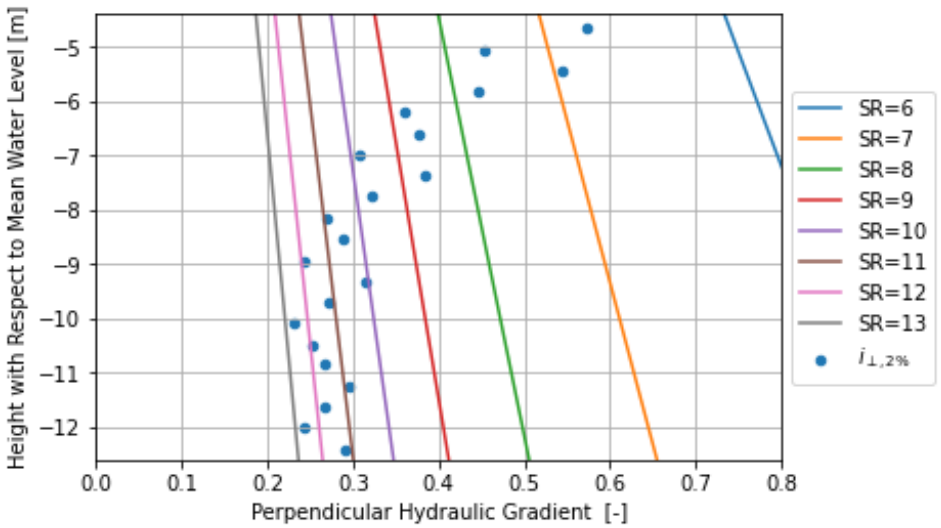

Figure 8.3: Design graph for the case study. This is a comparison of the critical perpendicular hydraulic gradient for a specific stability ratio (SR), and the perpendicular hydraulic gradient exceeded by 2% of the waves during a design storm ($I_{\perp,2\%}$).

8.2. Recommendations

The current study has provided new findings that contribute to the understanding of open inverted filters. However, new questions have also been raised. This section will give recommendations for the continuation of this line of research. Some considerations for the application of open inverted filters will also be given.

8.2.1. Practical for Continued Research

The following practical recommendations are made for continued use of the physical model.

Produce Greater Hydraulic Gradients It was not possible to induce erosion for a significant portion of tests. The setup needs to be modified to produce larger hydraulic gradients. Perpendicular hydraulic gradients of up to 1 and parallel hydraulic gradients of up to 0.5 need to be generated. This will allow testing of a wider range of stability ratios with a surcharge.

The main limiting factor in producing larger gradients was the plunger mechanism which turned the rotational motion to linear motion. This mechanism is limited to a relatively small amplitude. It also had connections which loosened with the repetitive raising and lowering of the plunger. The amplitude of the plunger largely determines the maximum hydraulic gradients generated. The amplitude needs to minimally increase to 60mm and mechanism needs to able to handle the forces at this amplitude.

Placement Differential Pressure Sensors Placing the differential pressure sensors further apart, this will lead to an increased accuracy of the hydraulic gradients.

Parallel Tests Due to leaking, there were perpendicular gradients present in the parallel tests in the current and previous studies. The parallel configuration used in this study had closed boundaries on the sides of the base material. This is more sensitive to leaking than the setup used by De Graauw et al. (1984), where the boundaries were open. A configuration where the top of the base material is sealed and the sides of both the base and filter material is open, is recommended for testing parallel hydraulic gradients. This will lead to significantly lower perpendicular hydraulic gradients when the setup leaks.

Measurement of Water Level The method this study used to measure the water levels in the compartments was less reliable than the methods used by Boersma (2020) or Van de Ven (2019). As such the methods used in these previous studies is recommended for use in further research.

8.2.2. Expanding the Knowledge

This study has lead to an increase in the understanding of the functioning of open inverted filter constructions. In this processes, new knowledge gaps have been identified and additional questions have been raised. The following recommendations will address these knowledge gaps and provide suggestions to help study these phenomena.

Influence of Compaction This study has investigates the influence of applying a surcharge to a granular filter in loose state. The effects of applying a surcharge are twofold: (1) the filter may be compacted and (2) the effective stress is increased. This combination has shown to lead to a significant increase in the critical hydraulic gradient.

Increased effective stress within the soil leads to an increased strength of the arching. However according to Indraratna et al. (2007) the increased compaction may also lead to an increased stability of the filter. Separately studying the effect of the compaction of the soil and the effect of increasing the effective stress is recommended. This could help determine the effect of each mechanism separately. The effect of the compaction of the filter can be investigated separately using a prestressing technique. The filter can be compacted by applying a surcharge. Subsequently the surcharge can be removed and the critical hydraulic gradient can be determined without the surcharge. This way, only the effect of the compaction is studied.

Influence of Wet Placement of Base Material For the experiments in this study the base material was placed on top of the filter in wet conditions. This is in contrast with tests by Van de Ven (2019) and the parallel tests by Boersma (2020). For these tests placement was done in dry conditions. The placement in dry or wet conditions determines the characteristics of the final sand. This possibly also influences the critical hydraulic gradient of a filter. For this factor the effect is unknown and should be investigated.

Verify the Pressure Distribution within the Base Material The numerical model was used to calculate the distribution of the hydraulic gradient within the base material. This model in unvalidated as there was insufficient data to do this. The verification of the numerical results by comparing the results with data from experiments. Placing a grid of pressure sensors within the base material during experiments is recommended. A comparison can then be made between the measured distribution and the computed distribution.

Expansion of Numerical Model The numerical model used to determine the spacial distribution of the hydraulic gradients only modelled the 2D effects in the base material and assumed laminar resistance in the entire filter construction.

It is recommended to expand this model to in include the filter material. Modelling the potential flow within the filter material will allow for the results of the spatial distribution of the hydraulic gradients to be included in an update of the water level.

Furthermore it is recommended to include the effects of inertial and turbulent resistance. In particular the flow within the filter material the laminar resistance assumption is not valid.

Inclination of Filter In the setup used in this study the filter-base material interface was horizontal. The application of this interface will be at an inclination. The effects of this have not been investigated and may be of significance as the forces due to gravity will act in a different direction.

There is space within the container to be able to preform inclined tests. For performing these tests it is recommended to use a filter with a constant thickness. A filter with changing thickness will add to the uncertainties about the flow already present.

8.2.3. For Application of Open Inverted Filters

This study has determined principles which apply for an open inverted filter, this is has been done with a model which simplifies reality. The following recommendations should be taken in to account when applying the results of this study for the design of an open inverted filter.

For Conditions Tested This study tested within specific conditions. The most important are hydraulic gradients upto 0.3, uniformly graded filters, a 2D situation and a surcharge upto 200kPa. It is recommended to limit application of the findings of this study to situations that also match these conditions.

Relations are Conservative The relationships determined are conservative. If more research is done these relationships can be made less conservative. Which can further reduce the amount of layers needed in a filter construction. This would make an open filter an even more attractive solution.

References

Abdelhamid, Y. and El Shamy, U. (2016). Pore-scale modeling of fine-particle migration in granular filters. *International Journal of Geomechanics*, 16(3):04015086.

Allsop, W. and Williams, A. (1991). Hydro-geotechnical performance of rubble mound breakwaters.

ASTM (2017). Standard test methods for uncompacted void content of fine aggregate (as influenced by particle shape, surface texture, and grading).

Bakker, K., Verheij, H., and De Groot, M. (1994). Design relationship for filters in bed protection. *Journal of Hydraulic engineering*, 120(9):1082–1088.

Bear, J. (1972). Dover Publications.

Belyashevskii, N., Bugai, N., Kalantyrenko, I., and Topchii, S. (1972). Behavior and selection of the composition of graded filters in the presence of a fluctuating flow. *Hydrotechnical construction*, 6(6):541–546.

Boersma, F. (2020). Inversed open granular filters in land reclamation structures: Modeling of the interface stability. Master's thesis, Delft University of Technology.

Bratli, R. K., Risnes, R., et al. (1981). Stability and failure of sand arches. *Society of Petroleum Engineers Journal*, 21(02):236–248.

Carman, P. C. (1938). Determination of the specific surface of powders i. transactions. *J. Soc. Chemical Industries.*, 57:225–234.

Carrier III, W. D. (2003). Goodbye, hazen; hello, kozeny-carman. *Journal of geotechnical and geoenvironmental engineering*, 129(11):1054–1056.

Chew, S. H., Tian, H., Tan, S. A., and Karunaratne, G. (2003). Erosion stability of punctured geotextile filters subjected to cyclic wave loadings—a laboratory study. *Geotextiles and Geomembranes*, 21(4):221–239.

CIRIA, CUR, and CETMEF (2007). *The Rock Manual. The use of rock in hydraulic engineering (2nd edition)*. C683, CIRIA.

Creel, L. (2003). *Ripple effects: population and coastal regions*. Population reference bureau Washington, DC.

De Graauw, A. F., Van der Meulen, T., and Van der Does de Bye, M. R. (1984). Granular filters: Design criteria. *Journal of waterway, port, coastal, and ocean engineering*, 110(1):80–96.

Editors of Encyclopaedia Britannica (2008). Arch.

Hazen, A. (2013). Xxiii. some physical properties of sands and gravels, with special reference to their use in filtration. In *State Sanitation: A Review of the Work of the Massachusetts State Board of Health, Volume II*, pages 232–248. Harvard University Press.

Heerten, G. and Wittmann, L. (1985). Filtration properties of geotextile and mineral filters related to river and canal bank protection. *Geotextiles and geomembranes*, 2(1):47–63.

Heibaum, M. (2004). Geotechnical filters-the important link in scour protection. In *2nd International Conference on Scour and Erosion. Singapore, 14-17 November, 2004. Conference Proceedings-Volume 1*, number 1, pages 13–28.

Hu, Z., Zhang, Y., and Yang, Z. (2019). Suffusion-induced deformation and microstructural change of granular soils: a coupled cfd–dem study. *Acta Geotechnica*, 14(3):795–814.

Indraratna, B., Raut, A. K., and Khabbaz, H. (2007). Constriction-based retention criterion for granular filter design. *Journal of Geotechnical and Geoenvironmental Engineering*, 133(3):266–276.

James, S. C., Jones, C. A., Grace, M. D., and Roberts, J. D. (2010). Advances in sediment transport modelling. *Journal of Hydraulic research*, 48(6):754–763.

Koninklijk Nederlands Meteorologisch Instituut (2021). Knmi klimaatsignaal'21.

Kozeny, J. (1927). Uber kapillare leitung der wasser in boden. *Royal Academy of Science, Vienna, Proc. Class I*, 136:271–306.

Lambe, T. W. and Whitman, R. V. (1991). *Soil mechanics*, volume 10. John Wiley & Sons.

Liu, X. X. and Chiew, Y.-M. (2012). Effect of seepage on initiation of cohesionless sediment transport. *Acta Geophysica*, 60(6):1778–1796.

Locke, M., Indraratna, B., and Adikari, G. (2001). Time-dependent particle transport through granular filters. *Journal of geotechnical and geoenvironmental engineering*, 127(6):521–529.

McKelvey, J. A. I. (1994). The anatomy of soil arching. *Geotextiles and Geomembranes*, 13(5):317–329.

Miller, W. G. (1994). Sand flow mechanisms at well casing perforations. Master's thesis, University of Alberta.

Muszynski, M. R. and Vitton, S. J. (2012). Particle shape estimates of uniform sands: visual and automated methods comparison. *J. Mater. Civ. Eng.*, 24(2):194–206.

NEN (2017). Geotechnisch ontwerp van constructies - deel 1: Algemene regels. NEN NEN 9997-1+C2:2017 nl, Stichting Koninklijk Nederlands Normalisatie Instituut, Nederland.

Nguyen, V. T., Rujikiatkamjorn, C., and Indraratna, B. (2013). Analytical solutions for filtration process based on constriction size concept. *Journal of geotechnical and geoenvironmental engineering*, 139(7):1049–1061.

Polidoro, A., Allsop, W., and Pullen, T. (2015). Exploring the need for geotextile filters for rubble bunds retaining sand-fill islands.

Powers, M. C. (1953). A new roundness scale for sedimentary particles. *Journal of Sedimentary Research*, 23(2):117–119.

Raut, A. K. and Indraratna, B. (2008). Further advancement in filtration criteria through constriction-based techniques. *Journal of geotechnical and geoenvironmental engineering*, 134(6):883–887.

Schiereck, G. J. and Verhagen, H. J. (2019). *Introduction to bed, bank and shore protection*. Delft Academic Press / VSSD, 2 edition.

Schürenkamp, D., Oumeraci, H., and Kayser, J. (2016). Stability of wide-graded granular filters under oscillatory flow.

Shields, A. (1936). Application of similarity principles and turbulence research to bed-load movement.

Sjah, J. and Vincens, E. (2013). Determination of the constriction size distribution of granular filters by filtration tests. *International Journal for Numerical and Analytical Methods in Geomechanics*, 37.

Sugii, T., Yamada, K., Yokawa, H., and Asano, N. (2016). Ground destabilization due to soil particle effluxes. *Japanese Geotechnical Society Special Publication*, 2(49):1732–1735.

Terzaghi, K. (1936). Stress distribution in dry and in saturated sand above a yielding trap-door.

Terzaghi, K. (1948). *Theoretical Soil Mechanics*. John Wiley and Sons.

Tien, H.-J. (1996). *A literature study of the arching effects*. PhD thesis, Massachusetts Institute of Technology.

Tutein Nolthenius, R. (2018). Sandfill-retaining rubble mound structures: Evaluating the behaviour of sediments at the interface of a rubble mound with a reclamation, by means of physical modelling. Master's thesis, Delft University of Technology.

US Army Corps of Engineers (1984). *ENGINEERING AND DESIGN: Drainage and Erosion Control Mobilization Construction*. DEPARTMENT OF THE ARMY Washington DC.

Van Burkalow, A. (1945). Angle of repose and angle of sliding friction: an experimental study. *Geological Society of America Bulletin*, 56(6):669–707.

Van de Ven, D. (2019). Granular open filter in rubble mound sand retaining structures: Physical model tests of a negative geometrically open filter layer. Master's thesis, Delft University of Technology.

Van Gent, M. (1995). Porous flow through rubble-mound material. *Journal of waterway, port, coastal, and ocean engineering*, 121(3):176–181.

van Gent, M. R., Herrera, M. P., Molines, J., and Jacobsen, N. G. (2017). Rock slopes on top of sand: Modelling of open filters under wave loading. In *Coastal Structures and Solutions to Coastal Disasters 2015: Resilient Coastal Communities*, pages 817–827. American Society of Civil Engineers Reston, VA.

van Gent, M. R. and Wolters, G. (2015). Granular slopes with open filters under wave loading. *Coastal Engineering*, 104:135–150.

van Gent, M. R. and Wolters, G. (2018). Effects of storm duration and oblique wave attack on open filters underneath rock armoured slopes. *Coastal Engineering*, 135:55–65.

Verhagen, H. J. and Jansen, L. (2014). Ratio between stone diameter and nominal diameter. *Communications on Hydraulic and Geotechnical Engineering 2014-01*.

Verheij, H., Hoffmans, G., Dorst, K., and Van de Sande, S. (2012). Interface stability of granular filter structures under currents. In *ICSE 6: Proceedings of the 6th International Conference on Scour and Erosion, Paris, France, 27-31 August 2012*. Société Hydrotechnqiue de France (SHF).

Verruijt, A. and Broere, W. (2011). *Grondmechanica*. VSSD.

Wilson, A. M., Moore, W. S., Joye, S. B., Anderson, J. L., and Schutte, C. A. (2011). Storm-driven groundwater flow in a salt marsh. *Water Resources Research*, 47(2).

Wittmann, L. et al. (1980). Filtrations-und transportphänomene in porösen medien.

Wörman, A. (1989). Riprap protection without filter layers. *Journal of Hydraulic engineering*, 115(12):1615–1630.

Ziems, J. (1969). *Beitrag zur Kontakterosion nichtbindiger Erdstoffe*. PhD thesis, TU Dresden.

A

Design of Plate

A top-plate was designed to distribute the concentrated load from the hydraulic press equally across the top of compartment B. This is necessary as a constant effective stress was assumed along the filter-base interface. This appendix will explain the design of the plate. Firstly the design requirements will be presented, then the design of the plate and finally the design will checked for deformation.

A.1. Design Requirements

The top-plate needs to distribute the load from the hydraulic press across the base material in compartment B. The most important requirements are as follows:

- The variation in effective stress in the base material must be at the top of compartment B must be less than 10% when the effective stress is 200kPa.
- The plate must be simple to construct and transportable.
- The plate must allow for pore pressure to dissipate through the plate.

A.2. Design of Top-Plate

The design that was chosen for the plate is a rectangular grid of ribs welded on a stainless steel plate (757mm by 347mm and 8 mm thick) with holes (30 mm diameter) to allow for the dissipation of pore pressures. The ribs are made of a stainless steel strip (10mm by 80mm). Lifting attachments are attached to the corners to allow for transport as the the plate is too heavy for lifting by hand. The design of the plate is shown in Figure A.1.

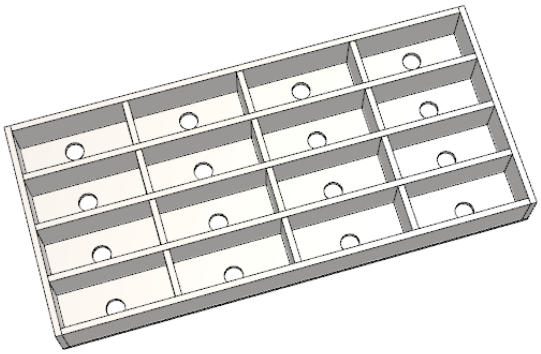

Figure A.1: The design of the top-plate

A.3. Check of the design of the Plate

The plate needs to have a larger relative stiffness when compared to the base material to ensure that the force from the hydraulic press is properly distributed across the base material. The distribution of the force was calculated using the FEM-Design module from the software Matrix-Frame. For this the top-plate was entered into the program as steel. The base material was modelled using a linear-elastic foundation with a stiffness of 20 kPa/mm. This corresponds to the bedding constant of a sand. The load from the hydraulic press is modelled as line loads on the centre-ribs. The finite element calculations were done using the linear elastic equation. The results of this analysis for the design are shown in Figure A.2.

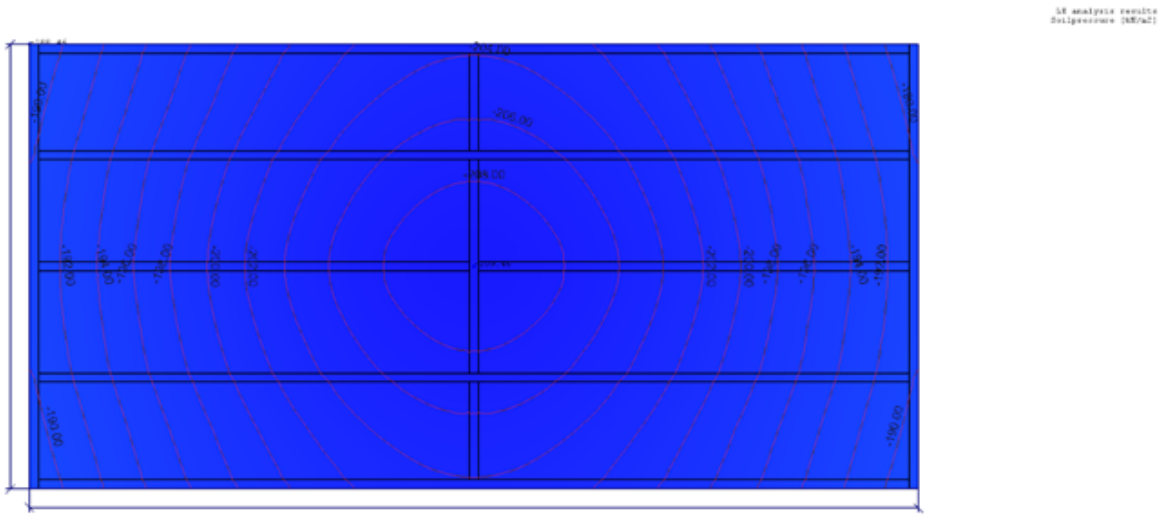

Figure A.2: Results of the finite element analysis of the deformation of the plate showing the effective stress in the soil in kPa.

From the FEM calculation we can see that the maximum deviation from the targeted 200 kPa is less than 10 kPa. The minimum is 191 kpa and the maximum is 209 kPa. This is a deviation of less than 5% and deemed acceptable.

B

Additional details of Numerical Model

Details about modelling the compressiblity of air will be included here. The compressiblity of air has been included in the Darcy model, as was explained in Chapter 4. This Appendix will first describe the parameters in the expanded model. Next the calculation of the compression of the air will be explained. Then the influence of this on the Darcy model will be explained. Finally a calculation will be made with the model.

B.1. Model Description

Within the The numerical model represents the experimental setup in the parallel configuration. The parameters used are shown in Figure B.1 and listed below:

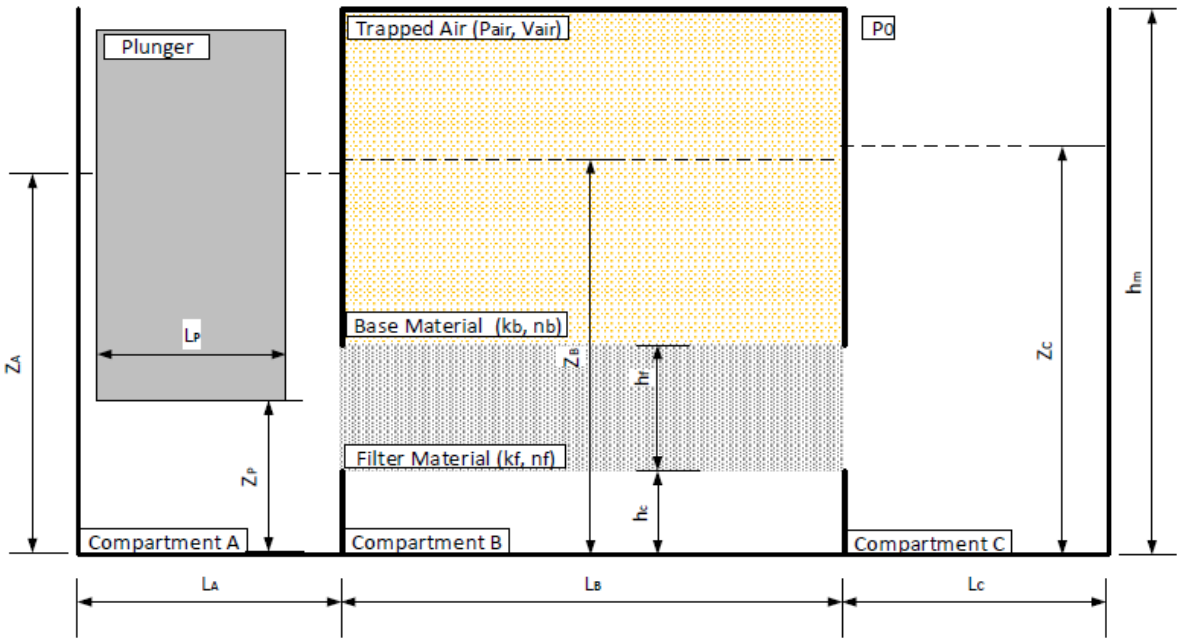

Figure B.1: The parameters in the numerical description of the experimental setup when compressible air is included

The parameters :

- z_A: Water level in compartment A [mm]
- z_B: Groundwater level in compartment B [mm]
- z_C: Water level in compartment C [mm]
- z_p: Level of bottom of plunger [mm]
- h_f: Filter layer thickness [mm]
- h_bc: Bottom cells height [mm]
- L_A: Length of compartment A [mm]
- L_B: Length of compartment B [mm]
- L_C: Length of compartment C [mm]
- L_p: Length of the plunger (2D representation of the area blocked in Comp. A) [mm]
- k_b: Permeability of the base layer [m/s]
- n_b: Porosity of the base layer [-]
- k_f: Permeability of the filter layer [m/s]
- n_f: Porosity of the filter layer [-]

B.2. Compressiblity of the Trapped Air

Within the model there is a pocket of air trapped within the pores of the sand above the waterline. As the top of the model is sealed this air cannot escape and is compressed when the ground water level in compartment B rises. The trapped air is modelled using the ideal gas law which is as follows:

$$P \cdot V = n \cdot R \cdot T \tag{B.1}$$

In which :

- P: The pressure of the gas.
- V: The volume of the gas.
- n: The number of gas moles. This is assumed to remain constant as the air is trapped.
- R: The universal gas constant, this value is always constant.
- T: The temperature of the gas. This is assumed to remain constant.

With these assumptions the $pressure \cdot volume$ of the trapped air is constant. Initially the air pressure is equal to the atmospheric pressure (P_0). The volume of the trapped air is calculated using the following equation:

$$V_{air} = (h_m - z_B) \cdot L_B \cdot n_b \tag{B.2}$$

Thus the air pressure at any time can be calculated based on the initial pressure and the volume of the air at that time.

$$P_{air}(t) = \frac{V_{air}(t = 0) \cdot P_0}{V_{air}(t)} \tag{B.3}$$

B.3. New Equations for the Perpendicular Hydraulic Gradients

Due to the trapped air in compartment B the hydraulic head is no longer equal to the water level in compartment B. The increased air pressure must also be included. The hydraulic head in compartment B (hh_B) is now calculated using the following equation:

$$hh_B = z_B + (P_{air} - P_0) \tag{B.4}$$

This influences the calculations of the perpendicular hydraulic gradients in the following way:

$$i_{A,\perp}(t) = \frac{(z_B(t) + (P_{air}(t) - P_0)) - z_A(t)}{z_B(t) - h_f - h_c} \tag{B.5}$$

$$i_{C,\perp}(t) = \frac{(z_B(t) + (P_{air}(t) - P_0)) - z_C(t)}{z_B(t) - h_f - h_c} \tag{B.6}$$

B.4. Example Calculation

The influence of the compressibilty of the trapped air has been calculated for the parallel configuration. It turned out that the seal leaked allowing air to escape. Therefore no pressure can build up and this process did not occur. However this calculation is still shows the influence that the compresibiltiy of the air can have if the seal was air tight. The Darcy model with compressible air was run for the situation in test . The results are presented in Figure B.2.

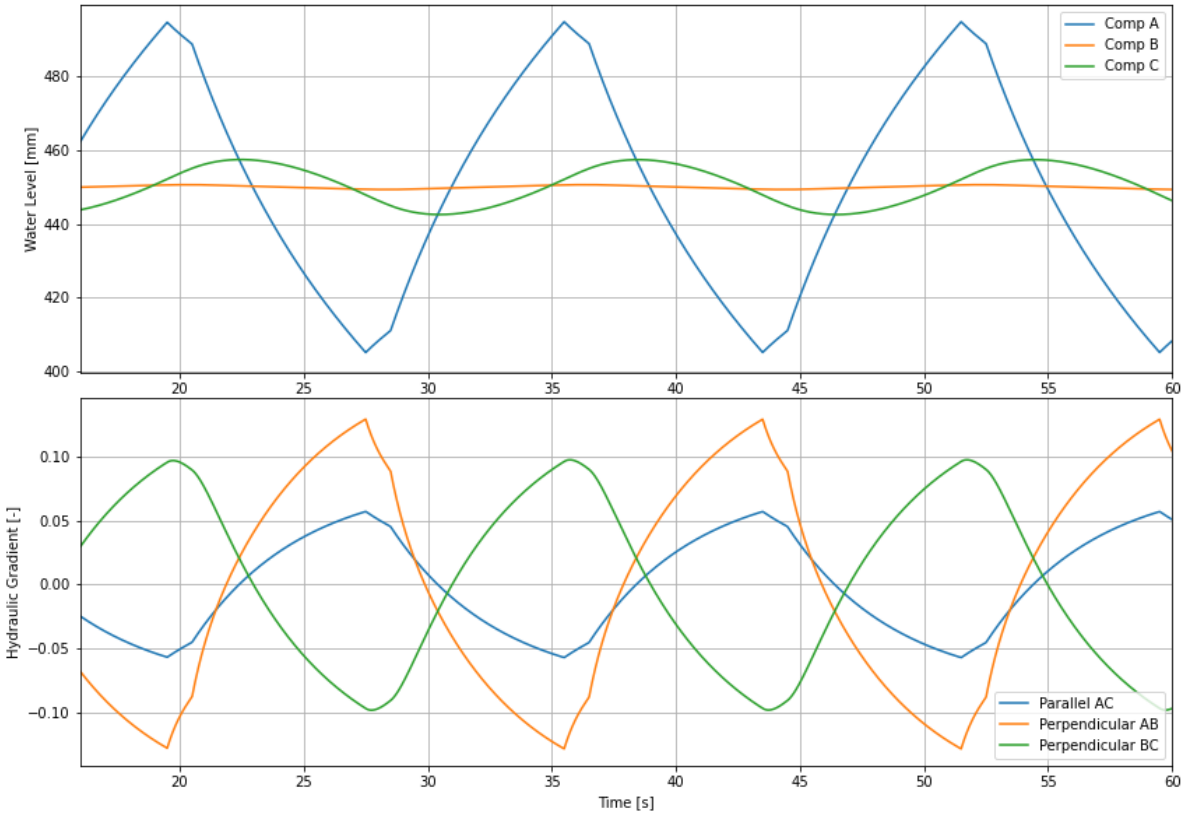

Figure B.2: Results of Darcy model for parallel setup with compressible air.

It can clearly be observed that the trapped air being compressible leads to significant perpendicular hydraulic gradients. These perpendicular hydraulic gradients are larger than the parallel hydraulic gradients and thus are likely governing. As such a setup with trapped air is not recommended for future testing as this does not allow for the testing for a parallel hydraulic gradient only.